Thermal efficiency improvement of closed hydrogen and oxygen fuelled combined cycle power plants with the application of solid oxide fuel cells using an exergy analysis method

Bram Schouten

student number: 4390504

to obtain the degree of Master of Science
at the Delft University of Technology,
to be defended publicly on Thursday the 9th of April, 2020 at 13:30 PM.

Abstract

Today's renewables, wind and solar power, have a fluctuating nature, making the grid less stable. However, with the increasing share of intermittent sources of renewable power, novel options have to be created to stabilize the power grid. One of these options is energy storage via the conversion of excess power to hydrogen, during periods of high generation from wind and/or solar. In periods of power shortages hydrogen is converted back to power.

In the literature fossil fuelled turbine cycles have been studied extensively, furthermore multiple fuel cell turbine cycles have been modelled. However, models with hydrogen and oxygen fuelled turbine cycles and fuel cell turbine cycles are scarce, leaving opportunity for further optimization of modeled hydrogen and oxygen fuelled cycles. The application of pressurized H_2/O_2 can lead to several improvements over conventional thermodynamic cycles and fuel cells.

In this work, a number of high efficiency hydrogen and oxygen fuelled thermodynamic cycles, based upon the Graz cycle and the Toshiba Reheat Rankine cycle, both a coupled closed Brayton cycle with a Rankine cycle, are investigated. Furthermore, the following thermodynamic improvements are proposed to fit the Graz cycle: an increased TIT (turbine inlet temperature), the use of a reheat combustor (the inclusion of a 2^{nd} combustor), condensate preheating and hybrid cooling (a combination of open loop and closed loop cooling) of the high temperature turbine blades. All upgrades together lead to an efficiency of 75% LHV. The rise of efficiency of the individual upgrades summed up is lower than the rise off all upgrades together. This is due to the fact that adding reheat and increasing TIT introduce extra high temperature turbine blade cooling needs and losses, which an improved cooling method counteracts. For this reason, the cooling method used is rather influential. Therefore, two cooling methods, open loop cooling and hybrid cooling, used in the Graz and Toshiba cycle respectively, are studied in this thesis.

Next to the thermodynamic improvements, an electrochemical improvement is studied, by adding fuel cell systems to the turbine cycles. Multiple fuel cells combinations are studied: a single low temperature solid oxide fuel cell (SOFC) and a low temperature, intermediate temperature and high temperature SOFC in series. Moreover, the type of fuel cell cooling is investigated, both cooling by adding steam to the cathode and recirculating excess oxygen in the cathode are studied.

The addition, of a triple SOFC cooled by oxygen recirculation, to an upgraded Graz cycle leads to a potential efficiency of 84% LHV. This efficiency is reached at a relatively low fuel cell fuel utilization of 58%. In this study the turbine cycle is not fully adapted to the fuel cell system or vice versa. Both systems are adapted to each other, leading to the unique triple fuel cell system operating in series, which is more easily coupled to a turbine cycle and can operate at an overall higher SOFC utilization, compared to a single fuel cell. However, from the fuel cell side 2 of the 3 fuel cells are less electrochemically favorable, as only one of the three fuel cells can operate in the best conditions. The overall system efficiency of the combined multiple fuel cell in series system with a turbine cycle, however is most efficient.

Acknowledgement

First and foremost, I would like to thank Prof.dr.ir. Sikke Klein for giving me the opportunity to work on this topic and for supervising this project. Also, at least as important, was his clear guidance keeping me from losing the broader picture. I also extend my sincere gratitude to Ir. T. Woudstra, Jelle Stam and S.A. Saadabadi for helping me out with some fuel cell related questions.

Furthermore, my gratitude goes to my study buddies working with me at the fluids lab for getting coffee with me whenever I needed to clear my mind. Thanks to my brother, for proof-reading my report and providing feedback.

Finally, I would like to thank my family, and friends for their support throughout and advice on things less technical.

Bram Schouten
Delft, April 2020

Contents

Nomenclature

Abbreviations

ASR	Area specific resistance
BFP	Boiler feed pump
CC	Combustor
CCGT	Combined cycle gas turbine
CIT	Combustor inlet temperature
CLS	Closed loop steam
CLSC	Closed loop steam cooling
Comp.	Compressor(s)
Deaer.	Deaerator
EQ	Equalized cycle
FC	Fuel cell
FC-OX	Oxygen recirculated fuel cell
FC-Steam	Steam cooled fuel cell
HC	Hybrid cooling
HEX	Heat exchanger
HPT	High Pressure turbine
HRSG	Heat Recovery steam generator
HTT	High temperature turbine
IRES	Interruptible renewable energy source
LPT	Low Pressure turbine
SOFC	Solid oxide fuel cell
TIT	Turbine inlet temperature

Variables and physical constants

$\chi_{molecule}$	Mol fraction of the relevant molecule

ϵ	$\frac{T_g - T_b}{T_g - T_{ci}}$	
η	Efficiency	
e	Exergy	$(\frac{J}{kg})$
E_0	Potential voltage	(V)
e_{ch}	Chemical exergy	$(\frac{J}{kg})$
e_m	Mechanical exergy	$(\frac{J}{kg})$
E_{nernst}	Nernst voltage	(V)
Ex	Exergy	(J)
F	Faraday Constant	$(\frac{C}{mol})$
G^0	Gibs free energy of formation	(J)
H^0	Enthalpy of formation	(J)
$Pp_{molecule}$	Partial pressure molecule	(Pa)
R	Gas Constant	$(\frac{J}{mol \cdot K})$
S^0	Entropy of formation	$(\frac{J}{K})$
A	Area	(m^2)
Bi	Biot number	
Cp	Heat capacity	$(\frac{J}{K})$
FOB	Fraction of the blade	
h	Heat coefficient	$(\frac{W}{m^2 K})$
HHV	Higher heating value	$(\frac{kJ}{kg})$
LHV	Lower heating value	$(\frac{kJ}{kg})$
n	Amount of electrons used in the reaction	
P	Pressure	(Pa)
POW	Power	(W)
Q	Heat	(J)
s	Entropy	$(\frac{J}{K})$
St	Stanton number	

T	Temperature	(K)
t	Thickness	(m)
U	Internal energy	(J)
V	Volume	(m^3)
v	Velocity	$(\frac{m}{s})$
W	Work	(J)

Subscripts

ano	Anode
b	Metal Blade
cat	Cathode
ce	Coolant exitting the blade
ci	Coolant going into the blade
c	Coolant
ex	External
g	Main gas
in	Internal
rxn	reaction
w	Wall

1 Introduction

The accumulation of greenhouse gasses (carbon dioxide, methane and nitrous oxide) is one of the worlds most challenging problems, that needs to be tackled. The greenhouse gasses create a layer that reflects the UV radiation and concentrates the incoming heat from solar radiation into the atmosphere of earth. As a consequence, the temperature rises on earth. It has been proven the increase in greenhouse gas concentration is the main reason for this increase in temperature. The OECD [1] predicts that at the 2011 emission rate, the temperature increase from 2011 to 2100 will range between 3 and 6 °C. Other very likely side effects of the greenhouse gas increase are more drought, more flooding, less ice and snow, more extreme weather incidents and a rising sea level [2]. From the greenhouse gasses carbon dioxide has the highest share. Without new policies, by 2050, more disruptive climate change is likely to be locked in, with global greenhouse gas (GHG) emissions projected to increase by 50%, primarily due to a 70% growth in energy-related CO_2 emissions [1]. Figure 1 shows the accumulation of greenhouse gasses and the global combined land and ocean surface temperature rise since 1850.

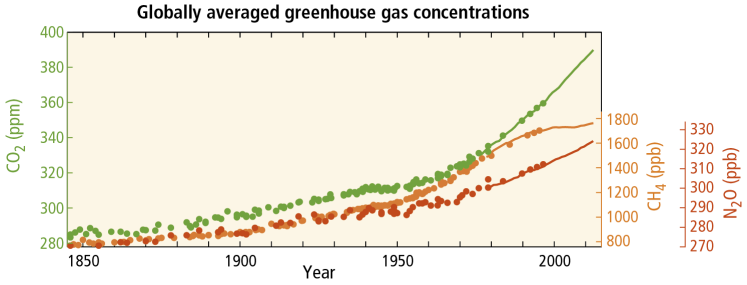

(a) Globally averaged concentrations of carbon dioxide (CO_2), methane (CH_4) and nitrous oxide (N_2O) determined from ice core data (dots) and from direct atmospheric measurements (lines).

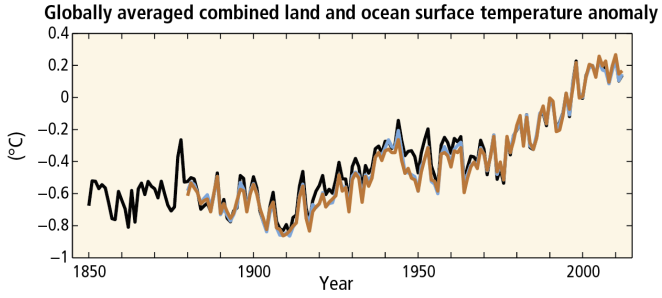

(b) Globally averaged combined land and ocean surface temperature anomalies relative to the average over the period 1986 to 2005. Colours indicate different data sets.

Figure 1: Observations of a changing global climate system [2]

More use of renewable energy seems to be the most logical next step. The power system already made significant changes during the last decade due to the large scale introduction of interruptible renewable energy sources (IRES) like wind and solar. It is expected that the power supplied from wind and solar will increase further at the expense of power from thermal power plants [3]. This change in the power system is driven by a combination of the increased attention to CO_2 emissions and the decrease of costs of IRES versus conventional plants [3]. When the stated policies are globally executed, the global power capacity is expected to look like figure 2. This further increase in interruptible supply from renewable sources will place challenges on the stability of the electricity system, with the decrease of fossil-fired thermal power plants. Storage of electricity will be required in the future electricity systems for stability reasons.

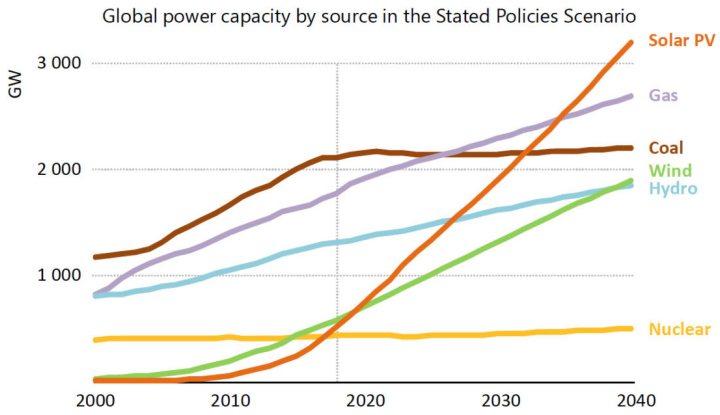

Figure 2: The distribution of generated power is being reshaped by the rise of renewables. In 2040, renewables account for nearly half of total electricity generation [3]

A potential storage option is hydrogen [4] in large scale volumes, such as salt caverns. Excess renewable power will be used to generate hydrogen and oxygen by electrolysis from water.

The power-to-power efficiency of hydrogen as an energy storage depends on a number of parameters, such as power to hydrogen conversion, compression, transport, storage and hydrogen back to power conversion. A full cycle, from excess electricity to the cycles modeled in this thesis, is depicted in figure 3. The most standard way for hydrogen back to power conversion is application in a fuel cell. A state of the art solid oxide fuel cell (SOFC) transforms 65% LHV of the converted fuel's energy into electricity [5]. Nowadays conversion efficiency of power to hydrogen in elektrolyzers is around 70% (ranging from 60-80%) LHV [6], the hydrogen fuelled SOFC fuel to power efficiency is 65%, making the maximum power-to-power efficiency of energy storage by hydrogen 46%, in this case transport losses, storage losses and compression power are neglected. Important improvements in this power-to-power round trip efficiency can be achieved by increasing the efficiency of the subsystems. In this thesis the focus will be on the improvement of the fuel (hydrogen) to power efficiency.

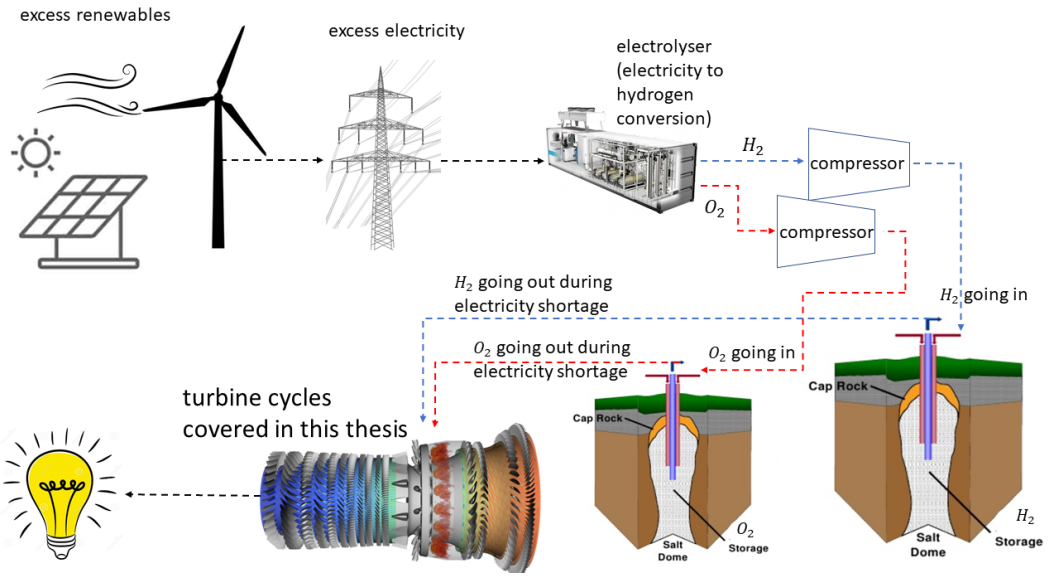

Figure 3: A full cycle from excess renewable energy, to an electrolyser, storing the obtained hydrogen in a storage facility (salt caverns) and converting this hydrogen back to power via the cycles discussed in this thesis

The utilization of both the hydrogen and the oxygen from the electrolysis, introduces the option to use both hydrogen and oxygen as a fuel for the turbine cycles. The use of hydrogen and oxygen makes path for common hydrogen and oxygen fuelled cycle principles. Steam can be used as the working fluid throughout the cycle, moreover the cycle can be used as a closed cycle. The advantages of these hydrogen and oxygen fuelled cycle principles are explained in the next paragraph. These cycles, result in electrical efficiencies over 70% LHV [7] [8] [9], while state of the art fossil fuelled CCGT (Combined cycle gas turbine) cycles have efficiencies around 60% LHV [10]. Two of these hydrogen/oxygen cycles, the modified Graz cycle developed by the Graz University [7] and the Toshiba Reheat Rankine cycle [8], will be studied in this thesis and potential optimizations and improvements will be identified.

These high efficiency hydrogen/oxygen cycles have a number of common principles:

1. *Cascading of thermal energy.* Like in CCGT power plants, the basic input is the combustion of fuel. The thermal energy is extracted in two phases: first in a high temperature turbine (HTT) at moderate pressures, comparable to pressures in a normal gas turbine, secondly the excess heat from the flow at the outlet of the HTT is transferred to a steam cycle using a heat recovery steam generator at different steam cycle pressure levels.

2. *Steam as working fluid for the cycle.* In a normal CCGT cycle, air is the working fluid for the Brayton Gas Turbine cycle. In the studied hydrogen/oxygen cycles steam is the working fluid in the combustor and the HTT part of the cycle. Hydrogen and oxygen are combusted at the stoichiometric ratio resulting in pure steam as product. The combustor temperature and the inlet temperature for the HTT are controlled by the addition of steam. Because no nitrogen is present, there is no risk of NO_X formation.

3. *Closed cycle.* The low temperature steam at the exit of the heat recovery steam generator (HRSG) is fed into the steam cycle making it possible to extract power from the available sensible and latent heat in this flow. The studied hydrogen/oxygen cycles therefore do not have a stack. The mass of water that is created in the combustor should be removed downstream of the condenser.

The simplified principle flow scheme of a hydrogen-oxygen cycle is shown in figure 4.

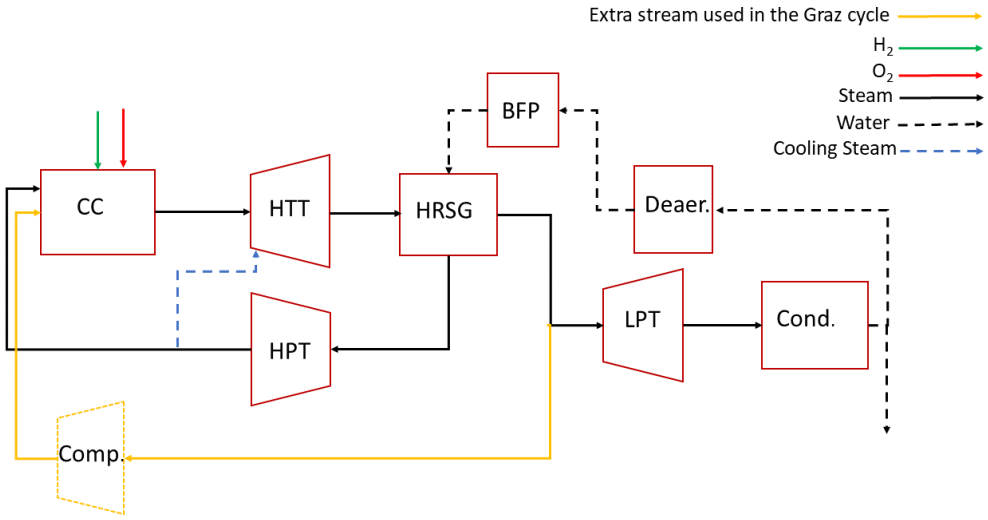

Figure 4: Simplified process flow diagram for the hydrogen and oxygen cycles. CC: combustor, HTT: high temperature turbine, HRSG: heat recovery steam generator, HPT: high pressure turbine, LPT: low pressure turbine, BFP: boiler feed pump, Cond.: Condenser, Comp.: Compressor, Deaer.:Deaerator. In the Graz cycle an extra steam compressor is added upstream of the combustor displayed in yellow. This steam compressor is not included in the Toshiba Reheat Rankine cycle.

1.1 Innovations in this thesis

In this thesis the following question will be answered:

How can one improve the configuration of a hydrogen and oxygen fuelled turbine cycle, for efficiency?

To answer the question fully, the following subquestions need to be answered:

1. How can one minimize the exergy losses throughout a hydrogen and oxygen fuelled turbine cycle?
2. How can one describe and model the high temperature turbine blade cooling needs in the hydrogen and oxygen fuelled turbine cycle?

3. What is the added value of a fuel cell system integrated into a hydrogen and oxygen fuelled turbine cycle?

4. What configuration of a fuel cell system integrated into a hydrogen and oxygen fuelled turbine cycle is most efficient?

1.2 Thesis outline

The theoretical background necessary is provided in chapter 2 in which both the thermodynamics behind power cycles and the physics behind the fuel cell is covered. Moreover, an analysis of existing hydrogen-oxygen cycles is made in this chapter.

The HTT cooling model is discussed in chapter 3. The physics behind CLSC and open loop cooling is explained. The implementation of open loop cooling into the open loop cooled models, of this study, is covered. Subsequently, the implementation of hybrid cooling into the hybrid cooled models, of this study, is covered (hybrid cooling is a combination of film cooling and closed loop cooling used in the Toshiba cycle [8]). The resulting hybrid cooling model and open loop cooling model are used in the succeeding chapters.

In chapter 4, the overall model is described and the existing cycles are validated and made comparable using an equal set of parameters. An exergy analysis is performed for both the Graz cycle [7] and the Toshiba Reheat Rankine cycle (also called Toshiba cycle) [8].

In chapter 5, a set of thermodynamic improvements are modeled and analyzed, the main objective is to quantify, for every upgrade, the reduction (or addition) of exergy losses through the components. The most important elements from both cycles will be included: reheat combustor, hybrid cooling in the hot section of the HTT and the compressor upstream of the combustor. The efficiency of this optimal cycle reaches 74-75% LHV, depending on the choices of the turbine inlet temperature.

The exergy analysis of this optimized cycle shows that the main exergy losses occur in the combustor part of the cycle. The potential improvement lays in the partial replacement of the combustor with an SOFC. An SOFC fits well with these kind of cycles due to its high operating temperature and efficiency. In chapter 6, the addition of a fuel cell to the turbine cycle is modeled, to further reduce the exergy losses going through the cycle. Two different set-ups with the SOFC are studied: First a single SOFC operating at 700 °C and then a set of three SOFC in series, operating at 700 °C, 850 °C and 1000 °C respectively. In the second situation the amount of exergy loss is further reduced. Moreover, the impact of two different operating philosophies for the cooling of the fuel cells will be discussed: in the first operating philosophy the fuel cell is cooled by an excess of oxygen that will be circulated over the cell, in the second approach the hydrogen and oxygen are supplied at the stoichiometric ratio and the fuel cell is cooled by steam addition to the oxygen (cathode side) flow. The electrochemical results of the various fuel cells are analyzed. Additionally, the fuel cell turbine cycles are exergetically analyzed. The result of the optimum fuel cell configuration in combination with the optimum thermodynamic cycle results in an efficiency of up to 83.8% LHV.

In chapter 7, the main conclusions are drawn. Recommendations and possible future research are discussed in chapter 8.

2 Thermodynamic and electrochemical power cycle analysis

In this chapter, the thermodynamics behind the power cycles are explained. The Carnot cycle (the most efficient thermodynamic cycle) is explained and will act as a reference cycle for cycles discussed in this thesis. Moreover, hydrogen and oxygen fuelled cycles from literature are covered. The differences between conventional fossil fuelled and hydrogen and oxygen fuelled cycles are discussed. Additionally, the Graz and Toshiba cycle are identified to illustrate the main aspects of hydrogen-oxygen fired turbine cycles. Thereafter, the SOFC (an electrochemical apparatus) is introduced and compared to thermodynamic power cycles. Moreover, the combination of a fuel cell and gas turbine is covered. Furthermore, the physics behind the fuel cell is explained in the final section of this chapter.

2.1 Thermodynamics of power cycles

A thermodynamic cycle consists of multiple thermodynamic processes transferring heat and work, while varying state variables (temperature, pressure, volume, enthalpy and entropy) and eventually returning to the systems initial state [11]. In this study, the goal is to produce power (mechanical work), for that reason the thermodynamic cycles, used in this thesis, are called power cycles. Power is obtained in a heat engine, which converts heat into power. The hydrogen combustion converts the chemical energy, of the fuel, into heat.

For thermodynamic cycles the first law of thermodynamic applies:

$$\Delta U = Q - W \tag{1}$$

Here ΔU is the change in internal energy of the system. Q is the net heat transferred to the system. W is the net work done **by** the system. Therefore, energy cannot be created, nor destroyed. However, energy can be transferred, from heat to work, for example.

The power produced in a cyclic process can be described by the following equation:

$$W = \oint p\,dv \tag{2}$$

Therefore, the net work can be visualized in a PV (pressure and volume) diagram as the enclosed area of the cycle [11]. The expansion of a pressurized system converts the internal energy into work, as done in a turbine where high pressures fluids are expanded. However, compression of a fluid needs energy. This is similar to what is done in a compressor, where fluids are pressurized. However, by adding heat to the cycle after the compression step and disposing less heat after the expansion process, net heat is added to the cycle. According to the first law of thermodynamics, net work must be created in this case (there is no internal energy change).

To first compress a liquid at the cost of work and directly expand the fluid to obtain work has no purpose, no net work will be obtained. However, by adding heat to the cycle after the compression step and disposing less heat after the expansion process, net heat is added to the cycle. According to the first law of thermodynamics (equation 1) net work must be created in this case (their is no internal energy change).

The heat (Q) input and output can be visualized in a Ts (temperature entropy) diagram. The highest possible theoretical exergy efficiency in a thermodynamic cycle is the Carnot efficiency. It provides an upper limit on the efficiency that any thermodynamic heat engine can achieve during the conversion of heat into work. This upper limit comes from adding heat to the cycle at the highest temperature (T_h), without temperature increase (nor decrease) during the heat addition. Moreover, heat is subtracted from the cycle at the coldest temperature (T_c), without temperature decrease (nor increase) during the heat addition. The use of the 4 ideal stages can be seen in the pressure volume and temperature entropy diagram in figure 5. It is not an actual (physical) thermodynamic cycle, but a theoretically constructed cycle.

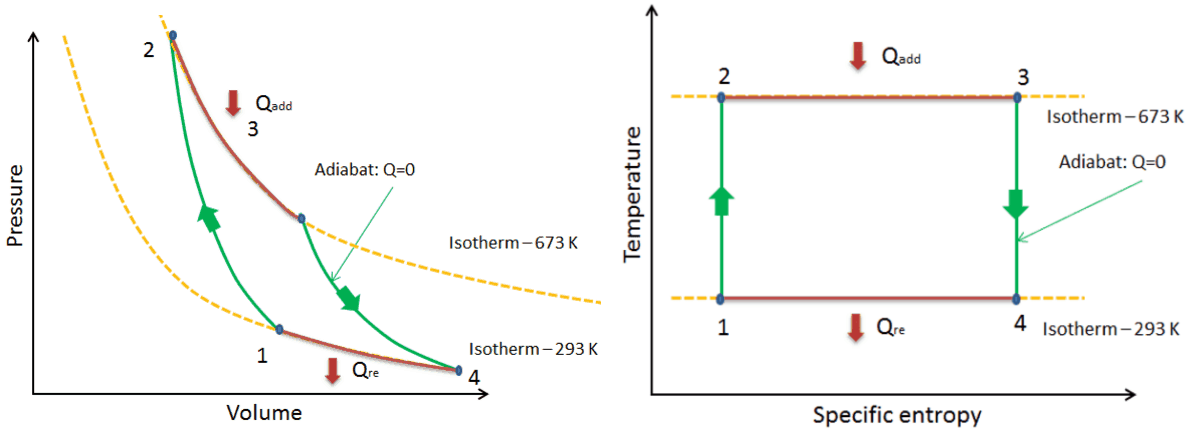

(a) Carnot cycle PV diagram

(b) Carnot cycle Ts (temperature entropy) diagram

Figure 5: Carnot cycle diagrams with a T_h of 673 Kelvin and a T_c of 293 Kelvin [12]. The heat inserted into the cycle is $Q_{add} = Q_h$ and heat removed from the cycle is $Q_{re} = Q_c$. The cycles consists of 4 theoretical stages, first (from point 1 to 2) the adiabatic compression from T_c to T_h, secondly the isothermal expansion at T_h (heat is added in this process), thirdly adiabatic expansion from T_h to T_c and lastly isothermal compression at T_c (heat is rejected during this process). The enclosed area of the process in both the PV and Ts diagram represents the amount of work produced.

The Carnot efficiency is defined as:

$$\eta_{carnot} = \frac{W}{Q_h} = \frac{Q_h - Q_c}{Q_h} = 1 - \frac{Q_c}{Q_h} = 1 - \frac{T_c}{T_h} \tag{3}$$

In which T_c is the coldest temperature to which heat is rejected (ambient temperature) and T_h the highest temperature achieved in the cycle. Increasing the firing temperature T_h and decreasing T_c will lead to an increased efficiency. For this reason, one wants to minimize Q_c and maximize Q_h.

The Carnot process is a theoretical process, in real life there are lots of irreversibilities that lead to entropy production such as friction, leakages and mixing. So this Carnot process can be used as a guideline and if a change in the model gives a quantitative improvement one can look for the qualitative resemblance in the Carnot cycle.

Real world thermodynamic cycles do not work in ideal conditions and have losses. A standard CCGT cycle (gas turbine cycle and steam cycle) scheme is depicted in 6 and the Ts diagram can be found in figure 7. This combined cycle contains both a Brayton cycle (gas turbine GT) and a Rankine (steam) cycle. The Brayton part of the cycle contains a compressor (1g-2g), a combustor (2g-3g), a high temperature turbine (3g-4g) and heat rejection in the stack (4g-1g). The Rankine part of the cycle contains a pump (1-2), heat addition (2-3-4-5), steam turbine (5-6) and condenser (6-1).

The cycles are coupled to each other, for this reason it is called a combined cycle. The Gas turbine cycle's heat rejection (4g-1g), in the stack, is not solely to the environment (as done in a conventional Gas turbine-only cycle), but most of the heat is passed through a heat recovery steam generator (HRSG) to the bottoming Rankine cycle. Consequently, the heat addition (2-3-4-5) is not done in a boiler (as done in Rankine-only cycle), but the heat is obtained in the HRSG from the Gas turbine cycle's otherwise wasted heat.

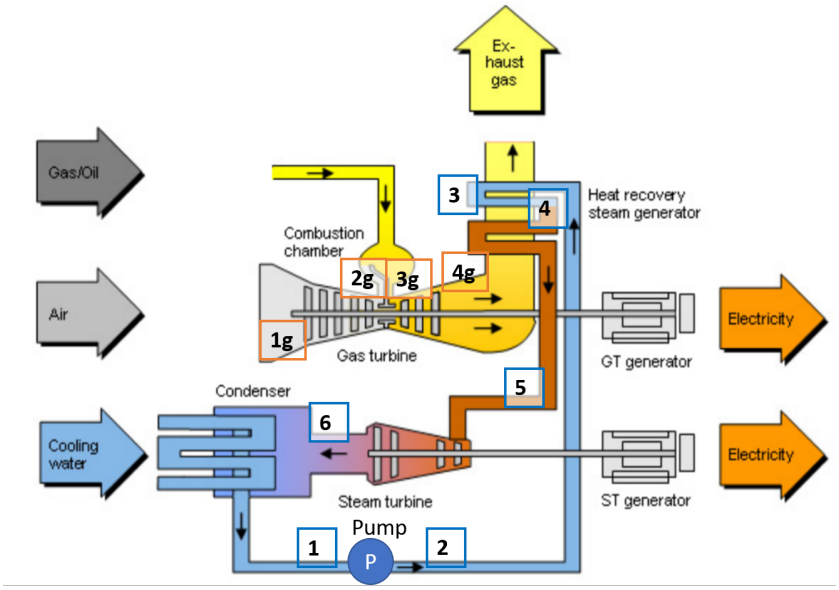

Figure 6: Fossil fuelled simplified CCGT cycle scheme [13]. The Brayton part of the cycle is numbered from 1g-4g and the Rankine part of the cycle is numbered from 1-6.

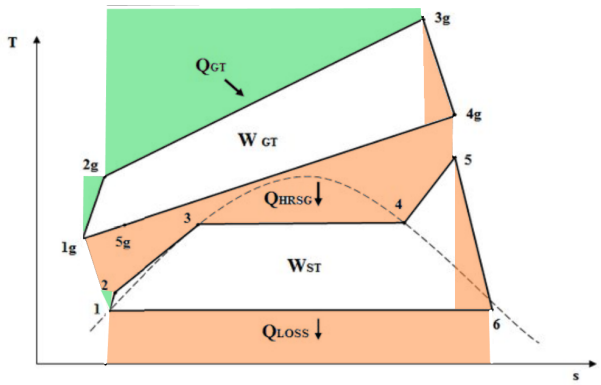

Figure 7: Standard CCGT Ts diagram, the points (numbered) correspond to the numbered components of the CCGT cycle depicted in figure 6. In green is the area depicted that can be incorporated into the cycle to increase efficiency (to look more like the reference Carnot cycle in figure 5b). The area in red should be reduced to increase efficiency. This is explained below.

Possible improvements to a standard CCGT cycle, to become more similar to the Carnot process and enhance efficiency are:

1. During the compression of the fluid, 1g-2g and 1-2, entropy is generated as friction occurs, this should be minimized. Furthermore, during the expansion process of 3g-4g and 5-6 entropy is generated due to friction, this also needs to be minimized.
2. The heat rejected from the gas turbine cycle is rejected from 4g-1g, this heat is used in the HRSG to heat the steam cycle from 2-5. The smaller the temperature difference between 4g to 5 and 1g to 2 is, the smaller the work free gap, inbetween the cycles. A smaller gap will fit the Rankine part to the gas turbine part better and consequently lead to a higher efficiency.
3. Temperature 2g (the combustor inlet temperature, CIT) and 3g (the turbine inlet temperature,TIT) should be maximized to increase the amount of work per unit of heat input. The increase in CIT and TIT, resulting in higher thermal efficiencies, is quoted on multiple occasions in this thesis.
4. The heat loss underneath the steam cycle (condensing process 6-1) should be minimized, therefore the temperature at point 6 and 1 should be minimized. The minimum temperature point 6 can reach is limited by the amount of condense the low pressure turbine can withstand at the chosen condenser pressure. When too much condense forms, the vapor quality is too low in point 6 and undesirable turbine blade erosion can occur.

2.2 Hydrogen fueled cycles

Hydrogen-oxygen fueled cycles differ from conventional fossil fuelled cycles in multiple ways. They do not produce CO_2, NO_x and other harmful emissions. Moreover, the exhaust gas is water, which is the working fluid as well. For this reason, the hydrogen CCGT cycles are closed and the GT and steam part of the cycle are more closely integrated. Creating a smaller work free gap in between the cycles as illustrated in figure 7. Moreover having steam as a working fluid throughout the cycle makes way for new cycle opportunities as used in the Graz cycle [7], discussed in section 2.2.2.

Hydrogen-oxygen cycles have first been studied during the late 1990's. In the recent years there has been a small revival in the study of these types of cycles. In this thesis a recent cycle, the Graz cycle [7], will be compared to the Toshiba cycle [8]. A number of other cycles have been evaluated.

The most efficient large scale hydrogen-oxygen fired cycles are CCGT cycles. The CCGT cycle extracts work from multiple pressure regimes by cascading energy throughout the cycle, using the waste heat of the Brayton part of the cycle to heat the Rankine part of the cycle. The most efficient hydrogen cycles minimize waste heat (like the most efficient fossil fuelled cycles). For this reason, the CCGT cycles are the most efficient hydrogen cycles, since they cascades energy through all pressure regimes of the cycle.

The SOFC also has been investigated. The SOFC can either be a standalone power generator, or can be coupled to a turbine cycle. Standalone operation cannot compete yet, with the class leading hydrogen fired turbine cycles. However, a fuel cell in conjunction with a turbine cycle can be competitive. Therefore, the addition of a fuel cell coupled to a turbine cycle is discussed in section 2.3.1.

The Westinghouse company has developed two hydrogen-oxygen fired CCGT cycles, named the Bannister-Westinghouse cycles [9], the research was led by Bannister. The cycles use reheat with a TIT of 1700 °C. The most promising cycle makes use of hybrid cooling and reaches an efficiency of 70.9% LHV.

The Toshiba cycle [8] is an improved Bannister-Westinghouse cycle [9]. The Toshiba cycle has broadly the same configuration, but includes low pressure turbine condensing heat extraction, for better performance. Moreover, the Toshiba [8] is operated at different temperatures, pressures and mass-flows than the Bannister-Westinghouse cycle. The Toshiba cycle (explained in detail in the next section) is a CCGT cycle that includes multiple extra performance extraction methods: hybrid cooling, reheat (the use of a second combustor) and low-pressure turbine condensing. All the performance enhancements lead to a remarkable high thermal efficiency of 72.9% LHV for the Toshiba cycle.

The Graz cycle [7] is a modification (explained in detail in section 2.2.2) to a standard CCGT cycle. The cycle is not enhanced with extra performance extraction methods and it operates at a relatively low TIT of 1500 °C. Nevertheless, the cycle reaches a high thermal efficiency (70.4% LHV).

The high efficiencies of these cycles with high TIT's (1500-1700°C), comes with a cost. The turbine blades can withstand metal temperatures between 750°C [7](obtained from table 1 of the respective paper) and 788 °C [8](obtained from figure 13 of the respective paper). The blades need to be kept at the right temperature, while the main gas in the first high temperature turbine stage is (1500-1700°C). Therefore, a significant amount of high temperature turbine blade cooling is needed. Cooling however, introduces complexity and losses, therefore a good turbine blade cooling solution is very important. The Graz cycle and the Toshiba cycle have been identified as cycles to illustrate the main aspects of the hydrogen-oxygen turbine cycles.

2.2.1 Toshiba cycle

The Toshiba cycle with reheat and recuperation [8] is stated as a cycle with a potential for very high thermal efficiencies (61.7% HHV, which equals 72.9% LHV) in the literature. The cycle can be considered as a CCGT cycle, with steam as the working fluid for both the Rankine part and Brayton part of the cycle. The principle flow scheme is shown in figure 8.

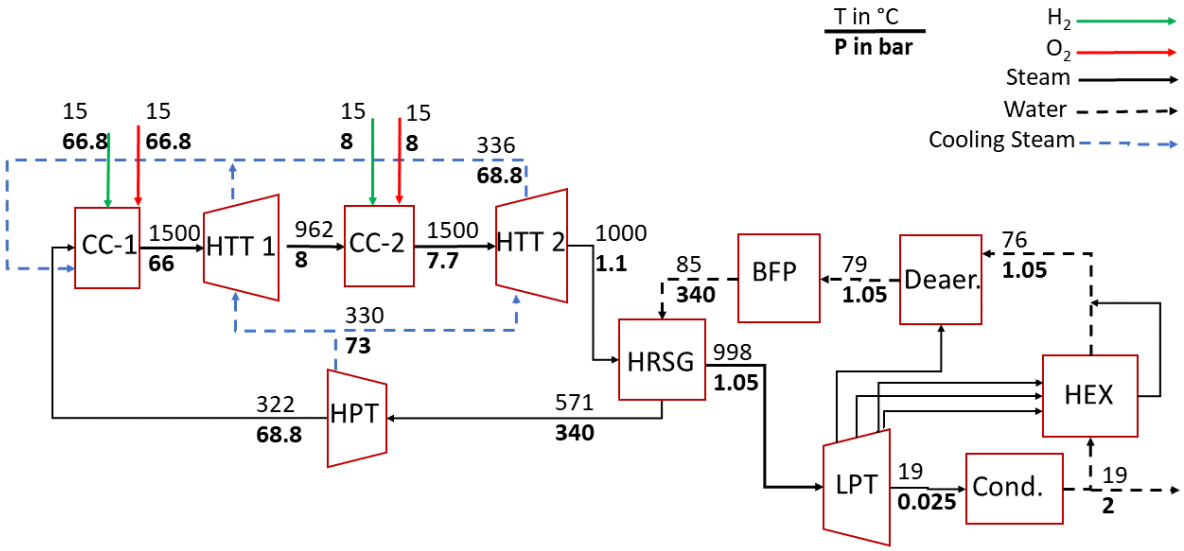

Figure 8: Principle flow scheme of the Toshiba cycle [8]. The temperatures and pressures are from the Toshiba-EQ cycle, this cycle is introduced in section 4.2. The detailed flow scheme of the Toshiba-EQ cycle is depicted in appendix B.2. The part at the left of the HRSG can be considered as a modified Brayton cycle with steam as a working fluid, the part at the right of the HRSG is a 'conventional' Rankine cycle

The cycle uses two hydrogen–oxygen combustors for heating and reheating with a turbine inbetween. At two locations steam is generated: (1) The combustors generate high-temperature steam at moderate pressures (66 bar in CC-1 and 7.7 bar in CC-2) by combusting hydrogen and oxygen and (2) in the HRSG at a high-pressure (340 bar) by boiling water. The steam generated in the combustors is expanded in two turbines (from 66 bar to 8 bar in HTT-1 and from 7.7 bar to 1 bar in HTT-2), the excess heat is transferred to a Rankine cycle via the HRSG after which the steam flow from the combustors is expanded in a condensing LP turbine. Heat is extracted from the LP turbine for feedwater heating. The high pressure steam flow generated in the HRSG is expanded in the HP turbine and fed into the first combustor. The steam flow from both the combustors and the Rankine cycle are fully integrated. The steam that is generated in the combustors has to be removed from the cycle downstream of the condenser.

2.2.2 Graz cycle

The original Graz cycle is a CH_4 and oxygen fuelled cycle for CO_2 capture which has been developed at Graz University of Technology since 1995 [14]. This cycle is further developed to become the hydrogen and oxygen fuelled Graz cycle [7], to be used as a reference cycle in this thesis.

The Graz cycle can be seen as a modification to a standard CCGT cycle, working with hydrogen as a fuel and pure oxygen as the oxidant, leaving steam as the combustion product and working fluid in the Brayton part of the cycle. Similar to the Toshiba cycle, the high temperature steam from the combustor is expanded in a HTT and transfers heat to a Rankine cycle in the HRSG. The steam from the 'stack' of the HRSG is partly expanded in a condensing LP turbine and partly compressed to 41 bar to be used for cooling the combustor. A principle flow scheme of the cycle is shown in figure 9. The overall efficiency of the Graz cycle is 70.4% LHV.

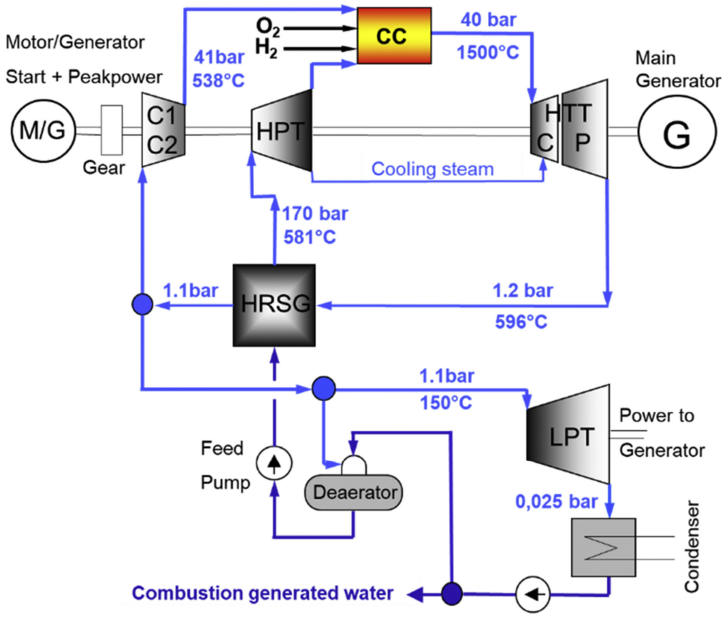

Figure 9: Principle flow scheme Graz cycle [7]

The direct compression of the steam downstream of the HRSG introduces an extra degree of freedom compared to the Toshiba cycle to secure the correct turbine inlet temperature of the HTT. This extra option enables a better energy balance over the HRSG and thereby a lower temperature difference in the heat transfer (from Brayton to Rankine part of the cycle) in the HRSG, this results in lower exergy losses. This can be visualized in figure 7 from section 2.1, the red area inbetween the two cycles is reduced.

2.3 The solid oxide fuel cell (SOFC)

The SOFC is a fuel cell (FC) with a solid oxide or ceramic electrolyte, the working principle of an SOFC is depicted in figure 10. The FC is an electrochemical cell that converts chemical energy directly into electricity and heat, whereas heat engines/cycles convert chemical energy into heat and then extract electricity from this heat. Therefore, the fuel cells efficiency is not limited to the Carnot efficiency, shown in equation 3, in section 2.1.

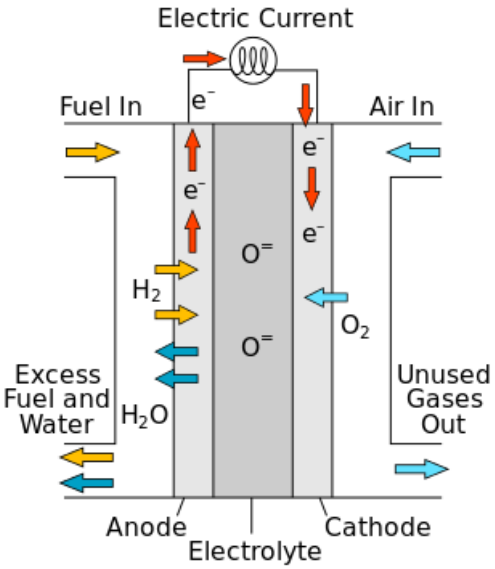

Figure 10: SOFC working principle [15]. The illustrated SOFC is operated with air as the oxidizer.

The efficiency is however limited by the available Gibbs free energy of formation.

$$\eta_{max} = \frac{\Delta G_{rxn}}{\Delta H_{rxn}} = \frac{\Delta H_{rxn} - T \cdot \Delta S_{rxn}}{\Delta H_{rxn}} \tag{4}$$

ΔH is the enthalpy of formation and ΔS is the entropy of formation. Contrary to heat engines the maximum obtainable electrical efficiency of electrochemical converters (fuel cells) decreases with an increasing temperature, as can be seen in equation 4. The efficiency curve of an ideal FC, operated at atmospheric pressure, is compared with a Carnot cycle at 90°C exhaust temperature in figure 11.

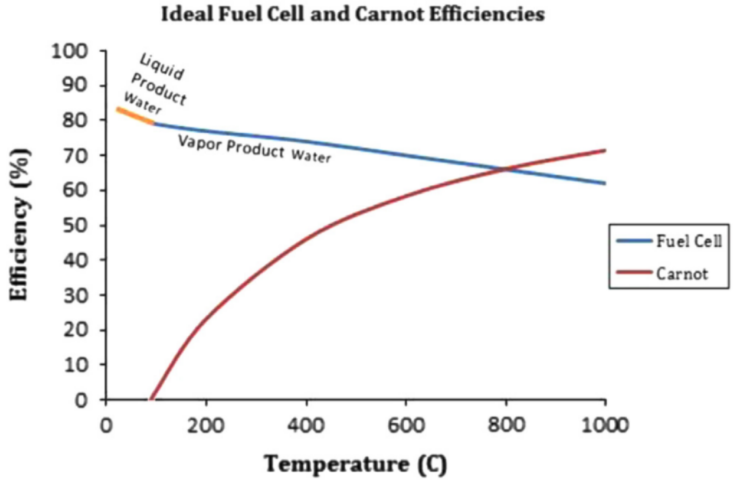

Figure 11: Ideal fuel cell operated at ambient pressure and Carnot efficiencies (using exhaust temperature of 90° C) as a function of temperature [16].

The reaction is driven by redox reactions as the reducer, the fuel hydrogen, flows through the anode. Oxygen, the oxygizer, flows through the cathode, ions (O^{2-}) are formed and conducted through the electrolyte into the anode where together with the H_2, water and electrons are formed. The cathode and anode half reactions are:

$$\frac{1}{2}O_2 + 2e- \longrightarrow O^{2-} \tag{5}$$

$$O^{2-} + H_2 \longrightarrow H_2O + 2e- \tag{6}$$

Resulting in the following reaction:

$$\frac{1}{2}O_2 + H_2 \longrightarrow H_2O \tag{7}$$

Thus for each mole of hydrogen 2 electrons are used. The stoichiometry is that for every mole of H_2 half a mole of O_2 is used. The lower the temperature the larger the theoretical maximum efficiency as equation 4 states. However, in practice the efficiencies of LT-SOFC's (low temperature solid oxide fuel cells) and HT-SOFC's (high temperature solid oxide fuel cells) do not differ significantly. Lower temperature fuel cells have higher resistances, as the resistivity of the materials used is inversely proportional with the temperature.

The latest spec high efficient SOFC's are planar SOFC's as these can reach higher power densities and efficiencies than their tubular counterparts [17]. The layout of both a tubular and planar FC is illustrated in figure 12. The electrons travel a longer path in the tubular counterpart, for that reason the resistance in tubular FC's is higher, resulting in a lower electrical efficiency. Generally, in planar SOFCs the electrolyte is made from yttria-stabilized zirconia (YSZ), a cathode made from lanthanum strontium manganite (LSM) and an anode consisting of nickel-YSZ (Ni-YSZ) [18].

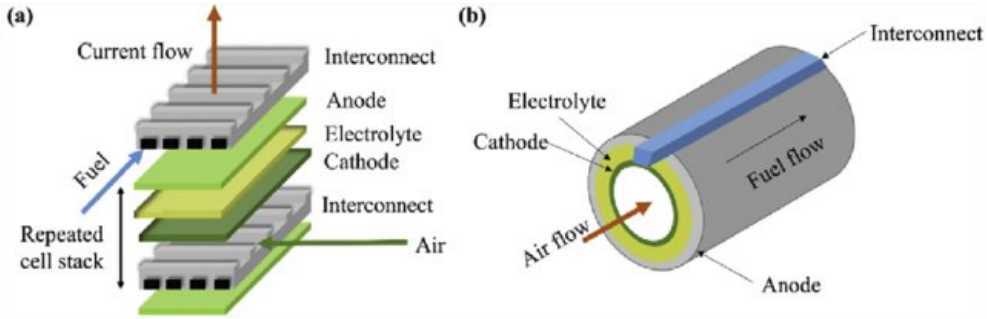

Figure 12: Planar and tubular SOFC [17]

Typically an SOFC is fuelled by gas using air as the oxidizer. The anode needs pure hydrogen for its half reaction. For this reason, the gas needs to be reformed. This can either be done in the FC or preliminary.

Today's operating SOFC's can have a working range from 550°C to 1000°C [17]. A state of the art SOFC transforms 65% of the converted fuel's energy into electricity [5]. In test conditions even 74% LHV is reached for the NELHI project [19]. The remaining energy is heat, which is absorbed by the gasses passing through the FC, and because of its high temperature, this released heat can easily be used in a bottoming cycle. An FC can be placed in front of the combustor, leading to an increased combustor inlet temperature and thus less exergy loss in the combustor.

2.3.1 Fuel cell-turbine cycle

Fuel cells (FC's) offer an interesting cycle improvement opportunity, to further reduce the exergy losses in the turbine cycle as the main exergy losses take place in the combustor. (Partial) replacement of the combustor by an FC can lead to a further reduction in exergy losses. The most promising FC for this application is the SOFC, having a high and broad operating temperature window. Turbine-SOFC cycles with air as a working fluid have been studied extensively and some units have been built, for example the Siemens-Westinghouse cycle [20]. This turbine cycle is coupled to a tubular SOFC, the cycle's priciple flow scheme is depicted in figure 13.

When an FC is directly fuelled with hydrogen and oxygen, no reforming of the fuels is required, which leads to better performance [18]. The efficiency, lifetime and power density are all higher without the reforming process [18]. Another compelling reason for combining the FC with a turbine cycle is that the driving force, the Nernst voltage, will increase with an increased pressure in the FC, as can be seen in equation 8 [18]. An increase in the Nernst voltage leads to a higher FC efficiency and a higher power density. Additionally, the use of pure hydrogen as fuel and pure oxygen as oxidizer increases the driving force of a fuel cell, as can be seen in equation 8.

$$E_{nernst} = E_0 + \frac{RT}{2F} ln\left(\frac{Pp_{H2}Pp_{O2}^{\frac{1}{2}}}{Pp_{H2O}}\right) \tag{8}$$

Pp indicates the partial pressure, while F indicates the Faraday constant, R indicates the gas constant and E_0 indicates the potential voltage.

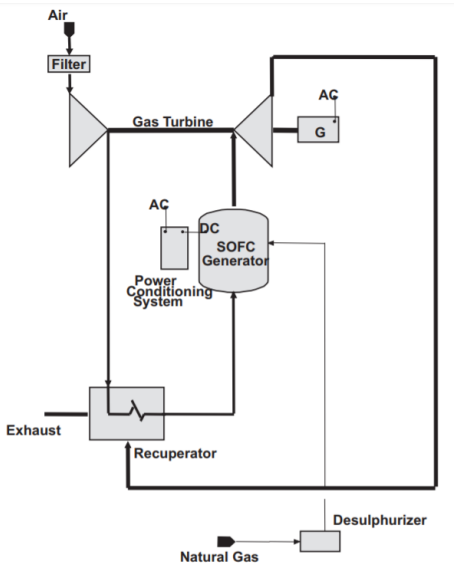

Figure 13: Principle flow scheme of the Siemens-Westinghouse cycle [20]. The cycle is fed with air and natural gas, for this reason the cycle needs a desulphurizer and the SOFC needs to reform the natural gas. The SOFC is placed in donwstream of the compressor and upstream of the turbine (in conventional cycles this is the place of the combustor).

2.3.2 Fuel cell physics model

The Gibbs free energy of formation (ΔG) indicates how favorable the chemical reaction is (if the reaction can take place spontaneously) [21]. The potential voltage is calculated as follows:

$$E_0 = \frac{\Delta G_{rxn}}{nF} \tag{9}$$

In which n equals the electrons released per mole of hydrogen which is 2 in our case.

$$\Delta G_{rxn,T} = \Delta H_{rxn,T} - T \cdot \Delta S_{rxn,T} \tag{10}$$

$\Delta G_{rxn,T}$ is lowered with an increasing temperature, for this reason the potential and Nernst voltage are lowered (see equation 9 and 8). Also, the FC efficiency decreases with an increasing temperature as can be seen in figure 11. The stoichiometry of the reaction needs to be taken into account.

$$\Delta H_{rxn,T} = \Delta H_{f,H_2O,T} - \Delta H_{f,H_2,T} - \frac{1}{2}\Delta H_{f,O_2,T} \tag{11}$$

$$\Delta S_{rxn,T} = \Delta S_{f,H_2O,T} - \Delta S_{f,H_2,T} - \frac{1}{2}\Delta S_{f,O_2,T} \tag{12}$$

In high temperature FC's the activation overpotential can be neglected as it is really small. Furthermore the concentration overpotential only becomes significant when the limiting current density is approached [18]. In this study efficiency is key and the high temperature SOFC is operated far away from

the limiting current density. Therefore, the ohmic resistance is the only significant resistance we are dealing with. For the planar (this study) case the resistance of the anode (component 1, c=1), electrolyte (c=2), cathode (c=3) and interconnect (c=4) are in series and the sum of these resistances is the total resistance.

$$R = \sum_{c=1}^{4} \frac{\rho_c t_c}{A_{crosssection}} \tag{13}$$

$$I_{cell} = \frac{E_{nernst} - E_0}{R} \tag{14}$$

$$C_{H2} = -\frac{I_{cell}}{2F} \tag{15}$$

C_{H2} is the consumption rate of H_2 in mole per second.

$$POW_{cell} = E_{cell} \cdot I_{cell} \tag{16}$$

$$\eta = \frac{POW_{cell}}{\Delta H_{rxn,T}} \tag{17}$$

The FC operates at unique operating conditions (high pressure $\sim$40 MPa, with hydrogen and oxygen as fuel). A conventional FC layout [22] is used. The design of an FC layout, tuned to these unique operating conditions, is not in the scope of this thesis. In table 1, the resistivity equations (from [23]) of the individual components of the FC stack are depicted.

Table 1: Geometry and resistances for the SOFC used in this thesis

Components	thickness t	Resistivity equations
Cathode (LSM-YSZ)	0.2 cm	$8.114 * 10^{-3} e^{\frac{600}{T}} \Omega cm$
Electrolyte (YSZ)	0.004 cm	$2.94 * 10^{-3} e^{\frac{10350}{T}} \Omega cm$
Anode (Ni-YSZ)	0.015 cm	$2.98 * 10^{-3} e^{\frac{-1392}{T}} \Omega cm$
Interconnect (metal)	0.01 cm	$100/(\frac{9.3*10^5}{T} \cdot e^{\frac{-1100}{T}}) \Omega cm$

3 Cooling of the high temperature turbine blades

In this chapter, in section 3.1 the physics behind closed loop cooling of the high temperature turbine blades is covered. Subsequently, in section 3.2 the physics behind open loop cooling of the high temperature turbine blades is discussed. In subsection 3.2.1 the result of the open loop cooling is validated with the build in Thermoflex open loop cooling method. In section 3.3 the implementation of open loop cooling into the open loop cooled models of this study is treated. Finally, in section 3.4 the implementation of hybrid cooling into the hybrid cooled models of this study is discussed. The different cooling methods are depicted in figure 14.

The different turbine cycle configurations, covered in this study, have different cooling needs, which is discussed in chapter 5. Additional cooling leads to more exergy losses in the cooled turbines. The two cooling methods discussed in this study are very different, especially in the cooling losses induced. No new blades are designed in this study, based on existing designs and the parameters associated with this, the required cooling mass flows are calculated. For this reason, a good cooling model is essential for a good performance/exergy analyses of the cycles.

Open loop cooling is the conventional method to cool down HTT blades in gas turbines [24]. Open loop cooling means a liquid is delivered to the blade and passes through (convecting heat away from the blade in the process) and then quenches into the main stream of the cycle. Both air and steam can be used to go through the blade. The open loop cooling method used in this thesis combines internal convection with film cooling. Internal convection cooling means the coolant convects the heat away via internal channels in the blade, going past cooling fins and impingements inside the blade. Subsequently, the coolant reaches the surface of the blade and reaches the film cooling holes. The fluid exits the blade through film cooling holes to form an active fluid film layer, that acts as an active thermal barrier. An open loop cooled blade is illustrated in figure 14a.

Closed loop steam cooling (CLSC) is a cooling method in which steam passes through the blade and is retrieved (it does not quench into the main stream of the cycle). The heat is convected away through fins and impingements inside the blade. The retrieved coolant can be used somewhere else in the cycle. The exergy losses are reduced because no steam is quenched into the main stream, however CLSC will lead to local high metal temperatures. For this reason, CLSC is not used in HTT's. A CLSC blade is shown in figure 14b.

Hybrid cooling is a combination of both CLSC and open loop cooling. This solution combines the exergetic advantage of CLSC (less quenching of steam into the main flow), with a flat metal temperature throughout the blade, made possible by the film cooling holes. In this cooling method part of the coolant is quenched via film cooling holes into the stream, however a fraction of the coolant is not quenched and retrieved. The Original Toshiba cycle [8] uses this cooling method. A hybrid cooled blade is depicted in figure 14c.

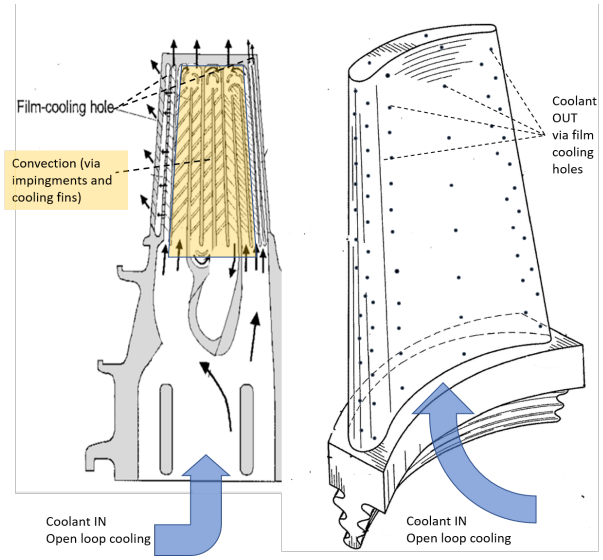

(a) Open loop cooling as used in the Original Graz cycle [7]. State of the art fossil fuelled CCGT cycles make use of this technology, making use of air as the coolant [24].

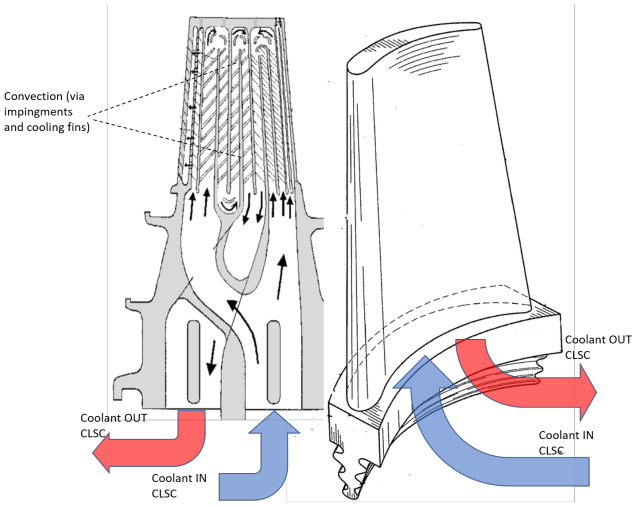

(b) CLSC (not used as a cooling solution in this thesis)

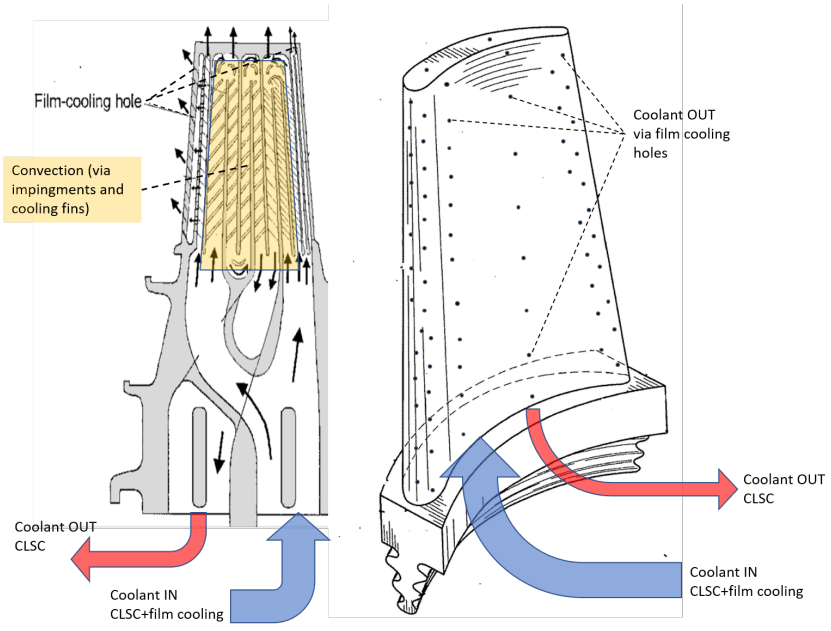

(c) Hybrid cooling as used in the Original Toshiba cycle [8]. The hybrid cooled blade differs from the conventional open loop cooled blade, as part of the coolant is retrieved.

Figure 14: Different cooling methods

The heat coefficients depend on the internal blade geometries (which are unknown). The amount of film cooling holes and impingements inside the blade are unknown. The temperatures T_{aw},T_w, T_{be} and T_{bi} are unknown, only T_g and T_b are known. Thus, a detailed cooling mass calculation, based on geometry data, will not be possible. For that reason, empirical relations are used to calculate the amount of coolant mass needed. The amount of stages per turbine are known. Therefore, an estimation of the amount of cooling must be based on the thermodynamic layout (the mass streams, their respective enthalpies, temperatures and pressures). For that reason, the cooling mass streams and the main gas streams are the given parameters.

The Original Toshiba cycle is a hybrid cooled cycle. Cycles designed in this thesis, that include hybrid cooling, are modeled to have the same cooling performance as the Original Toshiba cycle. The cooling performance parameters (tuning parameters, C_1 and C_2) together with the operating conditions dictate the amount of coolant necessary to keep the turbine blades from overheating. For this reason, (tuning parameters, C_1 and C_2) from the Original Toshiba cycle will be clarified and retrieved in section 3.4.

The Original Graz cycle is a open loop cooled cycle. Cycles designed in this thesis, that include open loop cooling, are modeled to have the same cooling performance as the Original Graz cycle. The cooling performance parameters (tuning parameter, C_{tune}) together with the operating conditions dictate the amount of coolant necessary to keep the turbine blades from overheating. For this reason, (tuning parameter, C_{tune}) from the Original Graz cycle will be clarified and retrieved in section3.3. The parameters used to tune the cooling methods and their resulting tuning parameters are depicted in table 2.

Table 2: Cooling parameters used for modeling hybrid and open loop cooled high temperature turbine blades

	hybrid cooling	open loop cooling
Reference cycle for obtaining tuning parameter	Replicated Graz cycle values	Replicated Toshiba cycle values
Physics used	a combination of CLSC and open loop cooling	open loop cooling
Bulk blade temperature	787.85 °C from figure 13 [8]	750°C from table 1 [7]
Enthalpy increase coolant CLSC **	342 KJ/Kg	there is no CLSC (part) used
Number of blade rows in HTT-1	5	2
Number of blade rows in HTT-2	4	4
Number of blade rows in HTT-3	non existent	2
Calculated tuning parameter(s) (Cooling performance parameters)	C_1=0.0021, C_2=0.0026	C_{tune}=0.0183
Cycles modeled with this method and the corresponding tuning parameter(s)	Toshiba-EQ, Graz-HC, U-Graz, U-Graz-1500°C, U-Graz-3FC-OX	Graz-EQ, Graz-1700°C, Graz-HEX, Graz-2CC, Graz-1FC-OX, Graz-3FC-OX, Graz-1FC-Steam, Graz-1FC-Steam

* Temperatures, mass flows and specific heats of the coolant individual streams can be retrieved from the principle flow schemes [7] and [8].

** The enthalpy rise equals the enthalpy of the CLSC coolant going out of the turbine blades minus the enthalpy of the CLSC coolant going into the blades.

3.1 Closed loop steam cooling (CLSC) physics

In this section the physics behind closed loop steam cooling is derived. CLSC is implemented as part of the hybrid cooling method used in this thesis. The heat resistance scheme through the CLSC and TBC coated blade is depicted in figure 15.

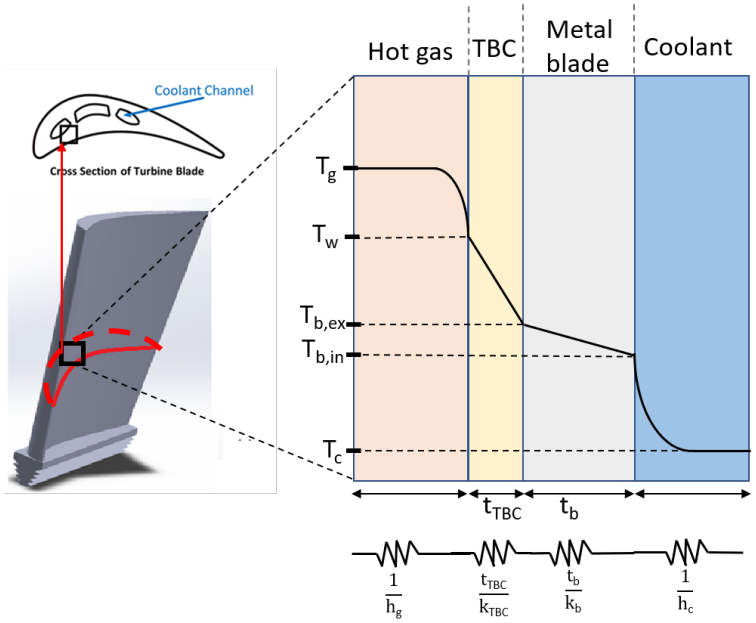

Figure 15: Temperature profile across a CLSC high temperature turbine blade with a TBC

CLSC is a closed cycle, thus the cooling steam will not enter the main flow contrary to open loop cooling. This is beneficial from an exergetic point of view, as the steam is not quenched into the cycle thus less losses occur. However, closed loop cooling will lead to certain hot points in the system, where film cooling can lead to a flat metal temperature profile throughout the blade. Moreover, film cooling is more effective (in bringing the turbine blade temperature down) per kg of coolant used.

$$R_{total} = \frac{1}{h_g} + \frac{L_{TBC}}{k_{TBC}} + \frac{L_b}{k_b} + \frac{1}{h_c} \tag{18}$$

The heat resistance scheme is solved in the next section, the following equation is the result:

$$\dot{m}_c = \frac{1}{Bi_{TBC}+1}\dot{m}_g \frac{Cp_g}{Cp_c} \cdot St \cdot \frac{A_g}{A_w} \cdot \frac{T_g - T_b}{T_{ce} - T_{ci}} \tag{19}$$

In which $\dot{m}_c$ equals the coolant going through one turbine stage, $\dot{m}_g$ equals the main gas mass flow going through the turbine stage. A turbine stage consist of one rotor row and one stator row. A_w is the area available for the main gas to flow through the blade wall. A_g is the surface area of the hot gas side on the blade.

3.1.1 Mathematical derivation closed loop steam cooling

The heat transfer is in steady state. Therefore, the heat flux is constant across the thickness of the blade. The heat flux through all parts of the blade is given in equation 20 and 21.

$$\dot{q} = h_g(T_g - T_w) = \frac{T_w - T_{b,ex}}{\frac{t_{TBC}}{k_{TBC}A_g}} = \frac{T_{b,ex} - T_{b,in}}{\frac{t_b}{k_b A_g}} = \dot{m}_c(h_{ci} - h_{ce}) \tag{20}$$

$$\frac{\dot{Q}}{A_g} = \dot{q} = \frac{T_g - T_c}{R_{total}} \tag{21}$$

The heat convected from the hot gas to the blade outer wall equals the heat conducted through the TBC coating. This heat equals the heat conducted through the metal blade, which in turn equals the heat that is removed by the coolant.

An approximation is made in equation 23 as $T_{b,ex} \approx T_{b,in}$. The metal blade conducts heat very well, for this reason there is very little temperature variation through the blade. The bulk temperature (T_b) will be very close to both the external blade and internal blade temperature, thus the following is assumed $T_{b,ex} \approx T_b$.

$$\dot{Q} = h_g A_g(T_g - T_w) \tag{22}$$

$$\dot{Q} = \frac{k_{TBC}}{t_{TBC}} A_g(T_w - T_{b,ex}) \approx \frac{k_{TBC}}{t_{TBC}} A_g(T_w - T_b) \tag{23}$$

$$\dot{Q} = \frac{k_b}{t_b} A_g(T_{b,ex} - T_{b,in}) \tag{24}$$

$$\dot{Q} = \dot{m}_c(h_{ci} - h_{ce}) \approx \dot{m}_c Cp_c(T_{ci} - T_{ce}) \tag{25}$$

The standard approach to calculate the cooling needs from these governing equations is from [25]. This approach does not contain a TBC coating. Therefore, the approach is adjusted later on in this study, to fit a turbine with TBC coating. The heat resistance scheme of a CLSC blade without a TBC is depicted in figure 16. The external metal blade is now in contact with the hot gas, thus the external metal blade is the wall. Therefore, T_w is used for this approach. Equation 22, 24 and 25 still hold for the uncoated blade.

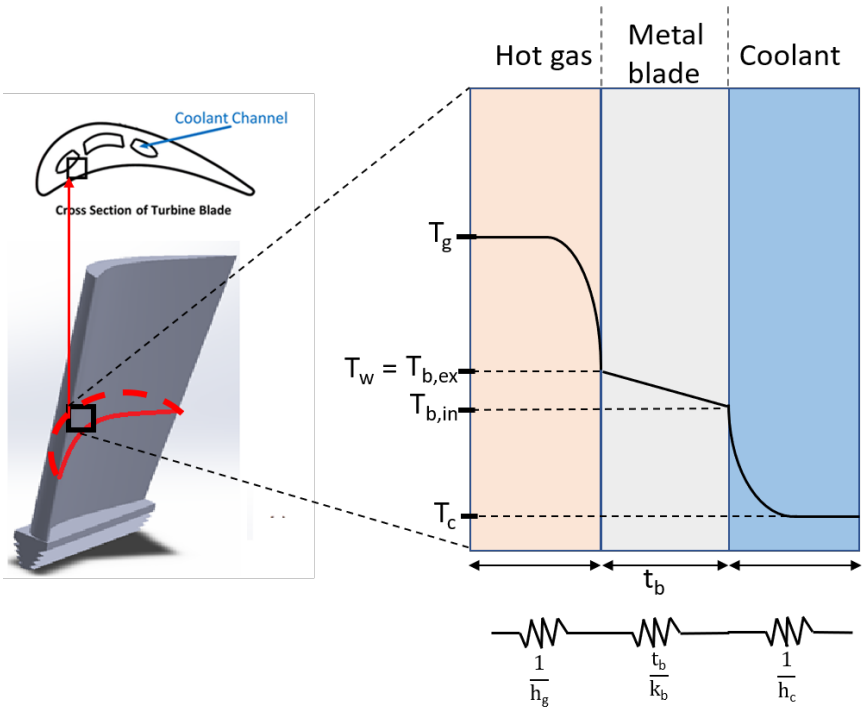

Figure 16: Temperature profile across CLSC turbine blade(without TBC coating)

$$St_g = \frac{h_g}{\rho_g \cdot v_g \cdot Cp_g} \tag{26}$$

The Stanton number (St) is a dimensionless number that measures the ratio of heat transferred into a fluid to the thermal capacity of the fluid, where v_g is the main gas velocity.

The total heat flow ($\dot{Q}$) equation 27 can be found by combining equation 26 and 22:

$$\dot{Q} = St_g \cdot \rho_g \cdot v_g \cdot Cp_g \cdot A_g(T_g - T_w) \tag{27}$$

$$\dot{m_g} = \rho_g \cdot v_g \cdot A_w \tag{28}$$

$$\dot{Q} = St_g \cdot \dot{m_g} \frac{A_g}{A_w} \cdot Cp_g \cdot A_g(T_g - T_w) \tag{29}$$

Combining equation 29 with equation 25 gives:

$$\frac{\dot{m_c}}{\dot{m_g}} = \frac{Cp_g}{Cp_c} \cdot St_g \cdot \frac{A_g}{A_w} \cdot \frac{T_g - T_w}{T_{ce} - T_{ci}} \tag{30}$$

This is the final result in the Masi [25] approach. This equation is the basic CLSC function in Thermoflex [26]. However, for our case, which includes a TBC coating, the wall temperature is not equal to the metal

blade temperature, as one can see in figure 15. The metal blade temperature T_b is known and the TBC outside temperature T_w is not. Therefore, one prefers a solution where T_b is a variable.
To achieve this, equation 22 and 23 are combined to:

$$Bi_{TBC} = \frac{h_g t_{TBC}}{k_{TBC}} \approx \frac{T_w - T_b}{T_g - T_w} \tag{31}$$

The Biot number of the TBC coating (Bi_{TBC}) displays the ratio between the transport by flow (convection) outside the TBC coating and the conduction of heat within the TBC coating.

The wall temperature (T_w) is eliminated out of the governing equation using the following algebraic trick:

$$\frac{T_g - T_w}{T_{ce} - T_{ci}} \cdot \left(\frac{T_w - T_b}{T_g - T_w} + 1 \right) = \frac{T_g - T_w}{T_{ce} - T_{ci}} \cdot \left(\frac{T_w - T_b}{T_g - T_w} + \frac{T_g - T_w}{T_g - T_w} \right) = \frac{T_g - T_b}{T_{ce} - T_{ci}} \tag{32}$$

$$\frac{T_g - T_w}{T_{ce} - T_{ci}} \cdot (Bi_{TBC} + 1) = \frac{T_g - T_b}{T_{ce} - T_{ci}} \tag{33}$$

$$\frac{T_g - T_w}{T_{ce} - T_{ci}} = \frac{1}{Bi_{TBC} + 1} \frac{T_g - T_b}{T_{ce} - T_{ci}} \tag{34}$$

Therefore, equation 30, for a CLSC blade with a TBC coating included, can be written as:

$$\dot{m}_c = \frac{1}{Bi_{TBC} + 1} \dot{m}_g \frac{Cp_g}{Cp_c} \cdot St \cdot \frac{A_g}{A_w} \cdot \frac{T_g - T_b}{T_{ce} - T_{ci}} \tag{35}$$

3.2 Open loop cooling physics

In this section the physics behind open loop cooling is derived. Open loop cooling is implemented as part of the hybrid cooling method and as a standalone open loop cooling solution. Open loop cooling is a combination of film, impingement and convection cooling. For the open loop case the heat network depicted in figure 17 is used. Equation 36 and 37 govern the heat network.

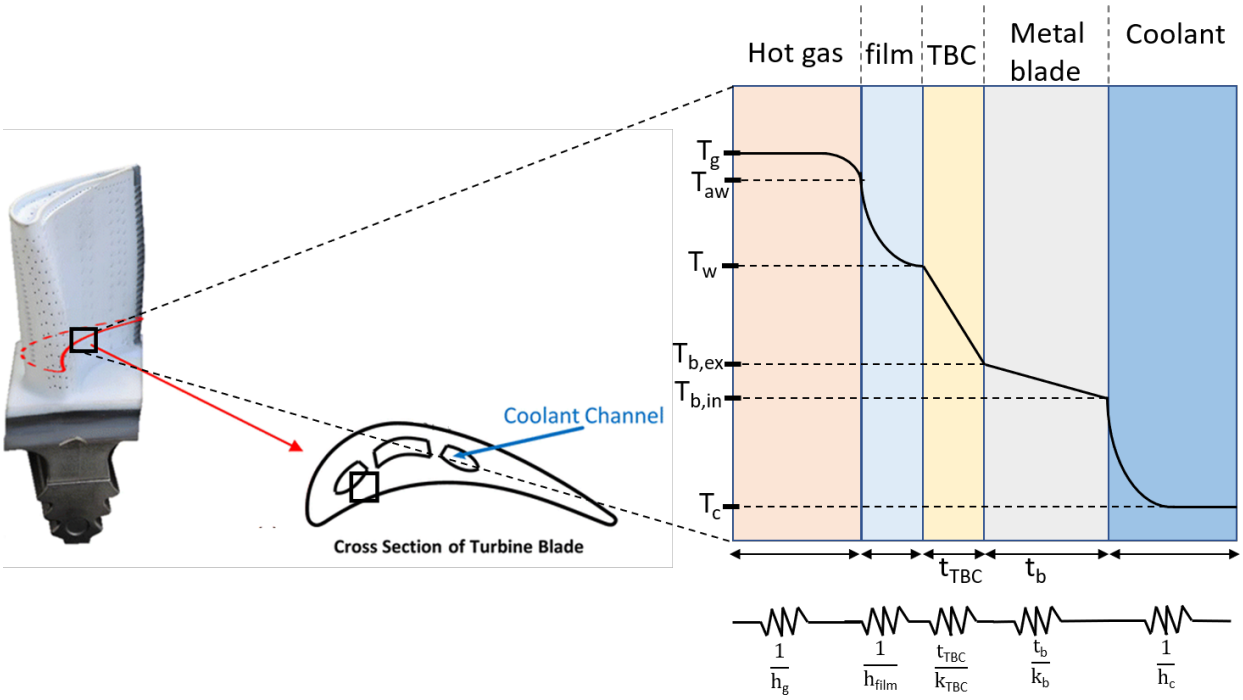

Figure 17: Temperature profile across open loop cooled and TBC coated turbine blade

The resistance scheme is:

$$R_{total} = \frac{1}{h_g} + \frac{1}{h_{film}} + \frac{L_{TBC}}{k_{TBC}} + \frac{L_b}{k_b} + \frac{1}{h_c} \tag{36}$$

$$Q = \frac{T_g - T_c}{R_{total}} = h_g(T_g - T_{aw}) = h_{film}(T_{aw} - T_w) = \frac{T_w - T_{b,ex}}{\frac{L_{TBC}}{k_{TBC}A}} = \frac{T_{b,ex} - T_{b,in}}{\frac{L_b}{k_b A}} = h_c(T_{b,in} - T_c) \tag{37}$$

The derivation done by [27] and better explained in [24] is done for a blade without a TBC coating. For that reason, the mathematical derivation of the system is done as if there is no TBC coating at first.

For the open loop case without TBC coating, the heat network depicted in figure 18 is used where equation 38 and 39 govern the heat network. Leading to the following resistance scheme and heat network:

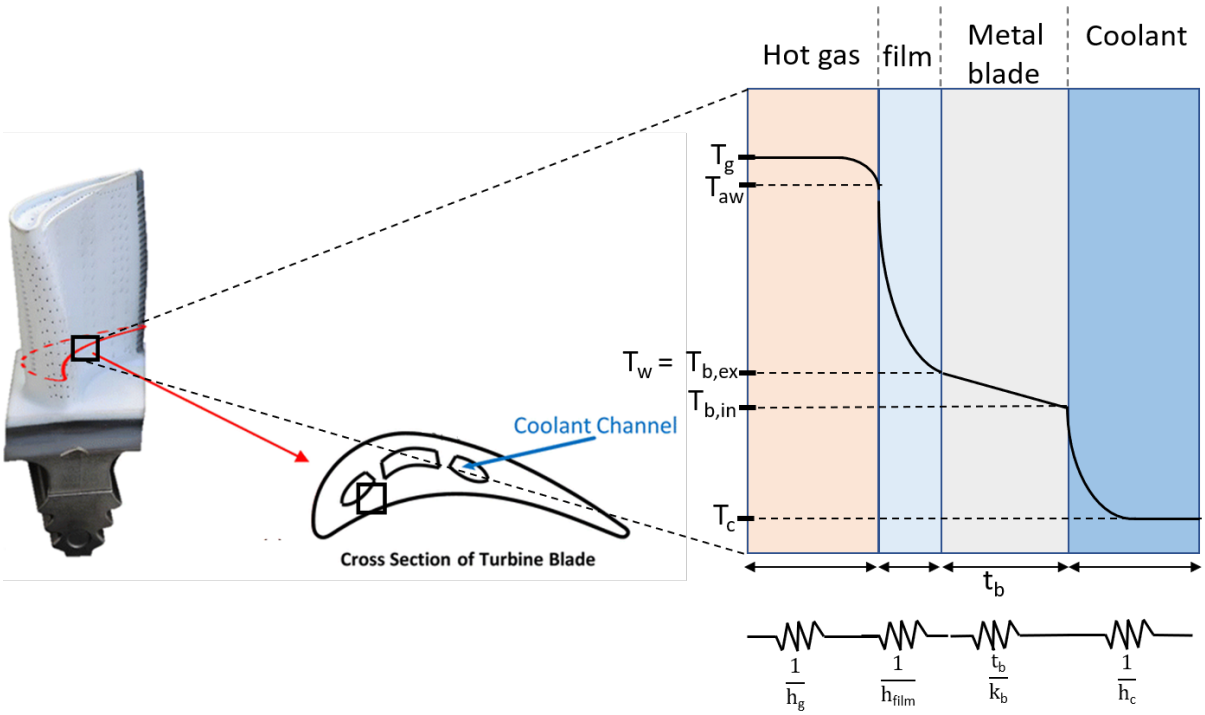

Figure 18: Temperature profile across film cooled and TBC coated turbine blade

$$R_{total} = \frac{1}{h_g} + \frac{1}{h_{film}} + \frac{L_b}{k_b} + \frac{1}{h_c} \tag{38}$$

$$Q = \frac{T_g - T_c}{R_{total}} = h_g(T_g - T_{aw}) = h_{film}(T_{aw} - T_{b,ex}) = \frac{T_{b,ex} - T_{b,in}}{\frac{L_b}{k_b A}} = h_c(T_{b,in} - T_c) \tag{39}$$

The heat resistance scheme of the open loop cooled blade without TBC is solved in appendix subsection A (Derivation open loop cooling), equation 40 is the result.

$$\dot{m}_c = \dot{m}_g St_g \frac{Cp_g}{Cp_c} \frac{A_g}{A_w} \frac{\epsilon}{1-\epsilon} \tag{40}$$

$$\epsilon = \frac{T_g - T_b}{T_g - T_{ci}} \tag{41}$$

For an open loop cooled turbine blade with TBC coating the result is:

$$\dot{m}_c = \dot{m}_g \frac{1}{1 + Bi_{TBC}} St_g \frac{Cp_g}{Cp_c} \frac{A_g}{A_w} \frac{\epsilon}{1-\epsilon} \tag{42}$$

This equation will be used for calculating the coolant flow in the open loop cooled cycles. The parameters are tuned to correspond to cooling solution used in the original Graz cycle. The tuning is done in subsection 3.3.

3.2.1 Validation of open loop cooling method, with Thermoflex method

In this section the open loop cooling physics result is compared to the Masi [25] approach (the method used in the Thermoflex program [26]). The calculated result is very similar to an empirically found equation by Masi [25]. In his study, Masi researched the significance of all the influencing parameters and came to the following equation:

$$\dot{m}_c = \dot{m}_g \frac{Cp_g}{Cp_c} ARC \cdot CF \left(\frac{\epsilon}{1-\epsilon} \right)^n \tag{43}$$

For pure film cooling n=0.9, for pure convection cooling n=1.25. Pure film cooling is not achievable and there will always be a fraction of convection. Therefore, n is often assumed to be 1 for film cooled blades [24]. CF is the cooling correction factor and equals $\frac{1}{1+Bi_{TBC}}$. ARC is the tuning parameter (area ratio coefficient), this parameter can be tuned to fit the cooling performance. When this equation is compared to equation 42, using n=1, it is exactly the same with:

$$ARC = St_g \frac{A_g}{A_w} \tag{44}$$

3.3 Open loop cooling implementation into the models of this thesis

Open loop cooling is used in a number of cycles modeled in the subsequent chapters. In this section, the tuning process is covered as the open loop cooling method is tuned to the open loop cooling used in the original Graz cycle [7]. Furthermore, the interaction between the stage by stage cooling model (Thermoflex) and the cooling script (MATLAB) is covered.

The blade temperature that the Graz cycle's cooling method can withstand is 750°C. The temperature of the coolant, the main gas stream mass and the specific heat of the streams are known per cycle, leaving the Biot number and Stanton number as unknowns. The Biot and Stanton number can be assumed constant throughout (all stages of) the turbine [24]. In this study, the same cooling performance for every turbine is assumed. Therefore, the Biot and Stanton number, are assumed constant through all turbine stages also in between the different turbines.

$$C_{tune} = \frac{1}{1+Bi_{TBC}} St_g \cdot \frac{A_g}{A_w} \tag{45}$$

The total coolant mass flow $\dot{M}_c$ for the original Graz cycle is given. $\dot{M}_c$ is the summation of all the blade rows (of all turbines) their $\dot{m}_c$, as depicted in figure 19. Therefore, C_{tune} (the cooling performance parameter) can be retrieved in an iterative manner, as the Biot number, Stanton number and the $\frac{A_g}{A_w}$ are assumed constant through all blade rows of all cycles using this cooling method.

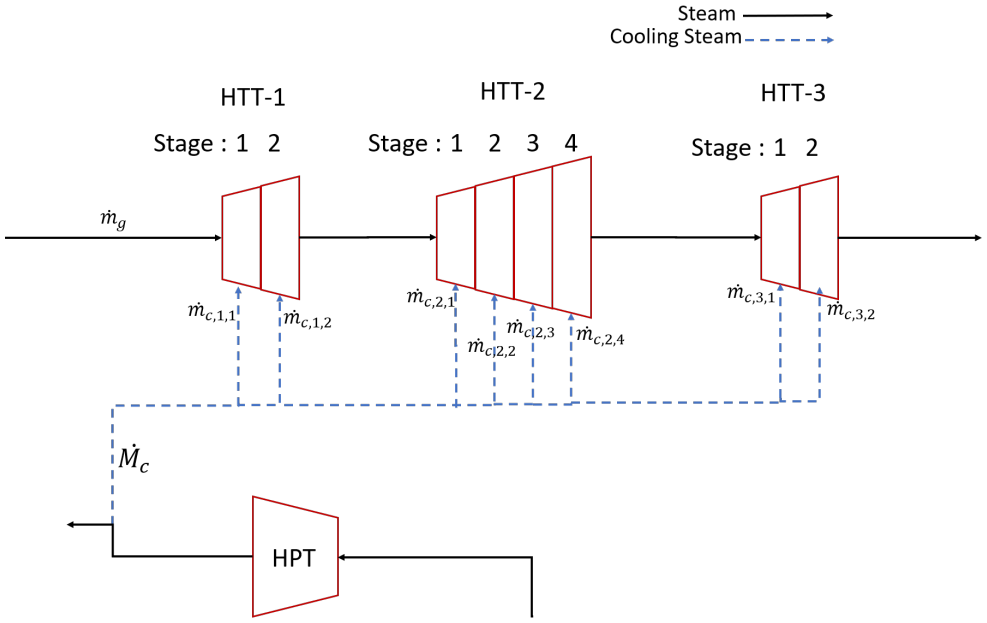

Figure 19: Simplified general open loop cooling, stage by stage cooling scheme. A detailed Thermoflex stage by stage cooling scheme is plotted in appendix B.3.1. $\dot{M}_c$ is the summation of all the blade rows (of all turbines) their $\dot{m}_c$. The individual stages have different temperatures and pressures leading to different individual cooling needs of $\dot{m}_c$ per stage, the needs are calculated in a MATLAB script using the tuned open loop cooling parameter.

An estimation of the coolant going into every blade row is made. The corresponding temperatures, specific heats and main gas flows can then be retrieved from the Thermoflex stage by stage cooling model. C_{tune} is tuned until its calculated $\dot{M}_c$ matches the $\dot{M}_c$ from the original cycle. The individual blade rows calculated $\dot{m}_c$ will be different from the initial estimation of $\dot{m}_c$ through every blade row. Therefore, the newly calculated $\dot{m}_c$ will act as the begin value of the new loop. These values are looped until $\dot{m}_c$ is within 0.5% of the previous iterations $\dot{m}_c$. The corresponding C_{tune} is used in all other cycles to calculate their coolant needs. In a nutshell, the tuning parameter is calculated as illustrated in figure 20.

This tuning parameter (combined Biot and Stanton number for film cooling) can be used to calculate the cooling needs of all designed open loop cooled cycles, using equation 46.

$$\dot{m}_c = \dot{m}_g C_{tune} \frac{Cp_g}{Cp_c} \frac{\epsilon}{1-\epsilon} \tag{46}$$

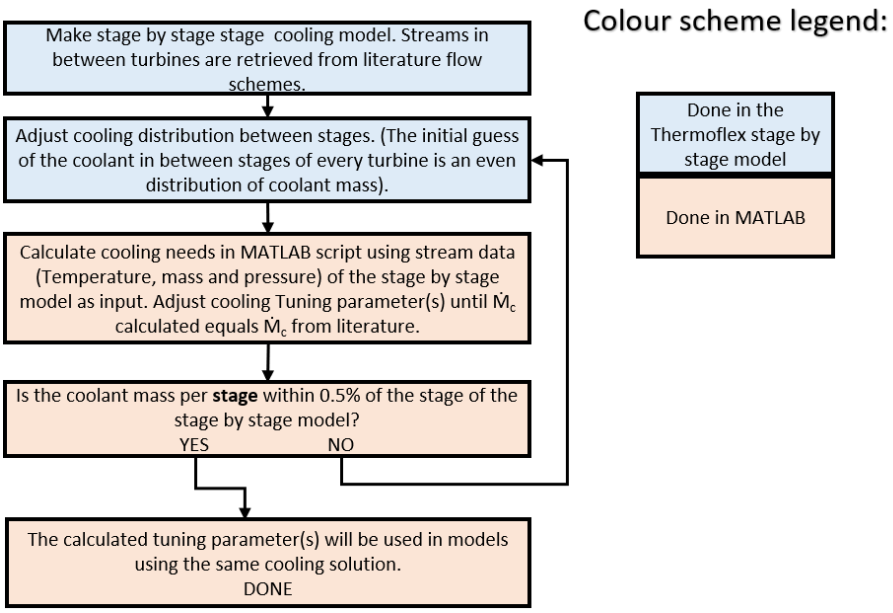

Figure 20: Retrieving the cooling Tuning parameter

3.4 Hybrid cooling implementation into the models of this thesis

Hybrid cooling is used in a number of cycles that are modeled in the subsequent chapters. In this section, the tuning process is covered as the hybrid cooling method is tuned to the hybrid cooling solution used in the original Toshiba cycle [8]. Furthermore, the results from the physical derivation of open loop cooled blade and the physical derivation of CLSC blade are assimilated into an approach to model a hybrid cooled blade (a partially CLSC and open loop cooled blade).

In the Toshiba cycle a combination of open loop and closed loop cooling is used. Closed loop cooling is beneficial as the steam is not quenched into the cycle and the film cooling (an open loop cooling method) will make sure a flat temperature profile is reached throughout the blade. For this reason, a combination of both is used where a fraction x (in the Original Toshiba cycle this part is $\frac{2}{3}$) of the cooling steam used is recovered (CLSC). The remaining 1-x part (in the original Toshiba cycle this fraction is $\frac{1}{3}$) of the used cooling steam used is discharged to the main stream through film cooling holes, so this part is open loop cooled.

As there are no equations for the combination of cooling, a combination of both equations is used. So the cooling needs for a hybrid cooled stage are calculated as if a part of the blade is solely film cooled and the rest is solely CLSC. In real life the full hybrid cooled blade is both CLSC and open loop cooled and there is interaction between the CLSC and open loop cooling. In real life a hybrid blade will have a thinner active film layer then a purely film cooled blade. A hybrid cooled blade is depicted in figure 14c.

To be able to model a hybrid cooled blade the CLSC part and open loop cooled part are separated. It is assumed and modeled as if part of the blade is solely CLSC and the other part is solely open loop cooled. The parts of the blade do not influence each other. This assumption can be visualized in figure 21. The open loop cooled part has all the film cooling holes and will have an active film layer, while the CLSC part will not have a film layer.

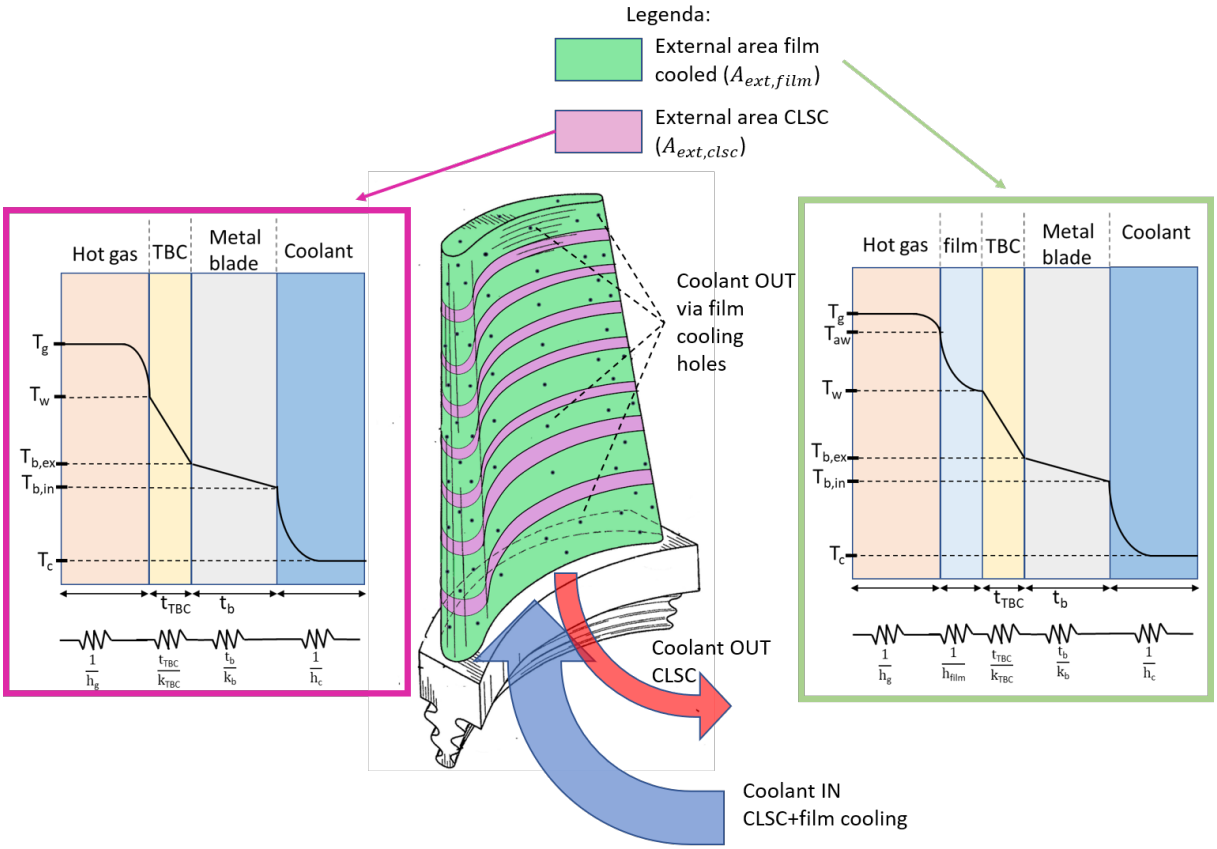

Figure 21: Modeling assumption visualized for hybrid cooling. The separation of the CLSC and open loop cooling part is a simplification, to be able to model the closed loop coolant mass flow and film cooled mass flow, going through, separately. In real life the blade will be CLSC and open loop cooled throughout the whole blade.

$$A_{ext,blade} = A_{ext,film} + A_{ext,clsc} \tag{47}$$

The fraction of the blade that is CLSC is called FOB_{clsc}.

$$FOB_{clsc} = \frac{A_{ext,clsc}}{A_{ext,blade}} \tag{48}$$

$$FOB_{film} = \frac{A_{ext,film}}{A_{ext,blade}} \tag{49}$$

Equation 19 still holds for a fully CLSC blade, however for a partially CLSC blade the introduced parameter FOB_{clsc} is added to the equation:

$$\dot{m}_{c,clsc} = \frac{1}{Bi_{TBC}+1}\dot{m}_g \frac{Cp_g}{Cp_c} \cdot St_{clsc} \cdot \frac{A_g}{A_w} \cdot \frac{T_g - T_b}{T_{ce} - T_{ci}} \cdot FOB_{clsc} \tag{50}$$

The tuning parameter to calculate the cooling needs of the CLSC part of the blade becomes:

$$C_1 = St_{clsc} \cdot \frac{A_g}{A_w} \cdot FOB_{clsc} \cdot \frac{1}{Bi_{TBC}+1} = \frac{\dot{m}_{c,clsc}}{\dot{m}_g} \frac{Cp_c}{Cp_g} \frac{T_{ce} - T_{ci}}{T_g - T_b} \tag{51}$$

The open loop cooled part of the blade is done in the same manner.

$$\dot{m}_{c,film} = FOB_{film} \cdot \dot{m}_g \frac{1}{1 + Bi_{TBC}} St_{film} \frac{Cp_g}{Cp_c} \frac{A_g}{A_w} \frac{\epsilon}{1-\epsilon} \tag{52}$$

$$C_2 = FOB_{film} \cdot St_{film} \cdot \frac{A_g}{A_w} \frac{1}{Bi_{TBC}+1} = \frac{\dot{m}_{c,film}}{\dot{m}_g} \frac{Cp_c}{Cp_g} \frac{1-\epsilon}{\epsilon} \tag{53}$$

Using the Toshiba cycles parameter with a blade temperature of 787.85 °C [8] (figure 13 in the article). The tuning parameters C_1 and C_2 can be retrieved using equation 51 and 53, making use of the temperatures, mass flows and specific heats of the Original Toshiba cycle. This is done in the same iterative manner as the open loop only cooling tuning parameter (C_{tune}) is retrieved. For hybrid cooling this is solved simultaneously for both tuning parameters, as both $\dot{M}_{c,clsc}$ and $\dot{M}_{c,film}$ are given for the Original Toshiba cycle. The cooling parameters (C_1 and C_2) are retrieved as illustrated in figure 20 from section 3.3.

With the obtained hybrid cooling tuning parameters, the coolant going into one hybrid cooled HTT stage can be retrieved using equation 54.

$$\frac{\dot{m}_c}{\dot{m}_g} = \frac{\dot{m}_{c,clsc}}{\dot{m}_g} + \frac{\dot{m}_{c,film}}{\dot{m}_g} = \frac{Cp_g}{Cp_c} \cdot C_1 \cdot \frac{T_g - T_w}{T_{ce} - T_{ci}} + \frac{Cp_g}{Cp_c} \cdot C_2 \cdot \frac{Cp_g}{Cp_c} \frac{\epsilon}{1-\epsilon} \tag{54}$$

The temperature/enthalpy increase of the steam in the closed loop cooling is limited by the thermal stresses. Therefore, the 342 kJ/kg enthalpy increase is used for all closed loop cooling cases (the coolant enthalpy retrieved is 342 kJ/kg higher than the enthalpy of the coolant going in). A simplified general hybrid cooling, stage by stage cooling scheme is depicted in figure 22.

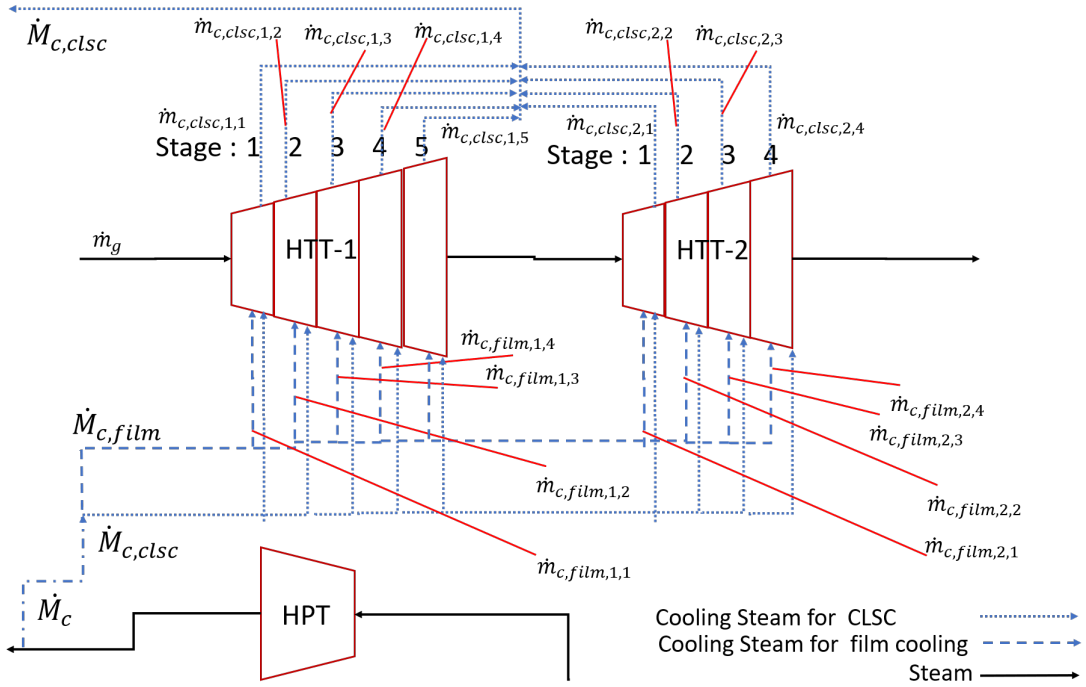

Figure 22: Simplified general hybrid cooling, stage by stage cooling scheme. A detailed Thermoflex stage by stage cooling scheme is plotted in appendix C.5.1. $\dot{M}_{c,clsc}$ is the summation of all the blade rows (of all turbines) their $\dot{m}_{c,clsc}$. The total film coolant mass $\dot{M}_{c,film}$ is the summation of all the blade rows (of all turbines) their $\dot{m}_{c,film}$. The individual stages have different temperatures and pressures leading to different individual cooling needs of $\dot{m}_c$ per stage, the needs are calculated in a MATLAB script using the tuned open loop cooling parameter, a script using hybrid cooling is depicted in appendix D.1.

4 Analysis of the Toshiba-Reheat-Rankine cycle and the Graz cycle

In order to find the optimal hydrogen-oxygen cycle, the Graz and Toshiba cycles are reproduced (with Thermoflex modelling software [26]) and validated to their original counterparts. The way the cooling model is integrated into the main model is described. Furthermore, the way the exergy analysis is made is covered. After the exergy analysis is explained, the main performance parameters of the Graz and Toshiba cycle are set to identical values and an exergy analysis is performed between the two cycles, resulting in the Graz-EQ and Toshiba-EQ cycle.

4.1 Comparison of the Graz and Toshiba cycles

To exactly rebuild the same cycle, all thermodynamic properties (mass flow, pressure, temperature and composition) must be known for validation. Furthermore, the component parameters (heat loss, pressure loss, efficiency, etc.) are required. There are some limitations in the available data from the literature as not all specifics are given in the papers, e.g. sometimes the turbine efficiency is given, but not the type of turbine efficiency (isentropic, polytropic, dry step).

The parameters used to build the cycles are depicted in table 3. The pressures and pressure losses off all streams and components throughout the system are depicted in the original flow diagrams in [7] and [8].

Table 3: Component efficiencies and important parameters used in the thermodynamic simulation of the replicated Toshiba and replicated Graz cycles

	Replicated Toshiba cycle values *	Replicated Graz cycle values *
Turbine inlet temperature	1700°C	1500 °C
Fuel and oxygen supply temperature	15 °C	15 °C
Ambient temperature	15 °C	15 °C
Property calculations	IF-97 Formulation	IF-97 Formulation
Excess oxygen	0%	0%
HPT inlet pressure	340 bar	170.4 bar
HTT inlet pressure	66 bar	40 bar
Condenser pressure	0.05 bar	0.025 bar
Turbine isentropic efficiency	93%	HTT 92% ,HPT,LPT: 90%
Compressor isentropic efficiency	**	88%
Pump isentropic efficiency	70%	70%
Combustor heat loss as %	0.3%	0.25%
Cooling flow as % of mass-stream after CC-1	32.4%	21.8%
Oxygen available and pressurized for	free	free
Hydrogen pressurized for	free	free

* For detailed cycle parameters the original detailed flow diagrams can be seen in [7] and [8].
** No such component in the cycle.

With the available information the cycles are recreated using the Thermoflex [26] software and validated with all the given performance parameters from table 4 and table 5. The replicated cycles represent their original counterparts very well. All main parameters of both cycles are within 1.1% of the literature values. The resulting efficiencies are within 0.2% of the literature values.

Table 4: Validation of the Toshiba Reheat Rankine cycle versus data from literature [8]

	Original Toshiba cycle values	Replicated Toshiba cycle values	Percentage off
Hydrogen Input	5.7 kg/s	5.685 kg/s	-0.3%
HPT Power	52.5 MW	52.2 MW	-0.5%
HTT-1 Power	183.8 MW	185.9 MW	+1.1%
HTT-2 Power	204.7 MW	206.7 MW	+1.0%
LPT Power	59 MW	59.2 MW	+0.3%
Gross output power	500 MW	498.3 MW	-0.3%
Gross thermal η	61.7 % HHV	61.8% HHV	+0.1%

Table 5: Validation of the Graz cycle versus data from literature [7]

	Original Graz cycle values	Replicated Graz cycle values	Percentage off
Power HTT turbine	231.8 MW	233 MW	+0.5%
Total Turbine Power	284 MW	285.2 MW	+0.4%
Compression Power	72.7 MW	73.2 MW	+0.7%
Thermal η	70.4% LHV	70.6% LHV	+0.2%

4.2 Making the cycles comparable

The main parameters from both the Graz cycle and the Toshiba cycle are made comparable to facilitate the analysis of both cycles. The most relevant changes from a thermodynamic point of view are depicted in table 6.

Only the thermodynamic properties of the cycles are of interest in this research. The new equalized cycles are called the Graz-EQ (equal parameters) cycle and Toshiba-EQ cycle.

All cycles designed in this study (except the replicated original cycles) are made in accordance with the rule-set of table 6.

Table 6: Equal comparison rule-set

Components	Value
Cycles conform rule-set	All cycles modelled except the Replicated Graz cycle and the Replicated Toshiba cycle.
Ambient temperature and pressure	15 °C, 1.01324 bar
LHV hydrogen	120.0 $\frac{kJ}{kg}$
Chemical exergy hydrogen	116.4 $\frac{kJ}{kg}$
Chemical exergy oxygen	0.25 $\frac{kJ}{kg}$
Chemical exergy water	0.07 $\frac{kJ}{kg}$
Property calculations	IF-97 Formulation, to get entropy and enthalpy for mechanical exergy calculation
Fuel and oxygen supply temperature	15 °C
Excess oxygen used in CC	0%
Turbine (uncooled) isentropic efficiency	HPT,LPT: 90%,HTT:92%
Pump and compressor efficiency	70%, 88%
HRSG or HEX minimum temperature difference	Superheater = 15K, Other heat exchange equipment = 5K
Heat exchanger heat loss	0
Oxygen and Hydrogen	Freely available and pressurized
Condenser subcooling	2K
Condenser pressure	0.025 bar
Deaerator and condenser pressure losses	0
Combustor pressure loss	$\frac{\Delta P}{P}$ =0.0425
Combustor Heat loss	$\dot{Q}_{CC,loss}$ =0.25% of the fuels energy burned in this combustor (LHV)
Coolant mass-flow	HTT blade cooling is altered as described in the chapter:'Cooling of the cycles'. The closed-loop cooling pressure loss is $\frac{\Delta P}{P}$ =0.0606
Other components pressure ratio's and losses	Are kept the same as their original cycle counterpart, except for*
Mechanical losses DC-AC converter and generator losses	Are not considered. As the thermal efficiency is of interest in this study
Single FC pressure loss	$\frac{\Delta P}{P}$ =0.02
Single FC Heat loss	2% of the heat converted in this FC (LHV)

* In the original Toshiba cycle a stream gains pressure in the HRSG this is deemed unlikely. Therefore, in the Toshiba-EQ cycle, the HTT-2 turbine expands to 1.1 bar (instead of the 1 bar in the original Toshiba cycle). Upstream of the LPT the pressure is 1.05 bar (instead of the original 1.3 bar) meaning a 5% HRSG hot-side pressure drop.

4.3 Path through the different models

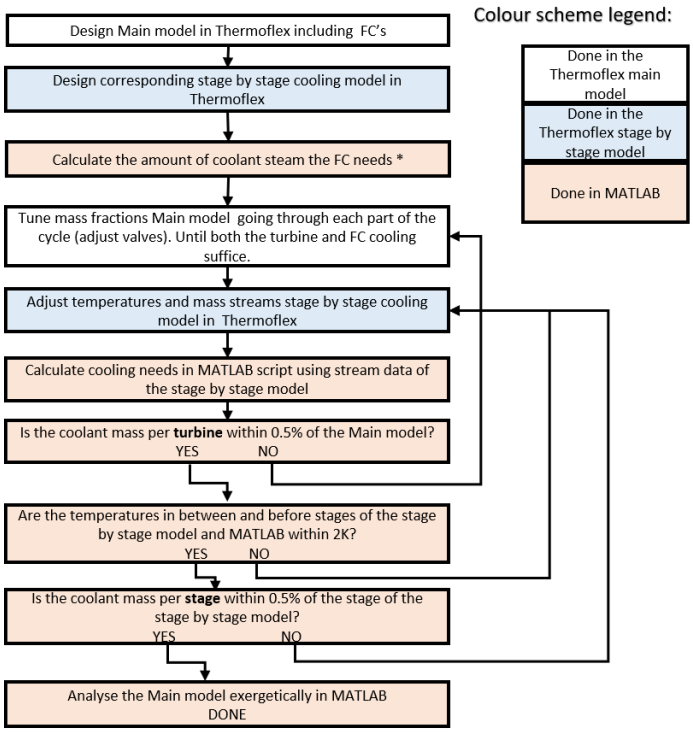

Figure 23: Path through the different models
* If an FC is included in the model

Using the cooling parameters ($C1$ $C2$ and C_{tune}), obtained in chapter 3, the cooling needs can be calculated and the different models can be modeled as done in figure 23. The main model simulates the cooling going into each turbine. A stage by stage modelling approach in the main model made the model too complex and buggy. For this reason, the main model models full turbines (not the stages in the turbines). Therefore, two separate Thermoflex models are used: the Main model and the Stage by stage cooling model.

4.4 Exergy analysis method

Exergy is the combination of the first and second law of thermodynamics and is defined as the maximum amount of work-potential a material or an energy stream contains, in relation to the surrounding environment. More loosely it is defined as the quality of different forms of energy in relation to a given environment. The loss of exergy generally provides an applicable quantitative measure of process inefficiency. Therefore, analyzing a cycle exergetically indicates the total plant irreversibility distribution among its components, identifying the components contributing most to overall plant inefficiency. The total exergy a stream contains is the combination of the mechanical and chemical exergy a stream

contains. The chemical exergy of the used substances is stated in table 6.

$$e_m = (h - h_0) - T_0(s - s_0) \tag{55}$$

$$e = e_m + e_{ch} \tag{56}$$

The value of e expresses the ability of the maximum work the working fluid (water/steam/hydrogen/oxygen) holds, until the external environmental state is reached. This is based on the second law of thermodynamics.

The available energy a subsystem generates ($W_{generated}$) or is inserted in the subsystem (-$W_{generated}$) is calculated in Thermoflex, moreover the streams (stream properties) are known. For this reason, the lost exergy (Ex_{lost}) per component can be calculated using equation 57.

$$Ex_{lost} = m(\Delta e_{in} - \Delta e_{out}) + W_{generated} = \Delta Ex_{in} - \Delta Ex_{out} + W_{generated} \tag{57}$$

The enthalpy h is obtained from the Thermoflex model (Thermoflex is set to use IF97 steam tables). The entropy s cannot be retrieved directly from Thermoflex. The temperature, pressure and enthalpy is known for each stream in Thermoflex, inserting these in the fluid prop (which also uses IF97 steam tables) calculator the entropy is retrieved. The IF 97 steam tables contain steam/water data, there is no database for hydrogen and oxygen, thus for the hydrogen and oxygen flows the entropy is obtained from the NIST (National Institute of standards and technology) web application [28].

To go through a whole cycle, the exergy losses of all components and stream mixers are combined to a total exergy loss. The percentage loss of a system, is the exergy loss divided by the exergy supplied to the cycle. The supply of exergy per kg of fuel used, differs from cycle to cycle as the supplied pressure of the fuels differ. Cycles that have 2 combustors have 2 supplies of fuel at different pressures.

The fuel **energy** supply of all cycles is the same. The hydrogen LHV is a given and is independent of the pressure. The statement stated earlier, the hydrogen is pressurized for free, is only relevant for the energy calculation. The exergy calculation takes the supplied pressure of the fuels into account.

4.5 Exergy analysis equalized (EQ) cycles

With the data set formulated in the previous section, the cycles are adjusted and can now be compared. The performance per component of the EQ-cycles is depicted in table 7. The performance of Toshiba-EQ cycle (fired at a TIT of 1500°C) is lower compared to the original Toshiba cycle, due to the original cycle's higher TIT of 1700 °C. The principle Toshibe-EQ cycle scheme shown is illustrated in section 2.2.1 in figure 8. The difference between the Graz-EQ cycle and the replicated Graz cycle efficiency is less than 0.2%.

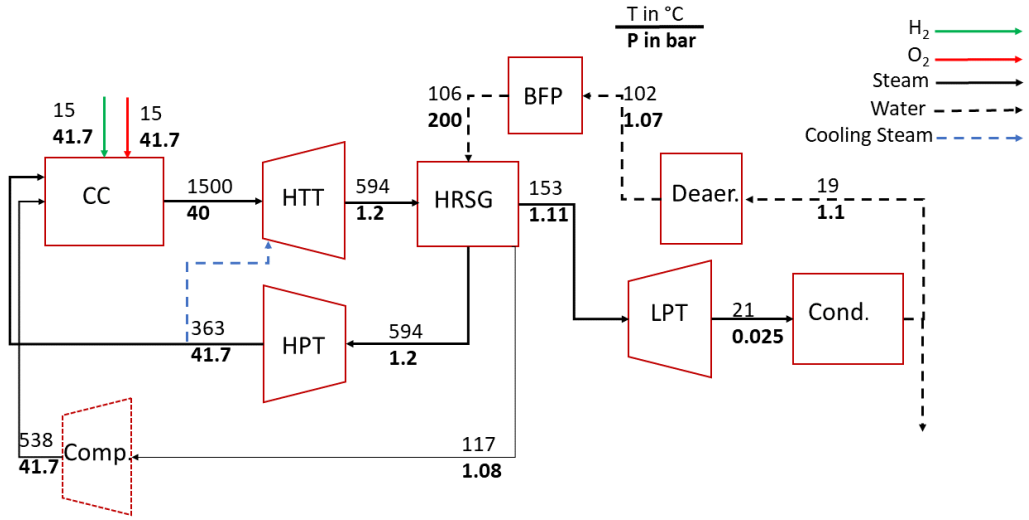

Figure 24: Principle flow scheme of the Graz-EQ cycle. The detailed flow scheme of the Graz-EQ cycle is depicted in appendix B.1.

Table 7: Exergy analysis equalized cycles

Exergy losses	Toshiba-EQ (TIT=1500°C)	Graz-EQ
Combustor 1	14.52% *23.18%	21.27%
Combustor 2	6.85% *18.33%	**
HRSG	4.63%	1.93%
Turbines	3.33%	5.49%
HTT's	1.56%	3.92%
HPT	0.29%	0.33%
LPT	1.48%	1.24%
Compressors	**	1.17%
Pumps	0.20%	0.11%
Condenser	0.96%	0.97%
Deaerator	0.27%	0.48%
Drainage	0.52%	0.52%
mixing	0%	0.11%
Exergy η	68.74%	68.06%
Thermal η_{LHV}	70.98%	70.43%
Principle flow scheme in	figure 8 section 2.2.1	figure 24 this section

* Relative combustor loss (loss if it was the only combustor)

** No such component in the cycle

The exergy losses in the different components of the cycle are calculated and compared. Both the individual performance of the components and the main cycle performance can be analyzed this way. From table 7, with the comparison of both cycles with identical main parameters, one can observe the following advantages:

Advantages of the Graz cycle:
• The Graz-EQ cycle HRSG exergy losses are significantly lower because of the small temperature difference in the HRSG (the heated steam downstream of the HRSG temperature is only 15°C lower than the exhaust HTT steam). The main reason is the direct compression of the steam downstream of the HRSG. This opens the options to optimize the mass flow over the HRSG. Additionally, in the Toshiba-EQ cycle the temperature differences in the HRSG are higher due to the higher exit temperature of the second High Temperature Turbine.
• The cycle combustor losses are the lowest (Toshiba's combined CC losses are 21.37%). The temperature of the entry steam in the first combustor is higher in the Graz cycle. The rise in entry temperature for the combustion chamber reduces the combustor exergy losses [11].
• The cycle works at lower pressure ratios. Both the HPT and HTT have a lower entry pressure, reducing the amount of turbine stages and thus reducing complexity and costs.

Advantages of the Toshiba Rankine Reheat cycle (1500°C) :
• Overall cycle efficiency is slightly higher than the Graz cycle.
• The relative exergy loss in the second combustor is very low (taking the fuel amount going in relatively), mainly due to the higher entry temperature.
• The deaerator losses are very low due to extraction of the heat from the LPT to preheat the condensate with a preheating HEX network.
• HTT exergy losses are lower as hybrid cooling of the turbine blades reduces cooling losses.
• Pressurization is only done in the water phase (pumping water instead of compressing steam) leading to lower overall pump and compressor losses.

The main advantages of the Graz EQ cycle are due to the extra degree of freedom by feeding the combustor with both steam from the HP turbine and the compression of the exhaust low pressure steam of the HRSG. In the Toshiba EQ cycle a larger part of the steam is condensated and has to be evaporated in the HRSG in order to function as cooling steam for the combustor.

The cycle efficiencies of the Toshiba-EQ cycle and Graz-EQ cycle are within 0.6% of each other. The strong points from the Toshiba-EQ cycle are: a second combustor, closed loop cooling in the HTT and extraction of heat from the LPT to preheat the condensate. These additions increase the cycle efficiency by more than 0.6%, this is confirmed in the next chapter (chapter 6) as the U-Graz-1500°C cycle is 3.2% more efficient than the (basic) Graz cycle. The inherent advantage of the Graz cycle is the inclusion of the steam compressor. Therefore, the Graz-EQ cycle is used as basis for the optimum hydrogen/oxygen cycle and is extended with a second combustor, hybrid cooling of the HTT and extraction of heat from the LPT to preheat the condensate.

5 Improvements to the Graz cycle

In this chapter, the improvements proposed in the previous chapter (hybrid cooling, the inclusion of a second combustor, condensate preheating and increased turbine inlet temperature) are implemented into the Graz cycle. Furthermore, all improvements together will be implemented as the U-Graz (upgraded Graz cycle), the cycle is depicted in figure 25. The resulting cycles will be analyzed based on exergy. Additionally, the temperature entropy diagrams of the cycles are plotted to compare the cycles from another angle.

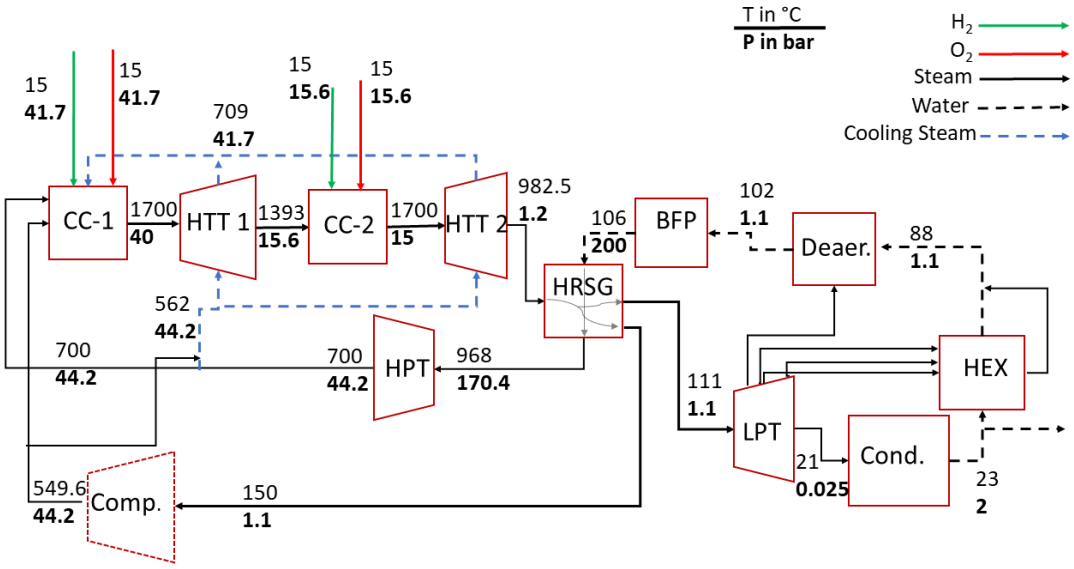

Figure 25: Principle flow scheme U-Graz cycle, a detailed flow scheme is depicted in appendix B.8. The flow scheme differs from the Graz and Graz-EQ cycle configuration, as depicted in figure 24, due to the following cycle adjustments. A second combustor (depicted as CC-2) is included. Hybrid cooling is used, now part of the HTT coolant is retrieved and is send into the first combustor (CC-1). Condensate preheating is applied, thus multiple streams are extracted from the low pressure turbine (LPT) to enter the heat exchangers (HEX). The turbine inlet temperature is increased from 1500° C to 1700° C (the stream between the combustor and HTT).

5.1 Individual cycle improvements

Hybrid cooling (Graz-HC): Hybrid cooling is a combination of film cooling and closed loop cooling used in the Toshiba cycle [8]. Hybrid cooling will lead to a reduction in turbine exergy losses as less cooling steam is quenched into the turbine main gas flow. The steam that is used in the closed loop cooling is fed back into the combustor. This results in a higher average steam inlet temperature entering the combustor. Due to the higher combustor inlet temperature and the fixed turbine inlet temperature, the increase of steam inlet temperature leads to a reduction of exergy losses. Closed loop cooling alone will lead to local hot-points in the metal. To enable the right metal temperatures throughout the blade, the closed loop cooling is combined with film cooling, this combination is called hybrid cooling.

Reheat (Graz 2-CC): The addition of a second combustor will decrease the relative combustor exergy destruction further. The steam entering the second combustor will be hotter than with a single combustor, leading to an overall higher average steam inlet temperature, resulting in lower exergy losses. The turbine loss is increased due to the addition of a second HTT as more cooling steam is required in the HTT turbines. The flue gas (steam) at the exit of the second HTT is hotter than in the reference case (the Graz cycle) leading to more heat transfer in the HRSG, but also to a higher temperature difference in the HRSG, therefore higher exergy losses. However, the reduction in combustor exergy loss is greater than the the increase in HRSG exergy loss. Furthermore, the increase of heat transfer in the HRSG reduces the amount of steam to be compressed for the combustor.

Condensate preheating (Graz-HEX): The bottoming cycle (Rankine part of the cycle) of the Toshiba cycle is copied completely. Steam extracted from the LPT is used to preheat the condensate before deaerator entry. This results in a smaller temperature difference over the deaerator, therefore the exergy loss is reduced.

Increasing the TIT (Graz-1700°C): Increasing the turbine inlet temperature to 1700°C improves the Carnot efficiency of the cycle. It will reduce the combustor exergy losses. The higher turbine inlet temperature will require increased cooling in the HTT, therefore the HTT exergy loss is increased.

Upgraded Graz cycle (U-Graz): All these upgrades together make the U-Graz cycle. The results of all these upgrades on the exergy losses are shown in table 8. As can be seen in table 8 the rise in efficiency of all the upgrades together (4.4%) is larger than the rises in efficiency from all the individual upgrades added up. The main contributions in the reduction of exergy losses are from the hybrid cooling and the increase of the TIT. The changes in the exergy losses for the combustor, HTT and HRSG dominate the differences between the other options. The main exergy losses in the U-Graz cycle are still in the combustor (17.7% of the total loss of 27.6%). The U-Graz cycle principle flow scheme can be seen in figure 25.

Table 8: Exergy analysis of improved Graz cycles.

Exergy losses in %	Graz EQ	Graz-1700°C	Graz-HEX	Graz-2-CC	Graz-HC	U-Graz-1500 °C	U-Graz
CC 1	21.27	19.67	21.24	12.73 * 20.85	21.12	14.51 * 20.34	12.87 * 18.42
CC 2	**	**	**	6.57 * 16.88	**	4.96 * 17.32	4.85 * 16.09
HRSG	1.93	1.88	1.94	2.45	1.81	2.86	3.40
HTT	3.92	4.71	3.94	5.08	2.07	2.35	2.57
HPT	0.33	0.36	0.33	0.46	0.27	0.29	0.27
LPT	1.24	1.31	1.32	1.45	1.35	1.40	1.36
Compressors	1.17	1.02	1.17	0.87	0.88	0.61	0.44
Pumps	0.11	0.11	0.11	0.12	0.10	0.10	0.10
Condenser	0.97	0.95	0.96	0.98	0.92	0.90	0.88
Dearator	0.48	0.47	0.23	0.50	0.45	0.21	0.20
Drainage	0.52	0.52	0.52	0.52	0.52	0.52	0.52
Mixing	0.11	0.04	0.11	0.00	0.12	0.05	0.10
Exergy efficiency	68.06	69.01	68.24	68.27	70.50	71.24	72.44
Efficiency LHV	70.43	71.47	70.60	70.43	72.96	73.63	74.86
Principle flow scheme in	figure 24	figure 24 ***	none	none	none	figure 25 ***	figure 25

* Relative combustor loss(loss if it was the only combustor)
** There is no second combustor
***Only the flow scheme fits the cycle. The displayed pressures and temperatures in the figure do not belong to this cycle.

5.2 Temperature entropy diagrams improved Graz cycles

The reference Graz cycle Ts (temperature entropy diagram) can be seen below in figure 26a next to the U-Graz cycle's Ts diagram in figure 26b. The figures are plotted with a clear differentiation between the Brayton and Rankine part of the cycle.

The following can be retrieved from the Ts diagrams. There is more Rankine and Brayton cycle area in the U-Graz cycle Ts diagram as the Rankine part goes into the higher temperatures (leading to the higher efficiencies) as it increases the Q_h without increasing the Q_c. Meanwhile, the theoretical maximum efficiency η of a Carnot cycle is $\eta = 1 - Q_h/Q_c$. The Brayton part of the cycle is wider (leading to more specific work) as more entropy is used and created and Q_h is higher. However, the amount of mass going though the different parts of the cycles differs from cycle to cycle, therefore no direct conclusion can be made solely from the Ts diagrams. For instance, the ratio of steam going through the first HTT and LPT is 1.13 for the U-Graz cycle and 1.84 for the Graz-EQ cycle. Thus, the Rankine bottoming cycle influences the efficiency of the U-Graz-cycle more. The plots are there to visualize the cycle in another way.

Noteworthy is the entropy reduction in the first high temperature turbine of the Graz-EQ cycle. Entropy is created during (non-reversible) turbine expansion. This can be explained by a significant amount of open loop cooling that is quenched into the HTT-1. The U-Graz cycle uses hybrid cooling, therefore less steam is quenched into the HTT-1 and the reduction in entropy is absent.

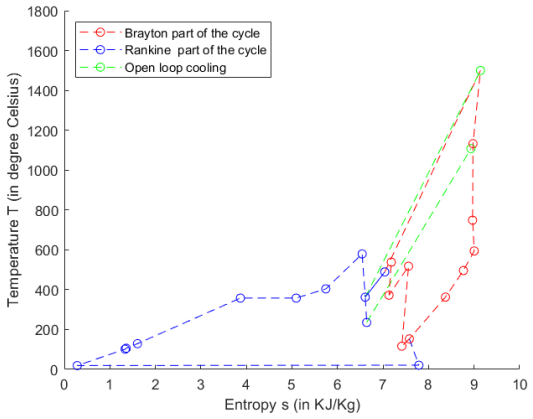

(a) Ts diagram Graz-EQ cycle

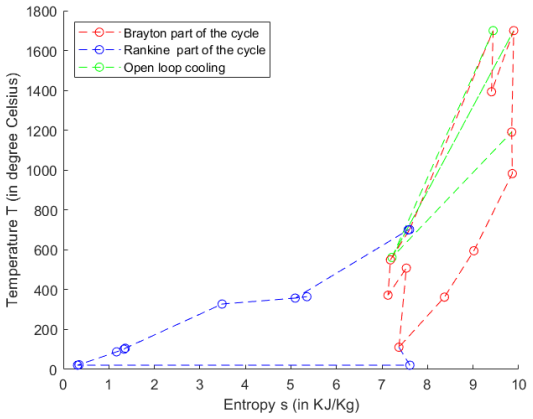

(b) Ts diagram U-Graz cycle

Figure 26: TS diagrams

6 Fuel cell addition to the Graz cycle

As discussed in section 2.3, the fuel cell is a very promising addition to a hydrogen and oxygen fired turbine cycle. As the pressurization of the fuel, the use of hydrogen and pure oxygen increases the driving force of the electrochemical reaction (the Nernst voltage equation 8). For instance, the U-Graz cycle transforms the heat (from the combusted fuel) into electricity with a LHV efficiency of approximately 75%. A state of the art SOFC transforms 65% of the converted fuel's energy into electricity LHV [5], thus 35% of this converted fuel LHV energy becomes heat. Thus if both cycles would fit to each other perfectly and the fuel utilization of the FC is 100% (no downstream combustor is required for complete fuel utilization) a combination of the two could lead to a $65 + \frac{35 \cdot 75}{100} = 91.2\%$ LHV efficiency. To come as close as possible to this perfect combination one would need an FC which can be fed with the fuel temperatures as given and exit the FC at TIT (1700°C) with 100% fuel consumption in the FC. Unfortunately, no such FC exist. The U-Graz cycle needs to be modified significantly to accommodate the FC.

For this reason, in this chapter the connection of FC system to a turbine cycle is investigated, furthermore the modifications that need to be made to the cycle are covered. This will be done for a single low temperature SOFC and a triple SOFC system containing low, intermediate and high temperature SOFCs. Moreover, the different cooling methods used to keep the SOFCs cool are covered, both the addition of steam and the use of excess oxygen is covered. The electrochemical operation and performance for the different SOFCs is investigated. Current density voltage (IV) curves are investigated. And finally, the different FC-Turbine cycles are exergatically analyzed.

6.1 Fuel cell connection to the Graz cycle

The FC is placed upstream of the combustor and the unutilized heated fuel, leaving the FC, is burned in the combustor. The combustor acts as an afterburner in this case. The full SOFC temperature range will be used in the system and the gasses are fed to the FC system at a temperature of 550 °C and exits at 1000 °C (the minimum and maximum operating temperatures for state of the art SOFCs). The broader this range the less thermodynamic adjustments that need to be made to fit the FCs. Today's FCs can have temperature deltas of 150 °C [17] per FC, therefore 3 FCs in series are required to achieve the 450 °C temperature delta. The fuel and oxidizer enter the first low temperature SOFC (LT-SOFC) at 550 °C and exit at 700 °C. For the intermediate temperature SOFC (IT-SOFC) entry is at 700 °C, while it exits at 850 °C. The high temperature SOFC (HT-SOFC) entry is at 850 °C, while it exits at 1000 °C.

An important aspect of the FC is the cooling. The waste heat must be extracted from the FC. Two options have been studied: (1) cooling via excess pure oxygen circulation at the cathode (cycles with FC-OX-abbreviation) and (2) cooling by dilution of the oxygen flow with steam (cycles abbreviated with FC-Steam). Both options will be compared.

Adding steam to the FC cathode for cooling, decreases the partial pressure of the oxygen resulting in a decrease in the electrochemical driving force (Nernst voltage) as can be seen in equation 8. The excess oxygen cooling has a higher Nernst voltage, but it requires an additional compressor (at high temperatures) for the oxygen recirculation. The addition of cooling steam to the anode side (hydrogen side) has also been evaluated. However, this has a very negative impact on the Nernst voltage as can

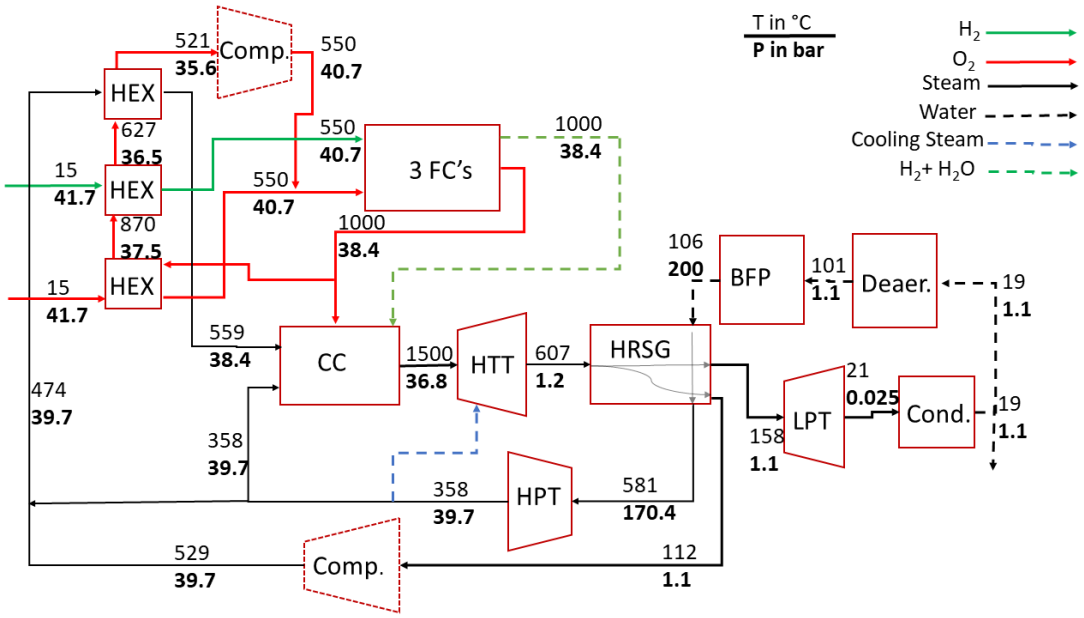

Figure 27: Principle flow scheme 3FC-OX-Graz cycle. A detailed flow scheme is depicted in appendix C.4. The FC is cooled using oxygen recirculation.

be seen in equation 8: the partial pressure of steam increases and the partial pressure of hydrogen decreases.

In the steam cooled FC, the hydrogen, steam and oxygen are preheated to SOFC inlet conditions. The HTT downstream steam preheats the flows. In the oxidant recirculated FC, the hydrogen and oxygen are preheated to SOFC inlet conditions. This heat is extracted from the excessive oxygen that exits the FC.

Moreover, the use of a single FC operating at a single temperature is compared to the use of three FCs. For the single FC configuration the LT-FC is chosen as it needs the same 550 °C feed as the 3FC configuration.

The steam cycles fuel utilization is limited by the amount of heated steam it can extract from the main cycle. The higher the fuel utilization in the SOFC, the less heat goes into the cycle. Therefore, less steam is needed in the combustor to get to the same TIT. Less steam in the combustor results in less steam through all parts of the cycle. Consequently, the compressors cannot feed enough steam to the FC entry. The 3FC-steam cycle is operated at this limit (at maximum fuel utilization in the FC) as the best efficiency is extracted at maximum FC usage. For a fair comparison the 3FC-OX cycle is operated at the same fuel utilization level as the 3FC-steam cycle. The 1FC-OX cycle uses the same amount of oxygen re-circulation as the 3FC-OX cycle. The 1FC-Steam cycle uses the same amount of fuel as the 1FC-OX cycle for a fair comparison.

Table 9: Fuel cell operating parameters

	1FC-OX	1FC-Steam	3FC-OX	3FC-Steam
Temperature out (°C)	700	700	1000	1000
Fuel used FC1(kg/s)	0.483	0.483	0.483	0.480
Fuel used FC2(kg/s)	*	*	0.483	0.482
Fuel used FC3(kg/s)	*	*	0.484	0.489
Fuel used total(kg/s)	0.483	0.483	1.450	1.450
Oxygen inlet (kg/s)	93.13	19.84	93.13	19.84
Oxygen utilization (kg/kg)**	0.041	0.193	0.124	0.580
Water inlet (kg/s)	0	34.19	0	33.80

* No such component in the cycle

** Oxygen utilization in kg oxygen reacted in FC's per amount of oxygen going into the first FC.

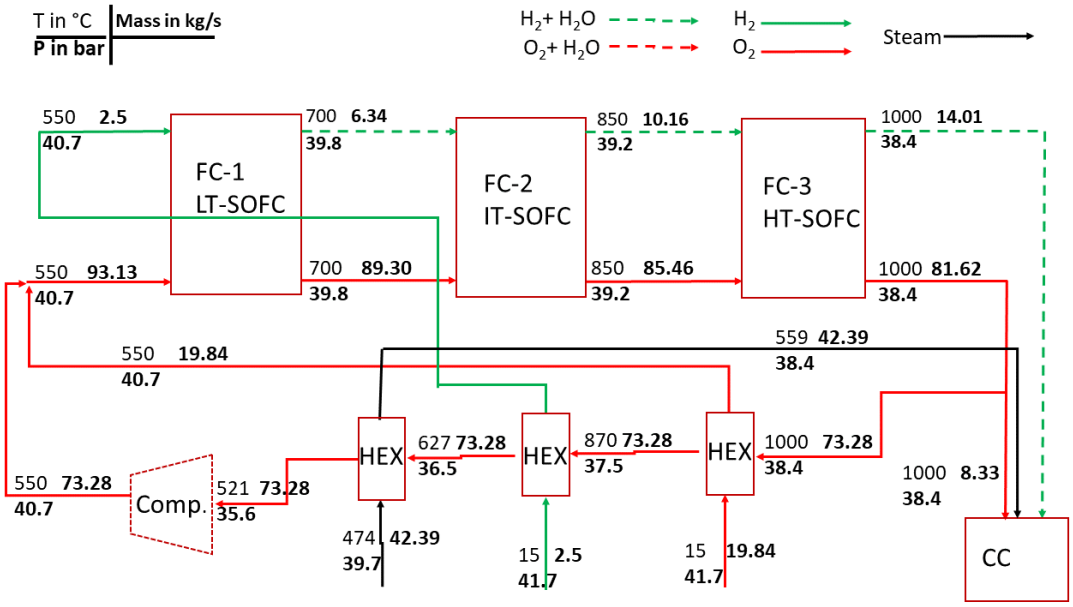

Figure 28: Fuel cell flow scheme 3FC-OX-Graz cycle. The FC is cooled using oxygen recirculation. A more detailed flow scheme is depicted in appendix C.4.

All these input values can be seen in table 9, the difference in the amount of oxygen utilization between the systems is particularly striking. A heat balance (equation 58) is calculated for each FC, which shows that the 3FC cycles are able to use 3 times the amount of fuel in the FCs for the same amount of coolant going in. The 3FC-OX principle flow scheme can be seen in figure 27. The recirculated oxygen preheats the fuels and heats the flow upstream of the compressor. A more detailed picture of the FC part of the cycle can be seen in figure 28. The 1FC-OX cycle flow scheme, as can be seen in figure 29, is different than its 3FC counterpart. One FC is not able to insert sufficient heat

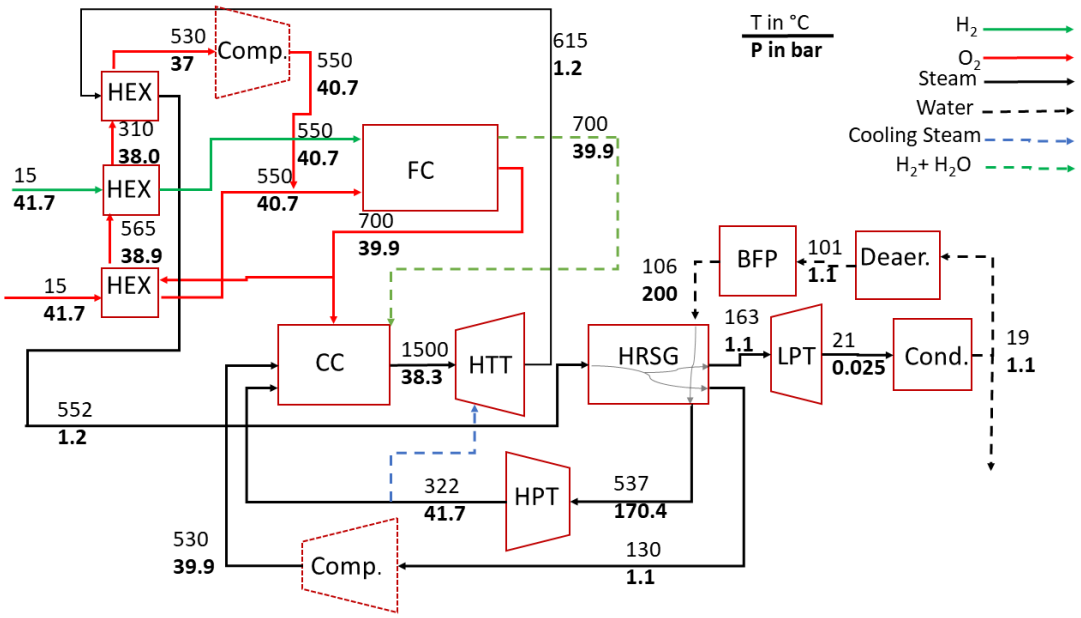

Figure 29: Principle flow scheme 1FC-OX-Graz cycle. A more detailed flow scheme is depicted in appendix C.3. The FC is cooled using oxygen recirculation.

in the recirculated oxygen (the oxygen exits this FC at 700°C), to preheat the fuel and oxygen to FC inlet conditions. Therefore, in the 1FC-Ox cycle the recirculated oxygen together with the steam downstream of the HTT preheats the fuels.

The 3FC-steam principle flow scheme can be seen in figure 30. This cycle uses the downstream gas from the HTT to preheat the gasses before FC entry.

The FC Steam cycles need to be fed a certain amount of steam (dependant on the FC operated fuel utilization) at 550°C and 40 MPa. This steam is needed to cool the FC (the OX-FC cycles use recirculated oxygen). The more fuel is utilized in the FC the more heat is generated in the FC (and more steam cooling is needed). The steam is extracted from the turbine cycle (the amount of steam available is however limited). The requirement to be fed an amount of 550°C and 40 MPa steam increases complexity. Therefore, the Steam-FC cycles are more difficult to design and regulate.

Increasing TIT or adding an extra combustor leads to less working fluid through the cycle, thus less (high temperature) steam is available to use elsewhere. The Steam-FC cycles need to be fed a certain amount of 40 MPa 550°C steam (the amount is dependant of the amount of fuel utilization in the FC). Therefore, not all cycle additions (operated configurations) are possible for steam cooled FC.

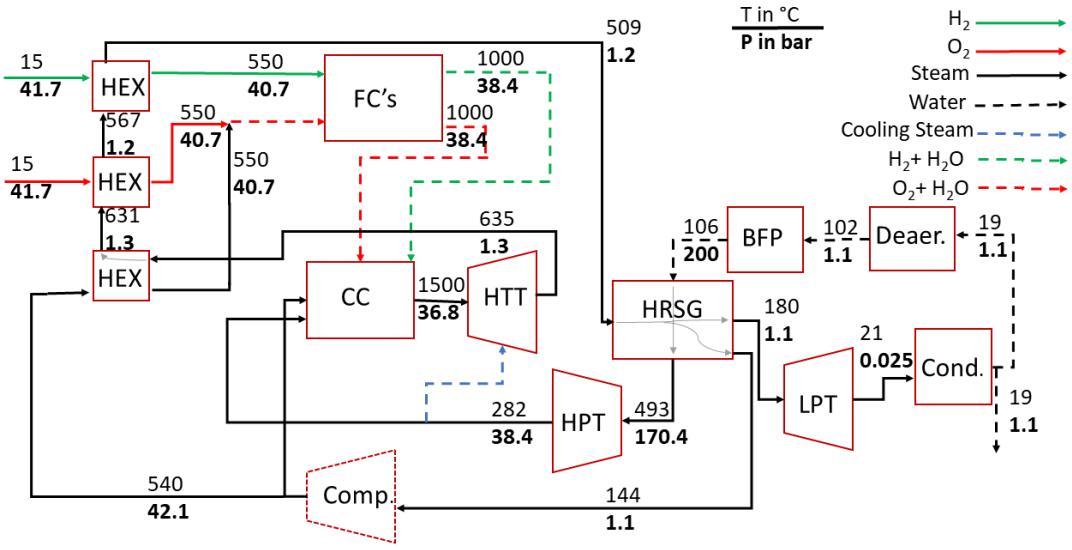

Figure 30: Principle flow scheme 1FC/3FC-Steam-Graz cycle, with the pressures and temperatures of the 3FC-Steam-Graz cycle. A more detailed flow scheme is depicted in appendix C.2. The FC is cooled by the addition of steam.

6.2 Electrochemical performance

To analyse the addition of FCs to the U-Graz cycle, all FCs are operated at 65% efficient LHV. A standard anode supported SOFC geometry as found in [22] is used with the materials and their respective resistivities from [23]. The resistivities and thicknesses of the components used in the FC stack are displayed in table 1. Losses occur due to electrical resistance (overpotential) in the FC. In high temperature FCs (all SOFCs are in this category) the activation overpotential is negligibly small [18]. Furthermore, the concentration overpotential only becomes significant when the limiting current density is approached [18]. In this study, efficiency is key and the SOFC is operated far away from the limiting current density. Therefore, the ohmic resistance is the only significant resistance in this study. The FC LHV efficiency is fixed at 65% and the inlet conditions are fixed, therefore the cell voltage is fixed as well. The FC model is used to estimate the power densities one can expect. Furthermore, the FC operates in steady state conditions, thus the following heat balance is valid, as can be seen in equation 58.

$$\dot{m}_{cat,in}h_{cat,in} + \dot{m}_{ano,in}h_{ano,in} = \dot{W}_{FC} + \dot{Q}_{Loss} + \dot{m}_{cat,out}h_{cat,out} + \dot{m}_{ano,out}h_{ano,out} \tag{58}$$

The subscript cat represents the cathode and ano represents the anode. The heat balance and the electrochemical operation both depend on the flows going in. Therefore, the equations are solved simultaneously. The heat loss ($\dot{Q}_{Loss}$) to the environment is assummed to be 2% LHV of the fuel reacting in the FC. Furthermore, the pressure loss per FC is assumed to be 2% (The 3FC pressure loss, therefore equals 6% in total).

A lumped parameter approach is assumed, meaning:

1. The FC temperature is constant in all directions.
2. The current density is constant.
3. The potential is constant, and therefore determined by the outlet compositions of the fuel and flow, since at this point the Nernst voltage is at its minimum.

The results for both the 3FC-OX and 3FC-steam cycle are shown in table 10. The resistivities of the SOFC materials are very temperature dependent as one can see from the reduction in the area specific resistance (ASR: the total FC electrical resistance divided by the total FC stack active area) when the FC temperature increases. The potential voltage E_0 decreases slightly with an increase in temperature. The driving force (the Nernst voltage) decreases even more in the downstream FCs as both E_0 decreases due to the increase in temperature and more steam is formed decreasing χ_{H_2} and χ_{O_2} (only in the steam cooled FCs). In the oxygen cooled cycle χ_{O_2} is always 1.

The power density of the 1FC-OX system is 0.324$\frac{W}{cm^2}$, while the power density of the 1FC-Steam system is merely 0.290$\frac{W}{cm^2}$. The power density of the 3FC-OX system is 0.409$\frac{W}{cm^2}$, while the power density of the 3FC-Steam system is merely 0.329$\frac{W}{cm^2}$.

Based on the difference in power density the required cell area for the 3FC-OX system is 24% smaller than the area for the 3FC-steam system, resulting in significant lower cost per kW [18]. Therefore, the recirculation of oxygen is superior to steam cooling, from an electrochemical point of view.

The 3FC-OX system has a 26% higher power density compared to the 1FC-OX system. Therefore, the use of multiple FCs is superior to the use of a single FC, from an electrochemical point of view.

Table 10: Elechtrochemical results 3FC-Steam and 3FC-OX configuration

	FC-1 OX	FC-2 OX	FC-3 OX	FC-1 Steam	FC-2 Steam	FC-3 Steam
Temperature FC exit (°C)	700	850	1000	700	850	1000
Pressure FC exit (bar)	39.9	39.2	38.4	39.9	39.2	38.4
Cathode χ_{O_2}	1	1	1	0.211	0.169	0.122
Anode χ_{H_2}	0.807	0.614	0.420	0.808	0.615	0.420
E_0 (V)	1.006	0.963	0.919	1.006	0.963	0.919
Nernst voltage (V)	1.143	1.074	1.001	1.111	1.031	0.952
Cell voltage (V)	0.834	0.838	0.840	0.834	0.838	0.840
ASR ($\frac{ohm}{cm^2}$)	0.794	0.398	0.303	0.794	0.398	0.303
Power density ($\frac{W}{cm^2}$)	0.324	0.496	0.445	0.290	0.407	0.310
Current density ($\frac{A}{cm^2}$)	0.389	0.593	0.530	0.348	0.485	0.369
Power (MW)	37.69	37.70	37.77	37.44	37.62	38.10

6.3 Electrochemical operation and IV curves

The IV curves and efficiency voltage curves, for the 3FC-OX and 3FC-Steam cycle are plotted in figure 31 and 32 respectively. The electrochemical results of table 10 are from the chosen operation at 65% efficiency. This is a choice taking efficiency and power density into consideration. The power density voltage curves are parabolas. A certain power density (except for the maximum power density) of a FC corresponds to 2 operational voltages, of which the higher voltage has the higher efficiency. For example, this can be seen from figure 31b as one can operate this FC at a 0.83 V (cell voltage) corresponding to a power density of 0.32 W/cm^2 with 65% efficiency or one operates it at 0.31 V corresponding to a power density of 0.32 W/cm^2 with 24% efficiency. Therefore, in general the logical operational voltage of a FC is at a voltage higher than the voltage corresponding to maximum power density.

For the LT-SOFC of the 3FC-OX system maximum power density occurs at 0.57 V, at 0.41 W/cm^2 power density, 0.72 W/cm^2 current density and 44% efficiency, as depicted in figure 31a and 31b . At the highest operatable voltage the efficiency is highest, but the power density is 0. Therefore, one wants to operate between these points, somewhere at a high efficiency with an acceptable power density. The operation at 65% seems to be very reasonable.

All three FC's operate at the same efficiency. This is however not the most optimal configuration. The fuel cells behave differently and for that reason have a different optimum operation point for a certain use case. The system can be optimized by operating all 3 FC's at a different efficiency, but reach the same overall system efficiency at a higher power density. However, this will be an optimization study on its own.

The 3 steam fed FC's operate at a lower power density compared to the oxygen recirculated FC's. For the HT-SOFC this difference is largest. The driving force of this fuel cell the Nernst voltage is lowest as depicted in table 10 and the difference in Nernst voltage compared to the oxygen recirculated FC's is largest. This can be explained by the low cathode oxygen mol fraction (0.122) as depicted in table 10. The low cathode oxygen mole fraction results in a lower Pp_{O_2} (partial oxygen pressure), thus the Nernst voltage is lower according to equation 8.

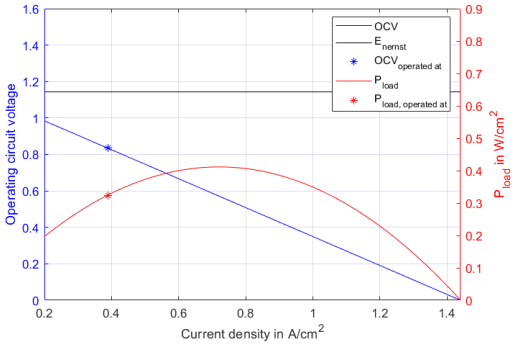

(a) LT-SOFC IV curve

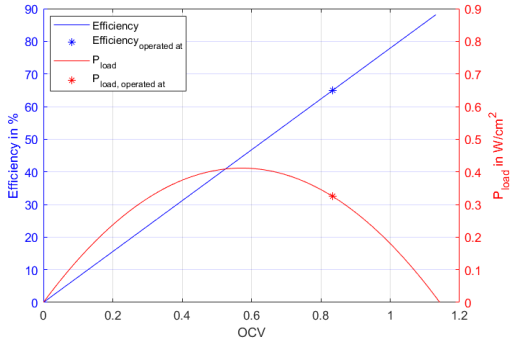

(b) LT-SOFC Efficiency to power-density

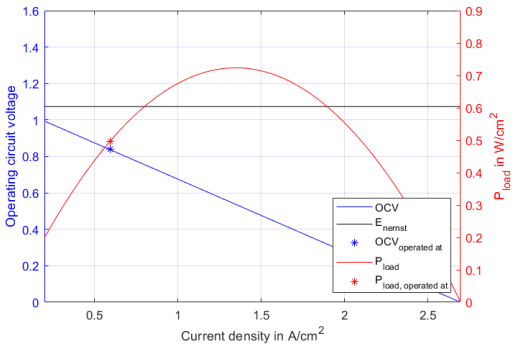

(c) IT-SOFC IV-curve

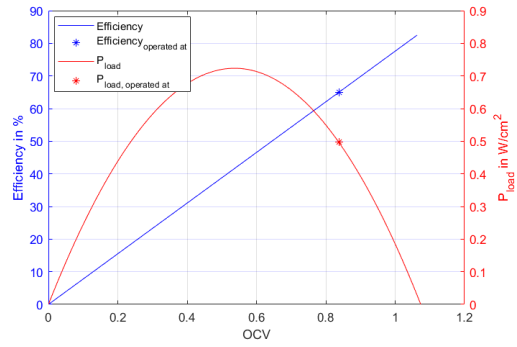

(d) IT-SOFC Efficiency to power-density

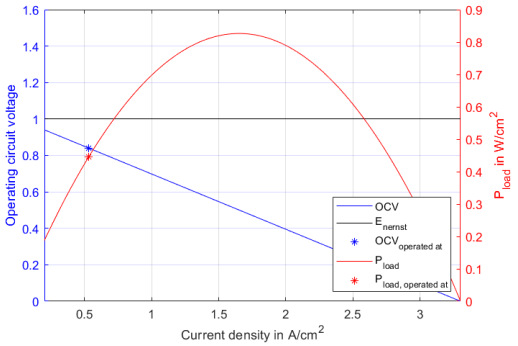

(e) HT-SOFC IV-curve

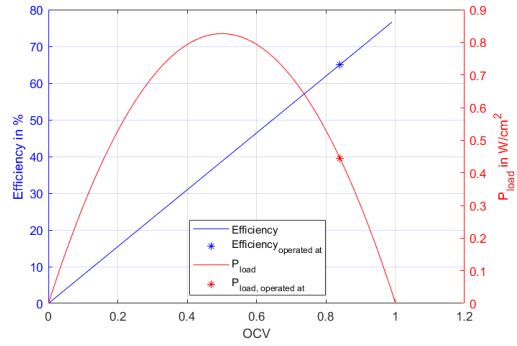

(f) HT-SOFC Efficiency to power-density

Figure 31: 3FC-OX IV-curves and efficiency power-density plots

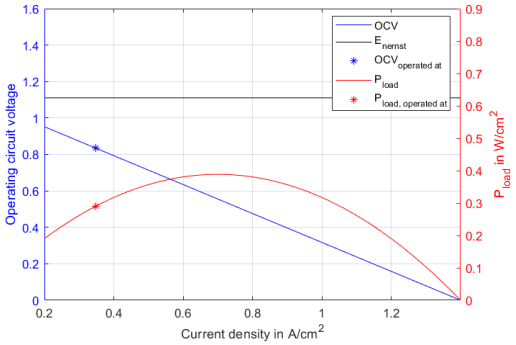

(a) LT-SOFC IV curve

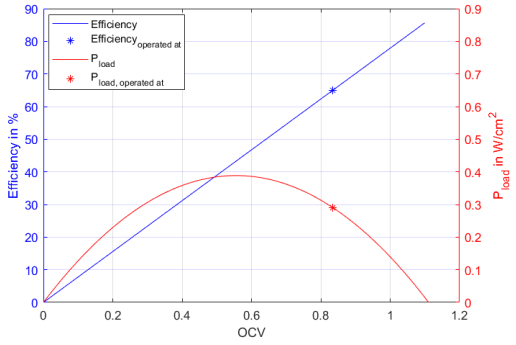

(b) LT-SOFC Efficiency to power-density

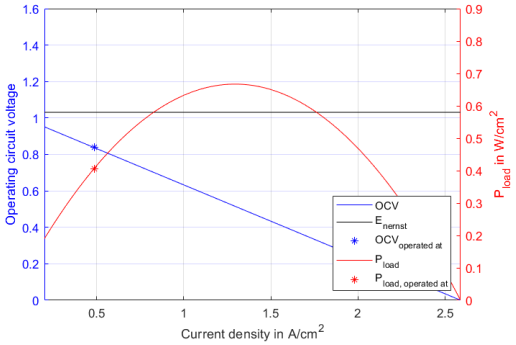

(c) IT-SOFC IV-curve

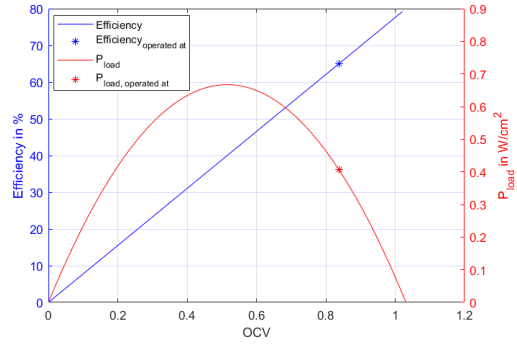

(d) IT-SOFC Efficiency to power-density

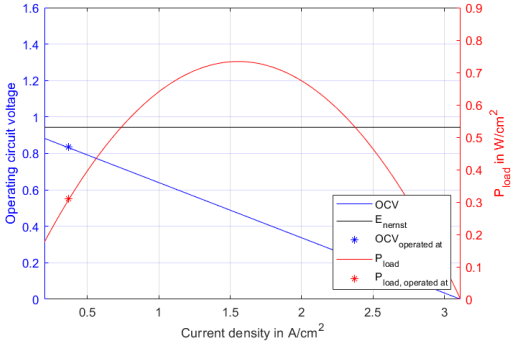

(e) HT-SOFC IV-curve

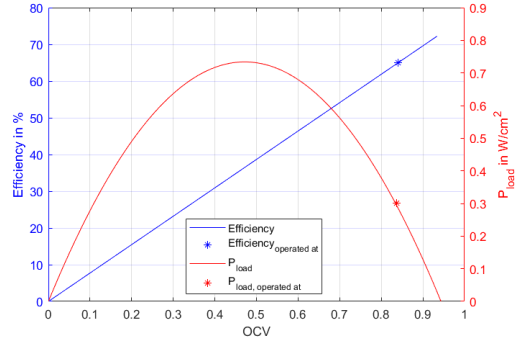

(f) HT-SOFC Efficiency to power-density

Figure 32: 3FC-Steam IV-curves and efficiency power-density plots

6.4 Exergy analysis FC-Graz cycles

6.4.1 1 fuel cell vs 3 fuel cells (1FC vs 3FC):

The FC acts as a preheating device for the combustor, heating the inlet flow to the combustor to 700 °C and 1000 °C for the 1FC and 3FC case respectively. The higher the inlet temperature of the combustor, the lower the combustor exergy losses. For that reason, the **relative** (and absolute) combustor losses drop due to the use of multiple FCs compared to a single FC. The absolute combustor losses drop even further, as the multiple FC cycles burn less fuel in the combustor, due to their higher overall FC fuel utilization. The 3FC combination has a clear efficiency advantage not only due to the higher conversion in the FC, but also due to the reduction of relative exergy losses in the combustor.

6.4.2 Steam vs Oxygen cooled fuel cells (Steam vs OX):

Both cooling options need different amounts of FC preheat at different utilizations of fuel in the FC. The FC-OX cycles are partly or fully preheated by the excess oxygen of the FC itself. The 1FC-OX cycle needs some extra heat from the HTT turbine, while the 3FC-OX cycle excess oxygen is too hot after preheat and needs to be cooled by streams after the HPT and compressors. The HPT and compressor streams differ in temperature from cycle to cycle. Therefore, the U-Graz-3FC-Ox cycle, Graz-3FC-Ox and Graz-1FC-OX have different HEX-Preheat FC exergy losses, as stated in table 11. Furthermore, the cycles introduce a very small compressor loss as the oxygen needs to be recirculated.

The Steam FC cycles preheat the fuel streams using only the main cycles heat (the HTT downstream). Therefore, the HEX-Preheat FC exergy losses are almost the same for the steam FC cycles, as stated in table 11. Furthermore, upstream of the HRSG there is less heat and thus less heat to be carried to the HPT. This results in lower temperature cooling water going into the combustor and HTT's, leading to reduced cooling mass needs (less HTT turbine exergy losses) and higher combustor losses.

In a nutshell, the steam cooled FC cycles extract more heat from the HTT downstream, leading to less heat upstream of the HRSG and therefore less heat downstream and upstream of the HPT. Less heat upstream of the HPT leads to less cooling mass required for the HTT turbine, thus less HTT exergy losses, but a cooler combustor inlet means more combustor exergy losses. The addition of a compressor to recirculate the oxygen adds a small compressor loss to the recirculated oxygen cycles. Overall, the oxygen cycle and steam cycles operate around the same efficiency, at some FC utilization rates the oxygen circulation efficiency is more efficient and at other fuel utilization the steam FC cycle is more efficient. Moreover, another advantage of the FC-OX cycles is their ability to operate at higher fuel utilization compared to the Steam-FC cycles, as they do not need a certain amount of steam feed at 550°C. For that reason, the FC-OX cycles have the prospect of becoming even more efficient, when operated at higher fuel utilization (than is done in this study).

6.4.3 The U-Graz-FC cycle

The best performing thermodynamic cycle the, U-Graz-1700°C, cannot be coupled to an FC cycle (with the same 0.58 fuel utilization in triple FC configuration). The system could not provide sufficient heat into the cycle, without huge adjustments (introducing multiple new heat exchangers and changing the inherent cycle design) and supplying the right amount of cooling to the HTT's.

Table 11: Exergy analysis FC enhanced cycles compared to Graz-EQ and U-Graz cycle

Exergy Losses in %	Graz-EQ	Graz-1FC-Ox	Graz-1FC-Steam	Graz-3FC-Ox	Graz-3FC-Steam	U-Graz	U-Graz-3FC-Ox
Fuel cell stack	**	1.56 *8.10	1.55 *8.00	3.78 *6.51	3.75 *6.46	**	3.78 *6.51
HEX-Preheat FC	**	2.52	2.03	3.16	2.00	**	3.33
FC Comp.	**	0.01	**	0.02	**	**	0.02
Combustors	21.27	14.77 *18.31	15.65 *19.39	7.10 *16.91	7.87 *19.83	19.47	6.63 *15.79
HRSG	1.93	1.69	1.71	1.18	1.21	2.86	1.55
Turbines	5.49	4.84	4.79	3.39	3.51	4.04	2.49
Pumps & Comp. excluding FC Comp.	1.28	1.10	1.10	0.59	0.70	0.71	0.22
Condenser	0.97	0.87	0.88	0.70	0.69	0.90	0.67
Deaerator	0.48	0.41	0.42	0.28	0.27	0.21	0.13
Energy η_{LHV}	70.43	74.49	74.21	82.48	82.65	73.63	83.79
Principle flow-scheme in	figure 24	figure 29	figure 30 ***	figure 27 ***	figure 30	figure 25	figure 33

* Relative FC/combustor loss (loss if it was the only fuel using device)
**Non existent
***Only the flow-scheme fits the cycle. The displayed pressures and temperatures in the figure do not belong to this cycle.

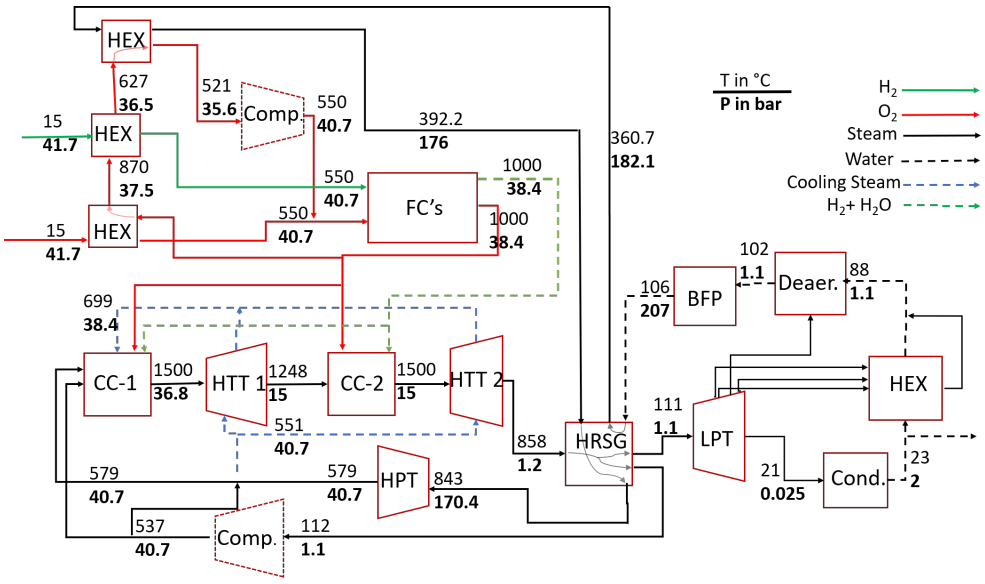

Figure 33: Principle flow scheme U-Graz-3FC-OX cycle. A detailed flow scheme is depicted in appendix C.5.

The 3FC-Steam cycle cannot be coupled to either the U-Graz-1700°C nor the U-Graz cycle (TIT of 1500°C). Due to the addition of FCs less heat is supplied to the cycles, therefore less working fluid is used throughout the cycle to be able to provide the same TIT. As a result, an insufficient amount of steam can be provided to the FC. The 3FC-OX cycle is therefore coupled to the U-Graz cycle as its TIT of 1500°C is reachable. The result is the U-Graz-3FC-OX cycle and is shown in figure 33. This combination is 1.3% more efficient as the Graz-3FC-OX cycle, as can be seen in table 11. This difference is less than half of the difference of the thermodynamic only Graz and U-Graz cycle (3.2% more efficient). This smaller effect can be explained by the fact that only 61% of the fuel energy is released as heat to the working fluid (41.9% of this heat is from the combustor and 19.1% from the FCs). Moreover, to incorporate the FCs, extra components (the FC itself and heat exchangers) are included, resulting in extra heat and pressure losses. A Sankey power diagram of the U-Graz-3FC-OX cycle is shown in figure 34, in which the energy (thus not the exergy) streams of the components are plotted.

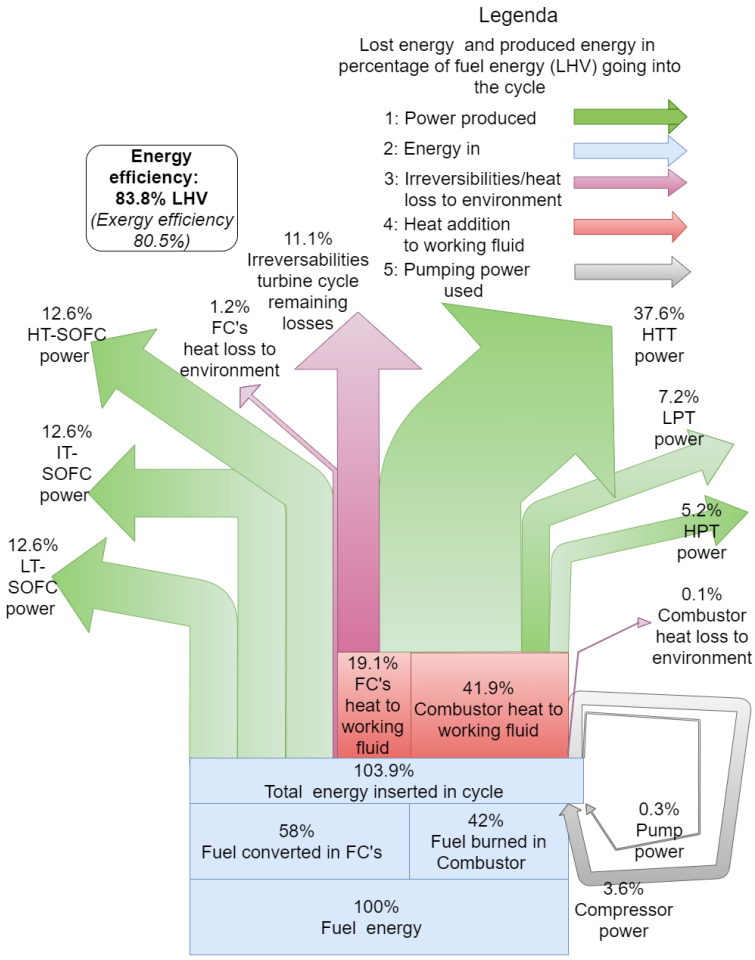

Figure 34: Sankey power (in LHV) diagram U-Graz-3FC-OX cycle.

The following can be noticed from figure 34: the power produced by the LPT and HPT falls short in comparison to the power produced by the HTT. This is a property of Graz cycles. In a Graz cycle, part of the steam, downstream of the HTT, skips the LPT and HPT and is compressed directly to enter the combustor. For this reason, the HTT power is more significant in Graz cycles than in conventional CCGT cycles.

7 Conclusions

This work presents the thermodynamic analysis of multiple very high efficiency hydrogen and oxygen fuelled electricity generating power cycles. The thermodynamic cycles are closed loop combinations of a Brayton and a Rankine cycle. Both a turbine-only-cycle and a cycle with the addition of FCs have been designed, followed by an analysis of all possible plant configurations.

The thermodynamic cycle (U-Graz-1700°C cycle) constructed is an adjusted Graz cycle, with added reheat combustor, hybrid cooling, extra heat exchangers to preheat the condensate and an increased TIT. These improvements result in a 74.9% LHV thermal efficiency, a 4.4% increase in efficiency over the Graz-EQ cycle. The main efficiency increase is generated by a lower overall combustor loss. However, the combustor loss is still the biggest exergy loss. Therefore, the integration of FCs before the combustor is investigated for further efficiency gains.

The addition of a turbine cycle to a FC is well known to extract performance from the otherwise wasted heat from a FC. This thesis examines the concept from the other side, a very efficient turbine cycle is developed and multiple FCs are placed there where they are most desired (from an exergetic point of view). The FCs are designed to fit the cycle. Furthermore, the cycle is adjusted to accommodate the FCs in the most efficient way. This leads to a turbine cycle with multiple FCs in series operating in different temperature regimes. FCs have not been modulated in series before, but the studied cycle has shown that it leads to the highest overall efficiency. Using oxygen recirculation as cooling method for the FC yields the best results, moreover the integration of the oxygen cooled FC into the cycle is less complex.

Moreover, the FC combination with 3 FCs in series combined with oxygen recirculation (3FC-OX) is most electrochemical favorable and results in the highest FC power density. The resulting efficiency is 82.5% LHV for the Graz-3FC-OX cycle and 83.8% LHV for the U-Graz-3FC-OX cycle. The FC decreases the role of the combustor and its exergy losses in the cycle. Therefore, all the methods used in the U-Graz cycle to decrease the combustor losses, which gave it a 3.2% efficiency benefit, have become less influential in the cycles with FCs. The U-Graz-3FC-OX cycle is only 1.3% more efficient than the Graz-3FC-OX cycle. Finally, the FC reduces the overall heat input in the cycle. Therefore, compromises need to be made to get to the same turbine inlet temperature. Both the thermodynamic (U) upgrades and FC addition mainly reduce the combustor exergy losses.

8 Recommendations for future research

The hybrid cooling model used for the hybrid cooled HTT blades is a new approach. In the approach it is assumed the blade can be modeled as if a fraction of the blade is solely CLSC and the rest of the blade is solely open loop cooled. In real life the full hybrid cooled blade is both CLSC and open loop cooled and there will be interaction between the CLSC and open loop cooling. Therefore, the approximation used is rather simplistic and should be improved in a future study.

An existing FC layout is used in this thesis. However, the operating conditions (a pressure of $\approx$ 40 MPa) fuelled with pure hydrogen and oxygen is unique. The SOFC design should be adapted to the unique operating conditions, to estimate the FC parameters (power density, operating voltage) corresponding to a chosen efficiency more accurately. The design of an SOFC layout that fits these unique operating conditions should be investigated in a future study.

Further efficiency improvements can be achieved by operating the SOFCs at higher fuel utilization, higher voltages or by an increase in operational temperature. Operation at higher voltages or higher fuel utilization will lead to lower power densities, resulting in a larger and costlier fuel cell. Moreover, in the 3FC cycles all three FCs are operated at the same efficiency, this is not the most ideal type of operation. The different FCs can be optimized to operate at different efficiencies each, but operate at the same overall efficiency with a lower total FC stack area. This can be done in a future optimization study.

An increase in the working temperature window of the fuel cells (now 550 to 1000°C) would lead to lower heat exchanger losses, resulting in an increased efficiency. Moreover, the inclusion of other types of fuel cells can be investigated, for example the proton exchange membrane (PEM) FC. PEM FCs operate around 100°C, the inclusion of a PEM FC would further increase the working temperature window of the FCs used.

The most efficient cycle, the 3FC-U-Graz cycle, is far too complex and expensive for near future use. It is in the earliest design phase, making an accurate estimation of the costs impossible at this point in time. A potential direction for further research is to develop a less complex cycle, based upon the 3FC-U-Graz cycle, incorporating the most important elements. A first step could be the coupling of a series of lab scale FCs to a simplified Graz cycle. The Graz cycle can be simplified by lowering the TIT to eliminate cooling needs. Additionally, one can reduce the turbines respective pressure ratios (reducing the amount of turbines stages/blade rows), or even remove the complete HPT.

Another research and development direction is to use the knowledge and insights from the 3FC-U-Graz cycle to study the option of modifying an existing CCGT cycle to a higher efficiency semi-closed H_2/O_2 cycle.

References

[1] K. Kitamori. OECD environmental outlook to 2050: the consequences of inaction. *International Journal of Sustainability in Higher Education*, 13(3), 2012.

[2] M. Jarraud and A. Steiner. Climate Change 2014 Synthesis Report. Technical report, IPCC, 2014.

[3] International Energy Agency. World energy balances: Overview. Technical report, International Energy Agency, 2019.

[4] Hans Christian Gils, Yvonne Scholz, Thomas Pregger, Diego Luca de Tena, and Dominik Heide. Integrated modelling of variable renewable energy-based power supply in Europe. *Energy*, 2017.

[5] M. Andersson and Froitzheim Jan. Technology review – solid oxide cells 2019. Technical report, Energiforsk, Malmö, 2019.

[6] Bruna Rego de Vasconcelos and Jean Michel Lavoie. Recent advances in power-to-X technology for the production of fuels and chemicals. *Frontiers in Chemistry*, 7(JUN):1–24, 2019.

[7] Wolfgang Sanz, Martin Braun, Herbert Jericha, and Max F. Platzer. Adapting the zero-emission Graz Cycle for hydrogen combustion and investigation of its part load behavior. *International Journal of Hydrogen Energy*, 43(11):5737–5746, 2018.

[8] Masafumi Fukuda and Yoshikazu Dozono. Double Reheat Rankine Cycle for Hydrogen-Combustion, Turbine Power Plants. *Journal of Propulsion and Power*, 16:562–567, 2000.

[9] Ronald L. Bannister, Richard A. Newby, and Wen Ching Yang. Final Report on the Development of a Hydrogen-Fueled Combustion Turbine Cycle for Power Generation. *Proceedings of the ASME Turbo Expo*, 2(January):8, 1999.

[10] C Hendriks, M Harmelink, K Burges, and K Ramsel. Power and heat production: Plants and grid. Technical Report January 2004, Rijksinstituut voor Volksgezondheid en Milieu, Utrecht, 2004.

[11] MJ Moran, HN Shapiro, DD Boettner, and MB Bailey. Principles of thermodynamics for engineering, 2008.

[12] Thermal Engineering. https://thermal-engineering.org/wp-content/uploads/2019/05/Carnot-cycle-pV-Diagram-min.png, 2020.

[13] A.J. Seebregts. Gas-Fired Power, https://refman.energytransitionmodel.com/publications/1960, 2010.

[14] Herbert Jericha, Wolfgang Sanz, Jakob Woisetschläger, and Morteza Fesharaki. CO2 - Retention Capapility of CH4/O2 - Fired Graz Cycle. *Cimac*, pages 1–13, 1995.

[15] Fuelcell store. https://www.fuelcellstore.com/fuel-cell-components/sofc-materials, 2020.

[16] Omar Z. Sharaf and Mehmet F. Orhan. An overview of fuel cell technology: Fundamentals and applications, 2014.

[17] K. H. Ng, H. A. Rahman, and M. R. Somalu. Review: Enhancement of composite anode materials for low-temperature solid oxide fuels. *International Journal of Hydrogen Energy*, 2018.

[18] Mark C. Williams. *Fuel Cell Handbook*. lulu.com, West-Virginia, 2004.

[19] Stephen J Mcphail, Sergei Pylypko, Shamil Nadorov, Dmitri Opalnikov, Alex Lattimer, and Stephen Bond. NELHI A new all-European technology for clean, efficient power. Technical report, Fuel Cells and Hydrogen Joint Undertaking, 2017.

[20] Klaus Hassmann. SOFC Power Plants, the Siemens-Westinghouse Approach. Technical report, Siemens, Erlangen, 2001.

[21] Robert Holyst and Andrzej Poniewierski. *Thermodynamics for chemists, physicists and engineers*. Springer Science & Business Media, 2012.

[22] Sanghyeok Lee, Hyoungchul Kim, Kyung Joong Yoon, Ji Won Son, Jong Ho Lee, Byung Kook Kim, Wonjoon Choi, and Jongsup Hong. The effect of fuel utilization on heat and mass transfer within solid oxide fuel cells examined by three-dimensional numerical simulations. *International Journal of Heat and Mass Transfer*, 2016.

[23] Norman F Bessette II, William J Wepfer, and Jack Winnick. A Mathematical Model of a Solid Oxide Fuel Cell. Technical Report 11, Georgia Institute of Technology, 1995.

[24] S. Can Gülen. *Gas Turbines for Electric Power Generation*. Cambridge University Press, Cambridge, Massachusetts, 2 2019.

[25] J F Louis, Astronautics K Hiraoka, and M A El Masri. A comparative study of the influence of different means of turbine cooling on gas turbine performance. Technical report, Massachusetts Institute of Technology, Cambridge, Massachusetts, 1983.

[26] Karsten Huschka. Thermoflex version 27, 2018.

[27] J. B. Young and R. C. Wilcock. Modeling the air-cooled gas turbine: Part 2-Coolant flows and losses. *Journal of Turbomachinery*, 124(2):214–221, 4 2002.

[28] NIST. https://webbook.nist.gov/chemistry, 2020.

A Mathematical derivation open loop cooling

A.1 Derivation open loop cooling without TBC coating

The derivation continues on the earlier made derivation of section 3.2. For the open loop case without a TBC coating the heat network depicted in figure 35 is used.

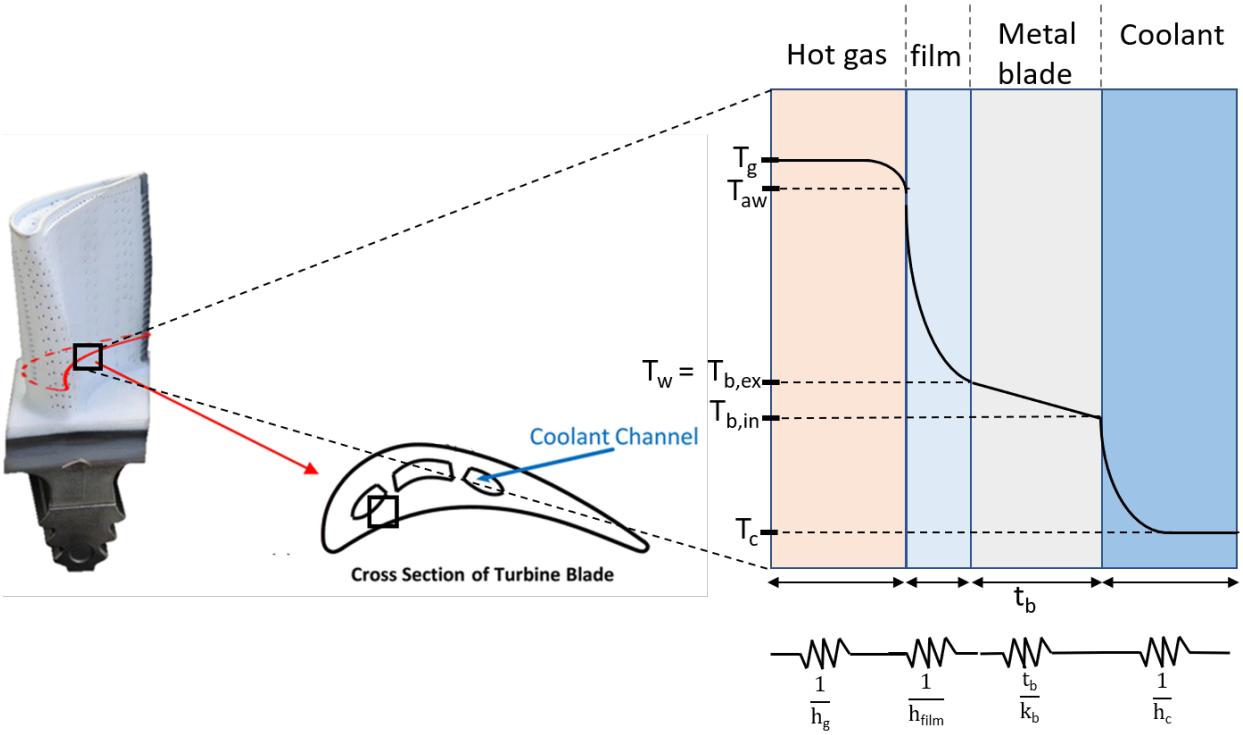

Figure 35: Temperature profile across film cooled and TBC coated turbine blade

The following parameters are introduced, to simplify the calculation:

$$\eta_c = \frac{T_{ce} - T_{ci}}{T_b - T_{ci}} \tag{59}$$

$$\epsilon = \frac{T_g - T_b}{T_g - T_{ci}} \tag{60}$$

The the metal blade conducts heat very well $T_{b,ex} - T_{b,in}$ is assumed to be negligible, therefore the bulk value will be used T_b for the interior and exterior wall. Moreover, Due to the assumptions made the governing equations become:

$$\dot{Q} = h_g A_g (T_{aw} - T_w) \approx h_g A_g (T_g - T_b) \tag{61}$$

$$\dot{Q} = \dot{m}_c(h_{ce} - h_{ci}) \approx \dot{m}_c Cp_c(T_{ce} - T_{ci}) \tag{62}$$

Together they form:

$$\frac{\dot{m}_c Cp_c}{h_g A_g} = \frac{T_g - T_b}{T_{ce} - T_{ci}} = m^* \tag{63}$$

Which can be rewritten to:

$$m^* = \frac{T_g - T_b}{T_g - T_{ci}} \frac{T_g - T_{ci}}{T_{ce} - T_{ci}} \tag{64}$$

Which can be further rewritten to:

$$\frac{T_{ce} - T_{ci}}{T_b - T_{ci}} + \frac{T_g - T_b}{T_{ce} - T_{ci}} - \frac{T_{ce} - T_{ci}}{T_b - T_{ci}} + \frac{T_g - T_b}{T_{ce} - T_{ci}} \cdot \frac{T_g - T_b}{T_g - T_{ci}} = \frac{T_g - T_b}{T_g - T_{ci}} \tag{65}$$

Which can be rewritten to:

$$\eta_c \cdot m^* = \frac{\epsilon}{1 - \epsilon} \tag{66}$$

At this point the following figures 36 and 37 illustrates the concept:

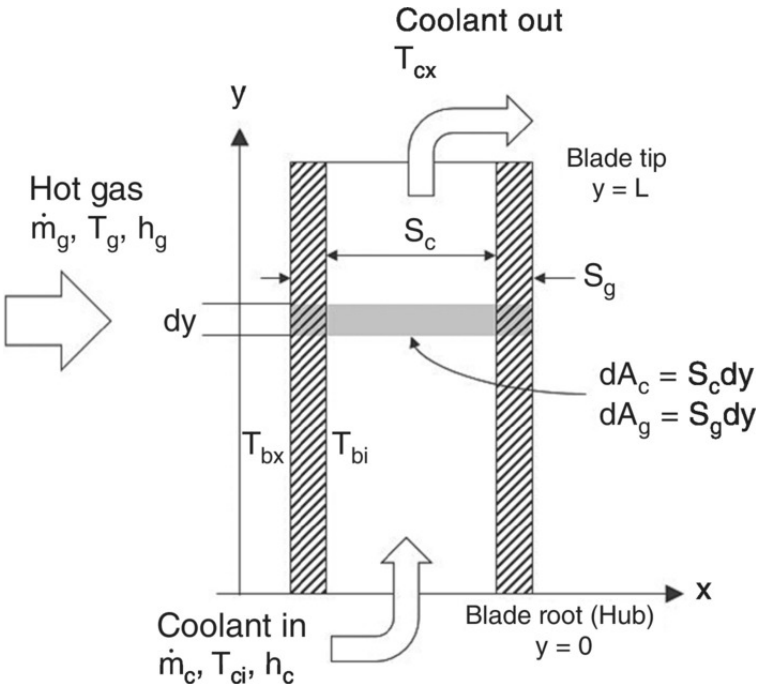

Figure 36: Simplified cross section of a single convection cooled blade[24]

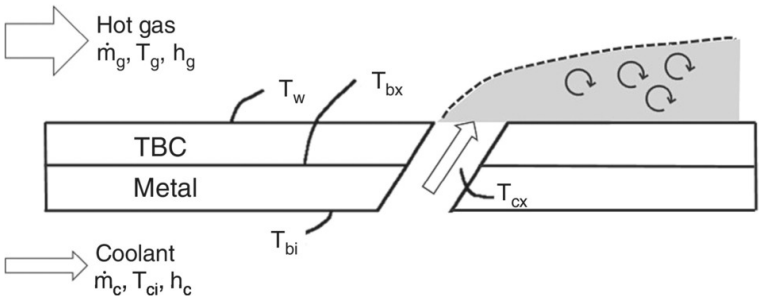

Figure 37: Simplified cross section of blade film cooling[24]

The heat balance of an elementary strip dy out of figure 36 is:

$$\dot{m}_c Cp_c dT_c = h_c S_c (T_b - T_c) dy \tag{67}$$

The left part is integrated from T_{ce} to T_{ci} and the right part of the equation is integrated from $y = 0$ to $y = L$. This leads to:

$$\frac{T_b - T_{ce}}{T_b - T_{ci}} = e^{-\frac{h_c S_c}{\dot{m}_c Cp_c} L} \tag{68}$$

$$\eta_c = 1 - e^{-\frac{h_c A_c}{m^* h_g A_g}} \tag{69}$$

A_c is the area of the cooled wall (including the fins inside). Combining equation 69 with equation 66 gives:

$$(1 - e^{-\frac{h_c A_c}{m^* h_g A_g}}) \cdot m^* = \frac{\epsilon}{1 - \epsilon} \tag{70}$$

$$(1 - e^{-\frac{\alpha}{m^*}}) \cdot m^* = \frac{\epsilon}{1 - \epsilon} \tag{71}$$

If $\alpha \gg m^*$ then $m^* \approx \frac{\epsilon}{1-\epsilon}$. For modern turbines this is the case as the cooling technology has increased a lot over time.
Using equation 63 one gets:

$$\dot{m}_c = \frac{h_g A_g}{Cp_c} \frac{\epsilon}{1 - \epsilon} \tag{72}$$

$$\dot{m}_g = \rho_g \cdot v_g \cdot A_w \tag{73}$$

$$\dot{m}_c = \frac{\dot{m}_g}{\dot{m}_g} \cdot \dot{m}_c = \frac{\dot{m}_g}{\rho_g * v_g * A_w} \cdot \dot{m}_c = \frac{\dot{m}_g}{\rho_g * v_g * A_w} \cdot \frac{h_g A_g}{Cp_c} \frac{\epsilon}{1 - \epsilon} \tag{74}$$

Combining this equation with the Stanton number leads to:

$$\dot{m}_c = \dot{m}_g St_g \frac{Cp_g}{Cp_c} \frac{A_g}{A_w} \frac{\epsilon}{1 - \epsilon} \tag{75}$$

A.2 Derivation open loop cooling with the TBC coating

The derivation of the previous subsection is for a blade without the TBC coating. As the blades of our study use a TBC coating this extra conducting part needs to taken into account in the heat transfer equation. This addition is done in the same way as in the CLSC case. Therefore, the resulting equation for the film cooling mass flow with a TBC becomes:

$$\dot{m}_c = \dot{m}_g \frac{1}{1 + Bi_{TBC}} St_g \frac{Cp_g}{Cp_c} \frac{A_g}{A_w} \frac{\epsilon}{1 - \epsilon} \tag{76}$$

$$\frac{\dot{m}_c}{\dot{m}_g} (Bi_{TBC} + 1) \frac{Cp_c}{Cp_g} \frac{A_w}{A_g} \cdot \frac{1 - \epsilon}{\epsilon} = St \tag{77}$$

B Thermoflex models without FC

The Thermoflex models are depicted in this part of the appendix. Fuel sources are depicted as an orange rectangle, the oxygen source is depicted as a red rectangle. The other components are explained on the Thermoflex website [26]. The full Thermoflex models include the operational parameters of the individual components. For those who want the full models please contact me (the author) via email.

The Exergatic analysis is done in MATLAB scripts. However, the stream and components power data is first copied to an Excel file, the MATLAB script reads the data out of the Excel file. The MATLAB script retrieves data from online fluid prop libraries. This fluid data is retrieved using certain function files. The right libraries need to be downloaded and one needs the right MATLAB files in the right folders. For this reason, contact me (the author) to access the MATLAB file folders, with an explanation.
The main Thermoflex models are depicted in subsection B.1-B.8. The stage by stage Thermoflex cooling model of the Graz-1700C cycle, is displayed in B.3.1. This cycle is open loop cooled.

B.1 Graz-EQ cycle Thermoflex model

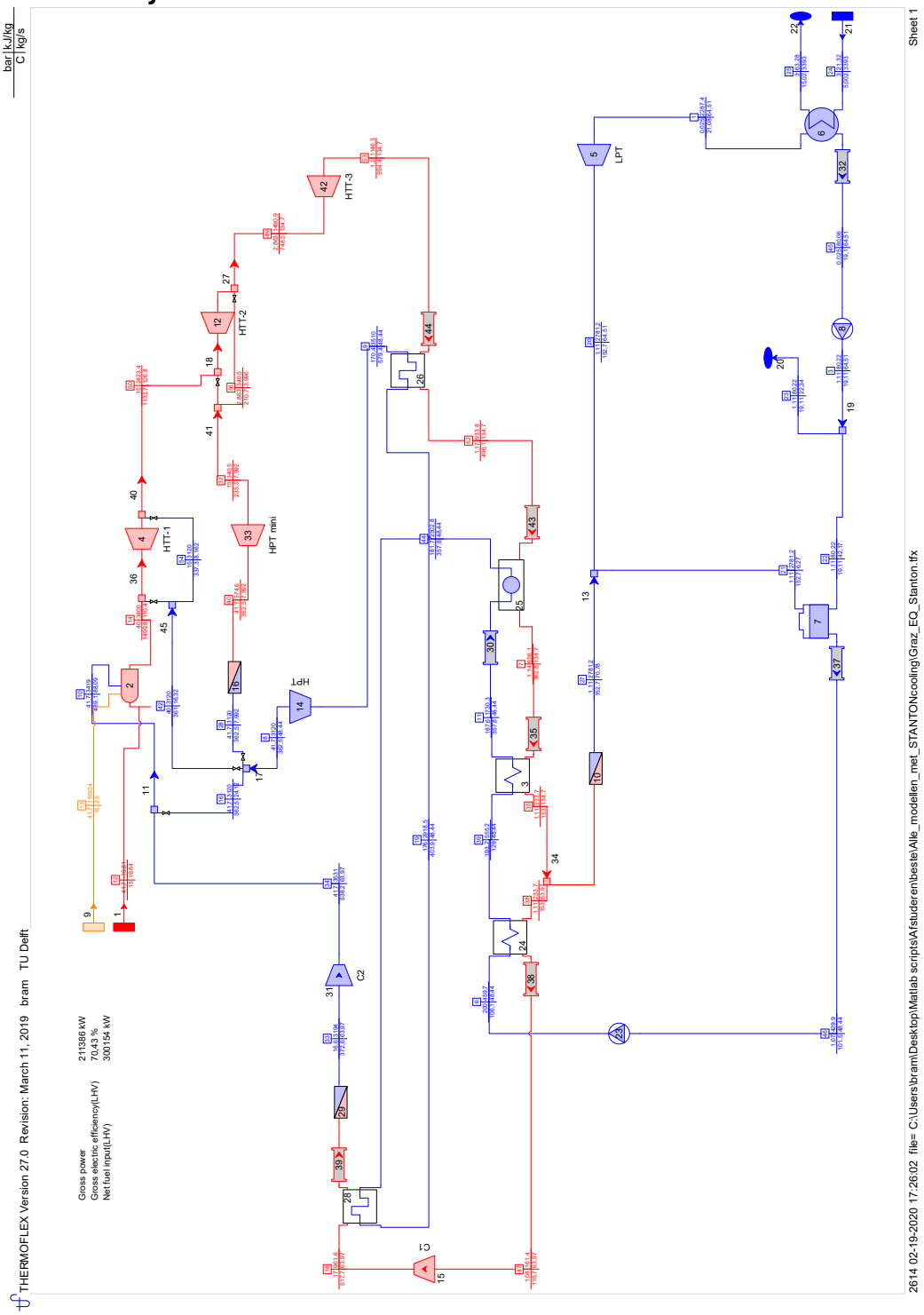

B.2 Toshiba-EQ cycle Thermoflex model

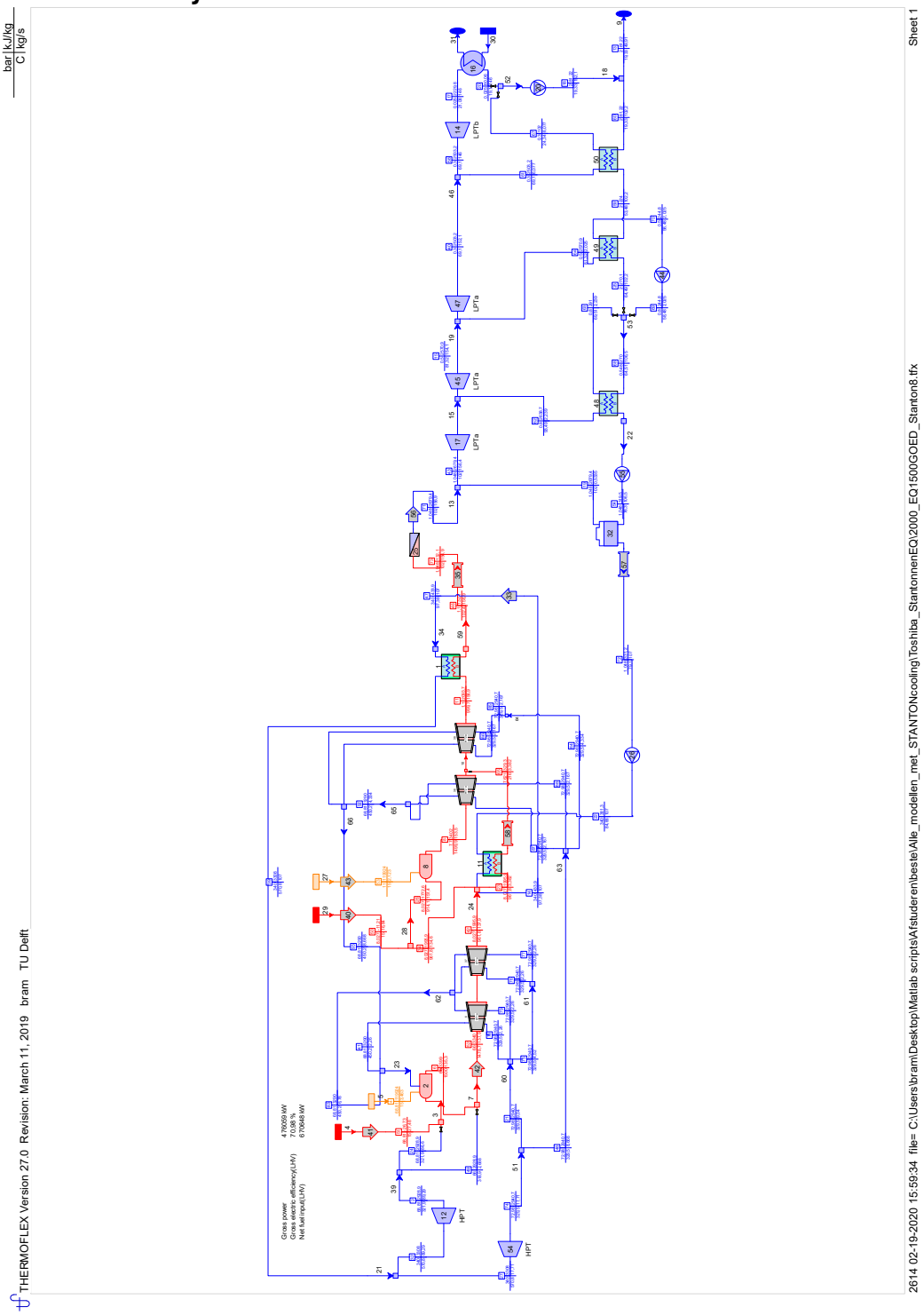

B.3 Graz-1700°C cycle Thermoflex model

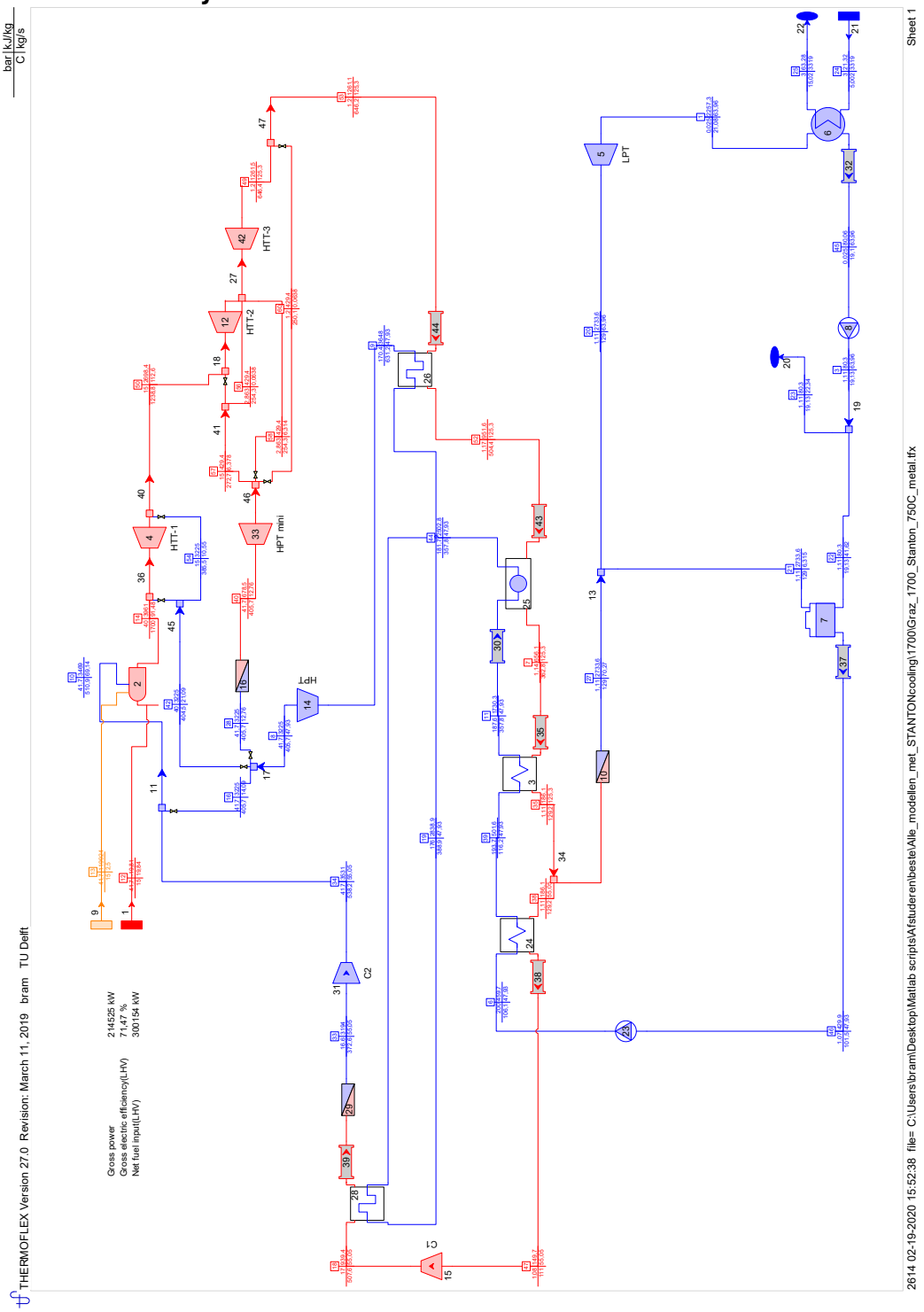

B.3.1 Graz-1700°C cycle Thermoflex stage by stage cooling model (open loop cooling)

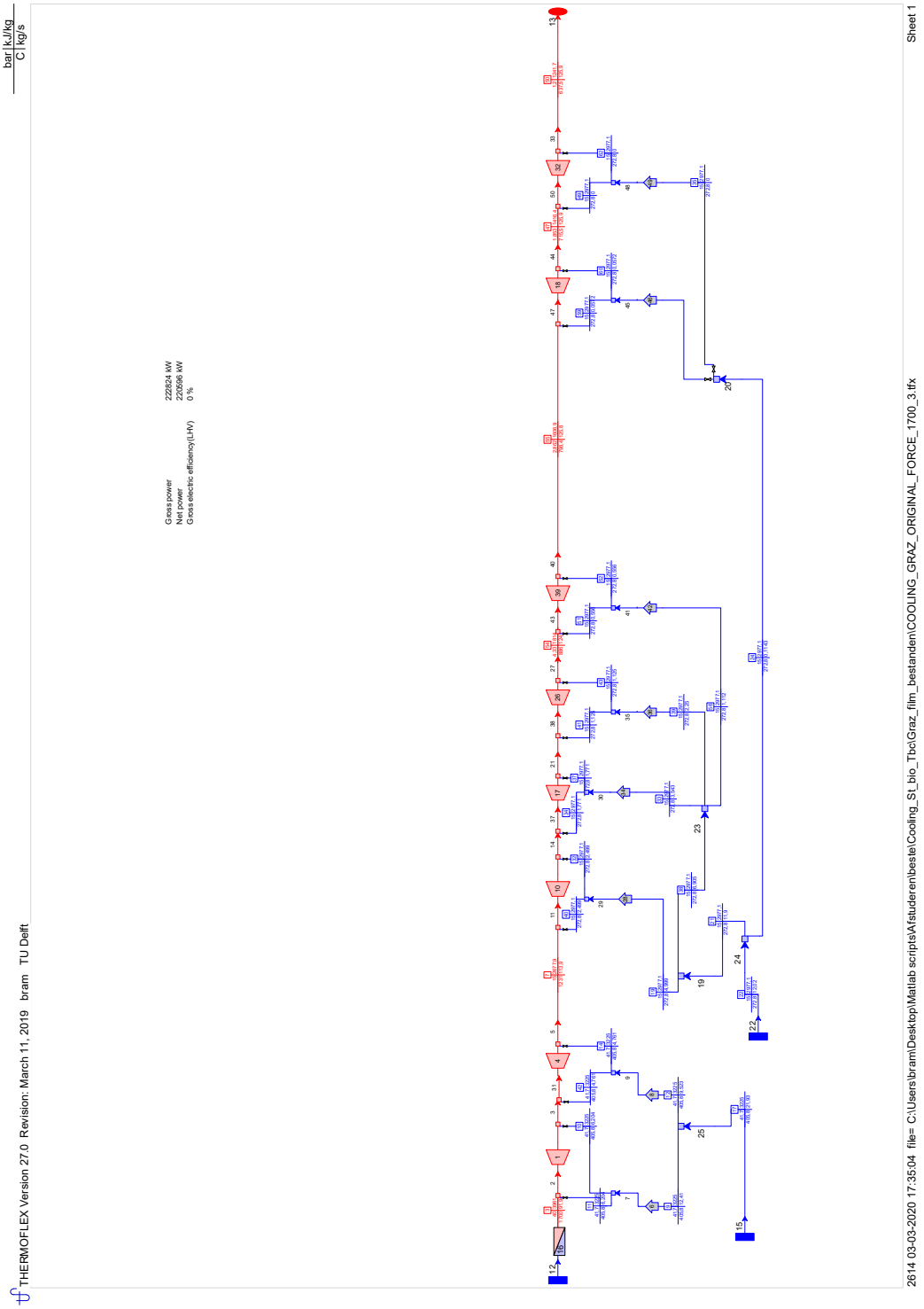

B.4 Graz-HEX cycle Thermoflex model

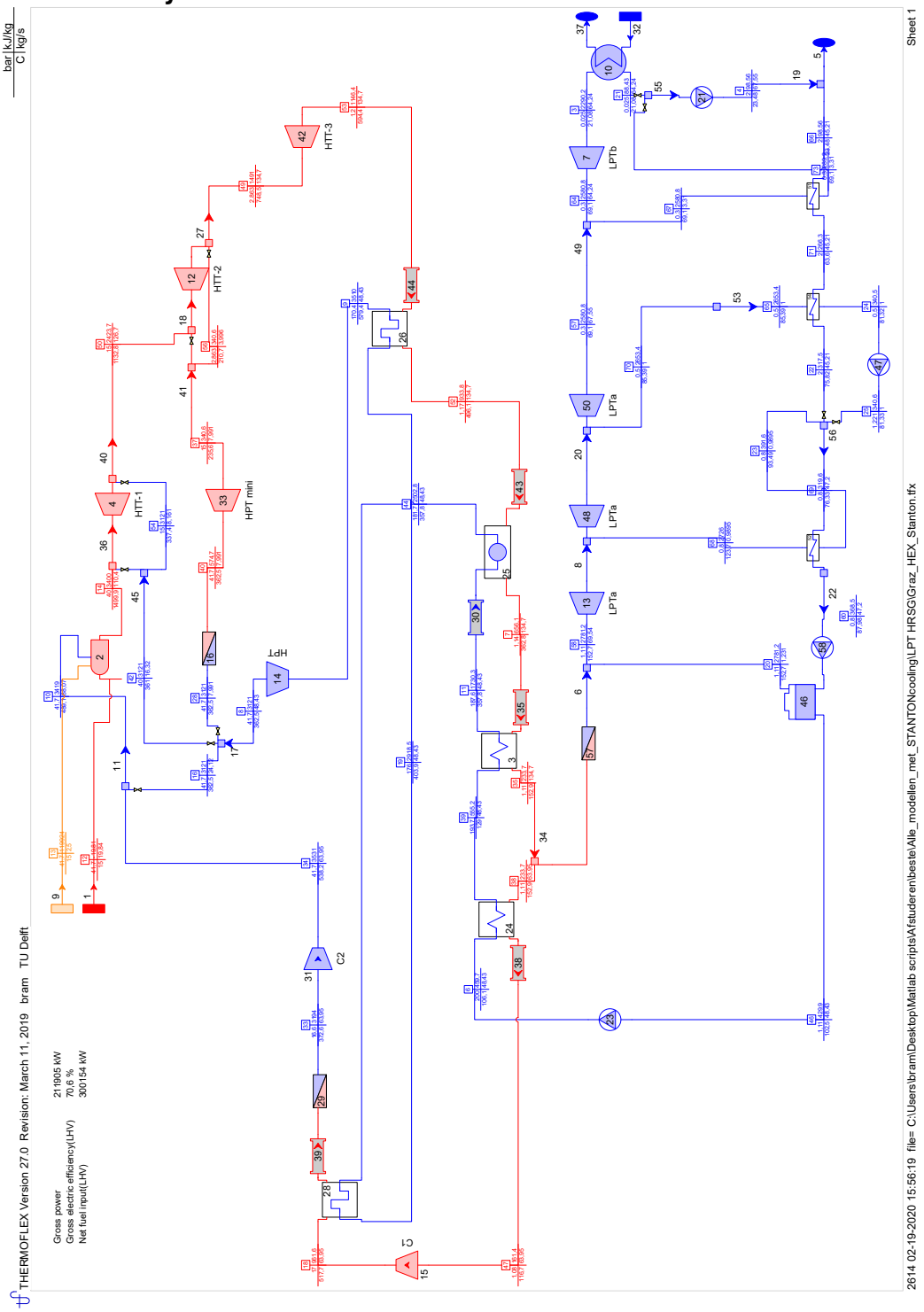

B.5 Graz-Hybrid cooled cycle Thermoflex model

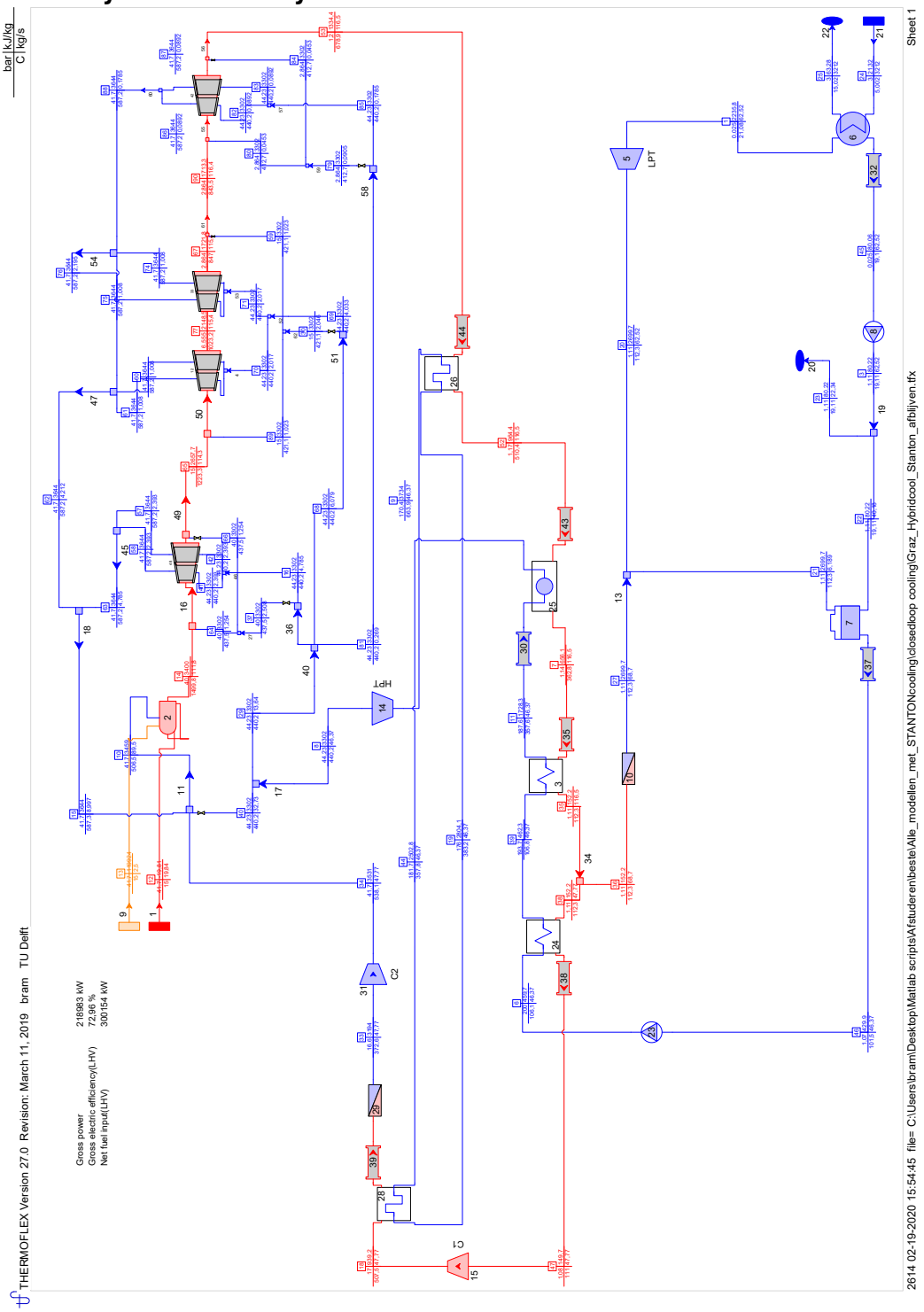

B.6 Graz-2CC cycle Thermoflex model

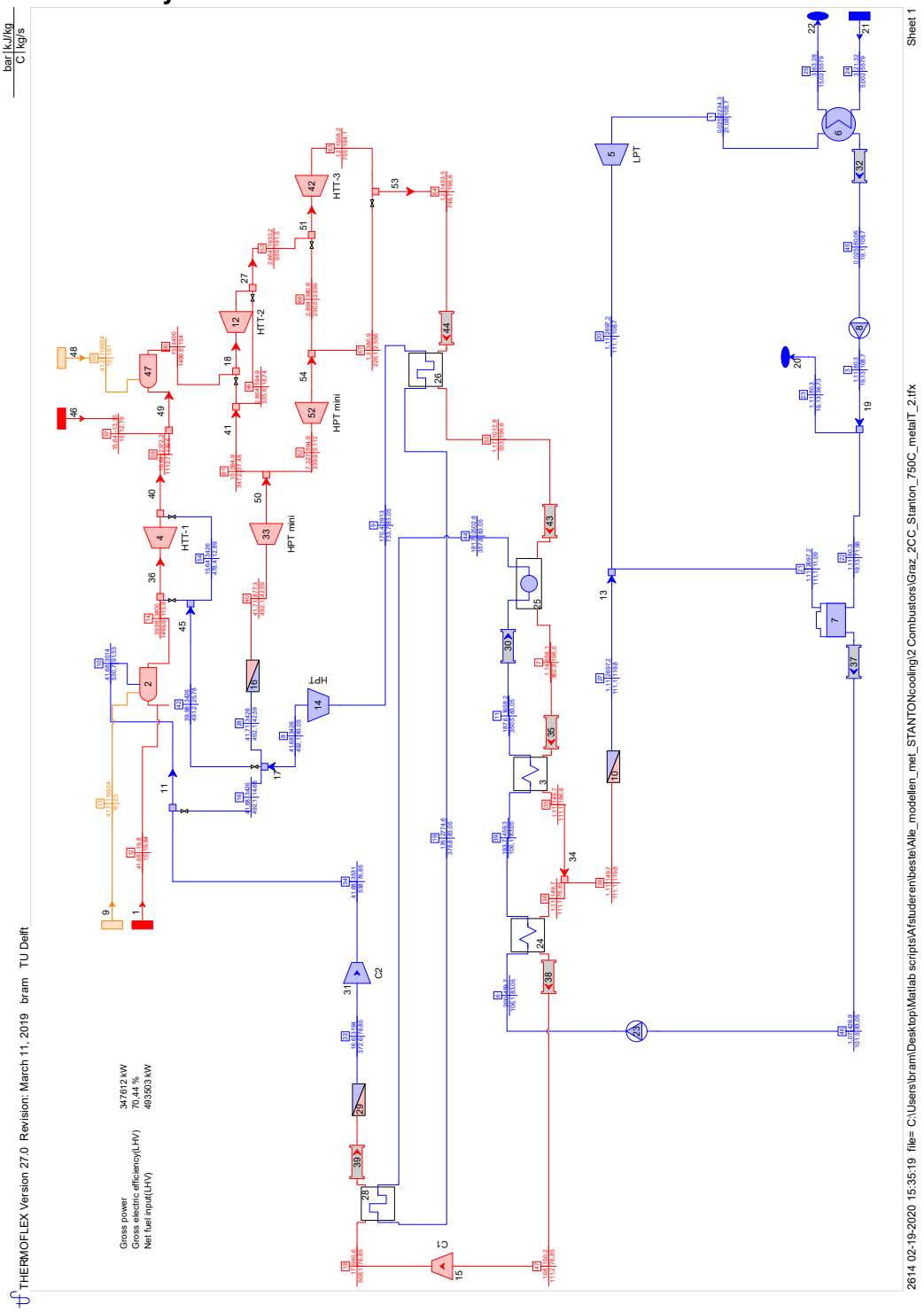

B.7 U-Graz-1500°C cycle Thermoflex model

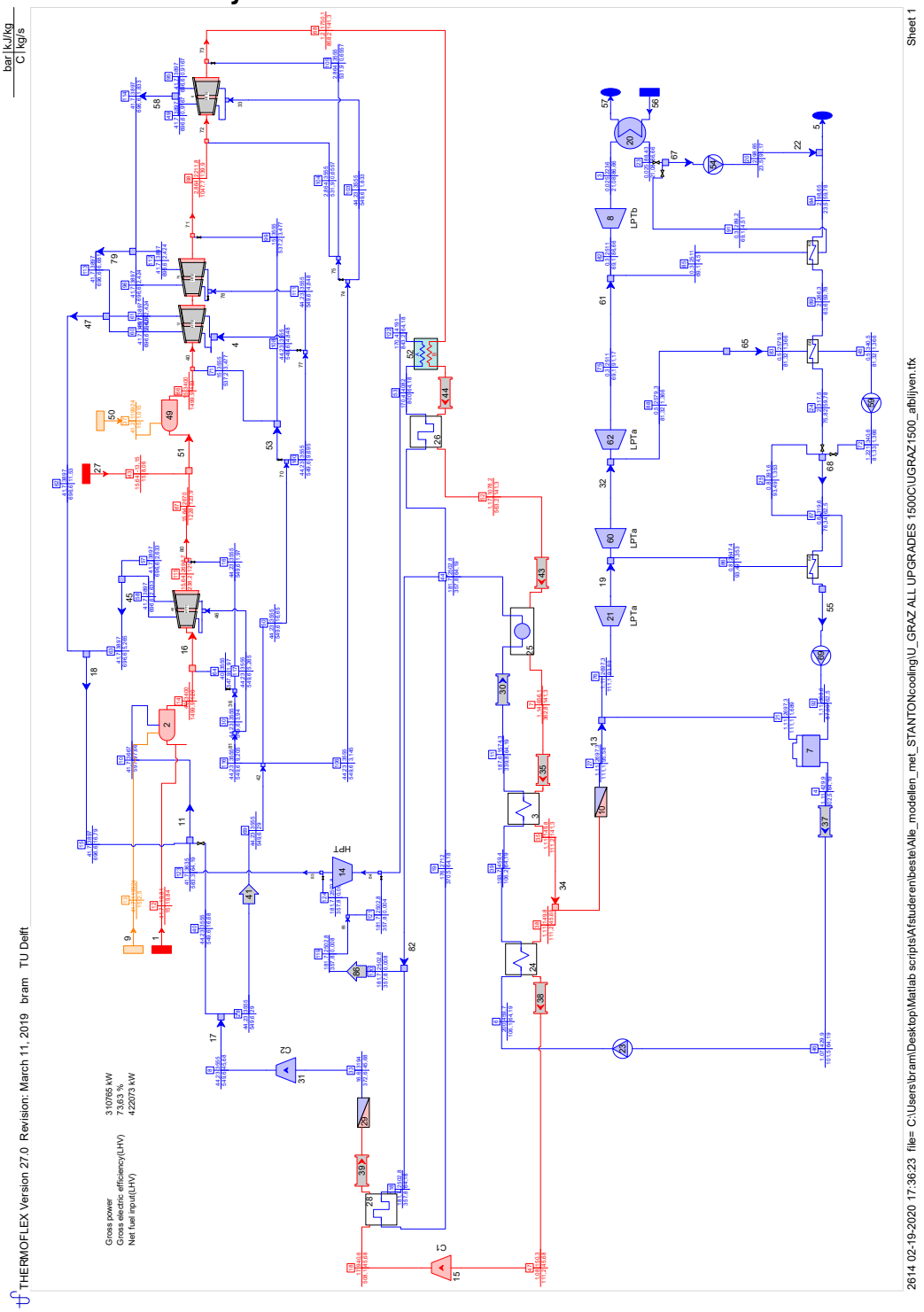

B.8 U-Graz cycle Thermoflex model

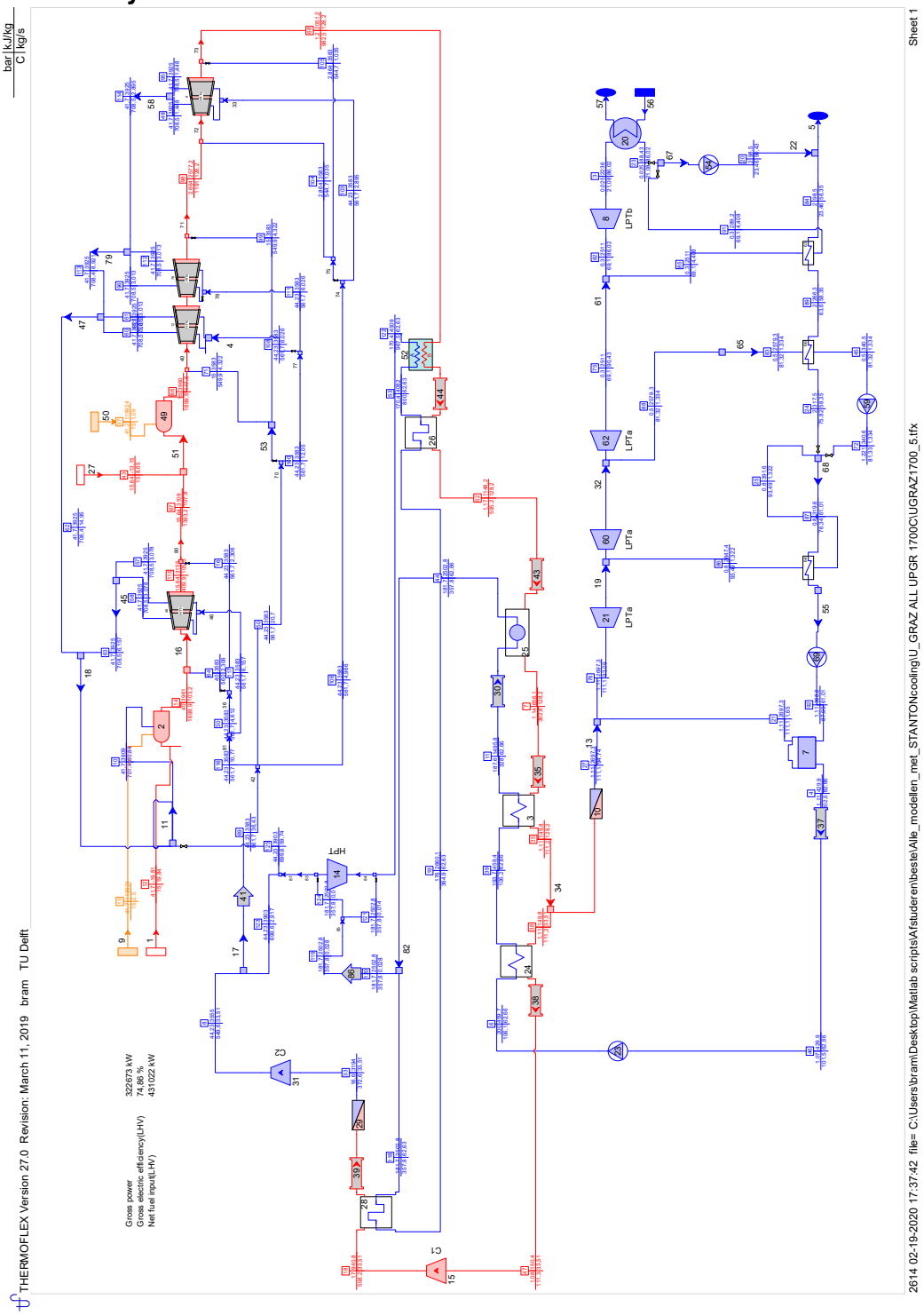

C Thermoflex models with FC

The schemes with the FC's operate with a "blackbox" around the FC part, this part is calculated in MATLAB, therefore only the turbine cycle power is displayed. Some trickery is applied to calculated to model the streams going through this part. The first combustor of the cycle acts as a FC, however only 35% of the energy is transferred to heat in the gasses going through. Therefore, the heat adder devices (displayed as Q+) subtract the surplus of added heat from the working fluids. Therefore the first combustor and the heat adder devices can be seen as "blackbox" items calculated in separate MATLAB script. The amount of oxygen recirculation, steam addition for an amount of fuel utilization is calculated per FC in MATLAB. For a detailed explanation of this integration and for the code email the author.

The main Thermoflex models are depicted in subsection C.1-C.5. The stage by stage Thermoflex cooling model of the U-Graz-3FC-OX cycle, is displayed in C.5.1. This cycle is hybrid cooled. The MATLAB code accompanied to calculate the stage by stage model cooling mass is displayed in appendix D.

C.1 Graz-1FC-Steam cycle Thermoflex model

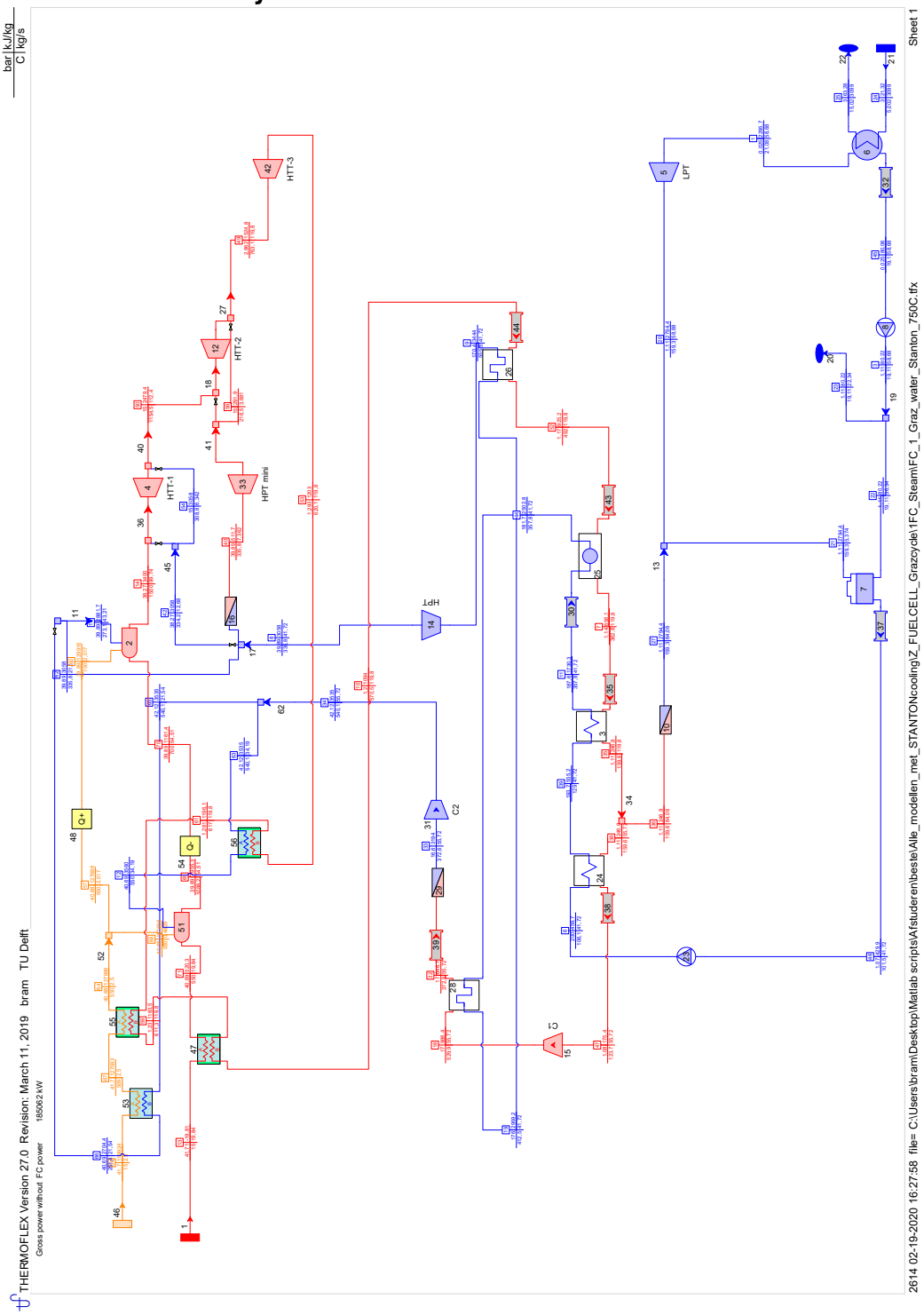

C.2 Graz-3FC-Steam cycle Thermoflex model

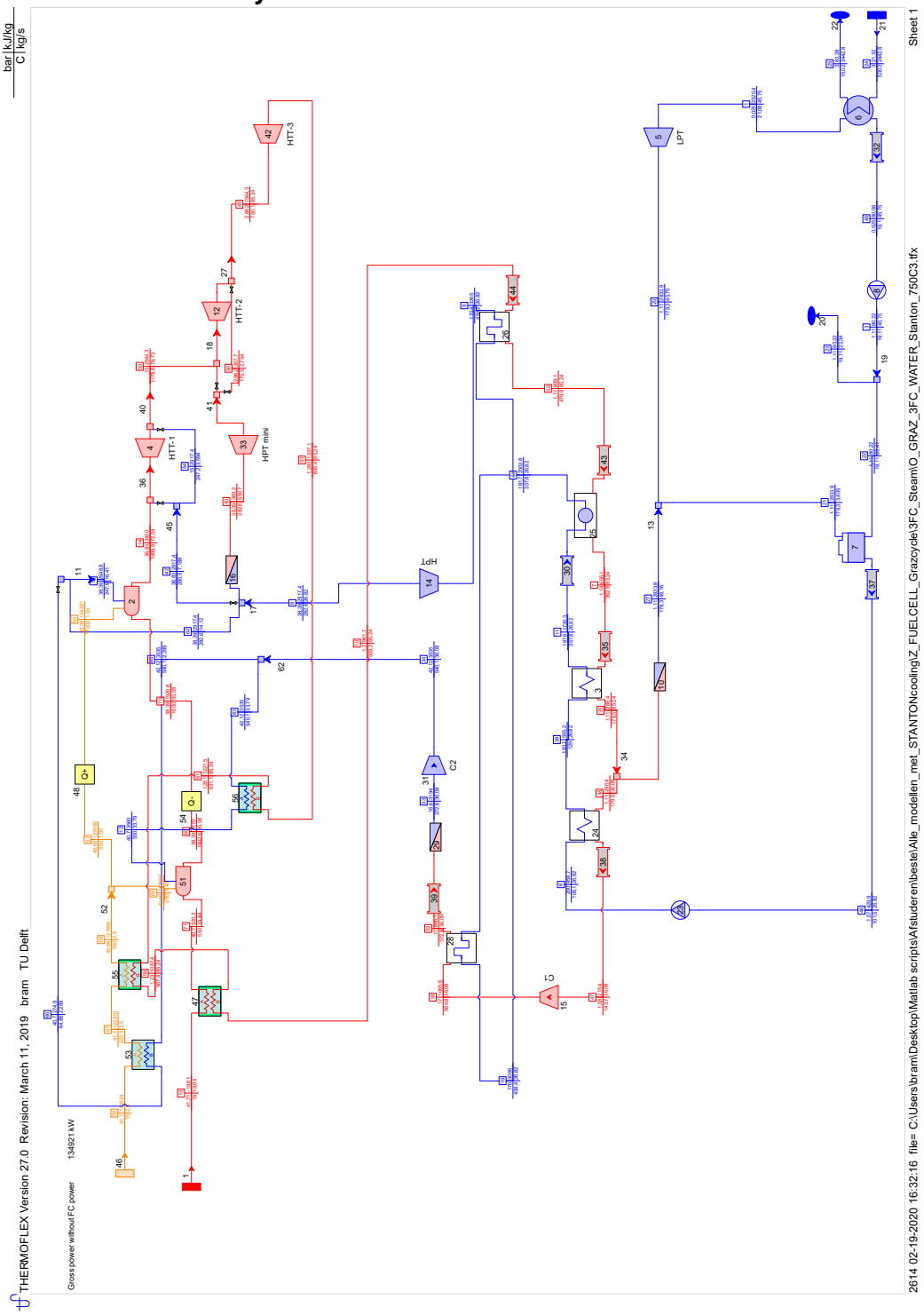

C.3 Graz-1FC-OX cycle Thermoflex model

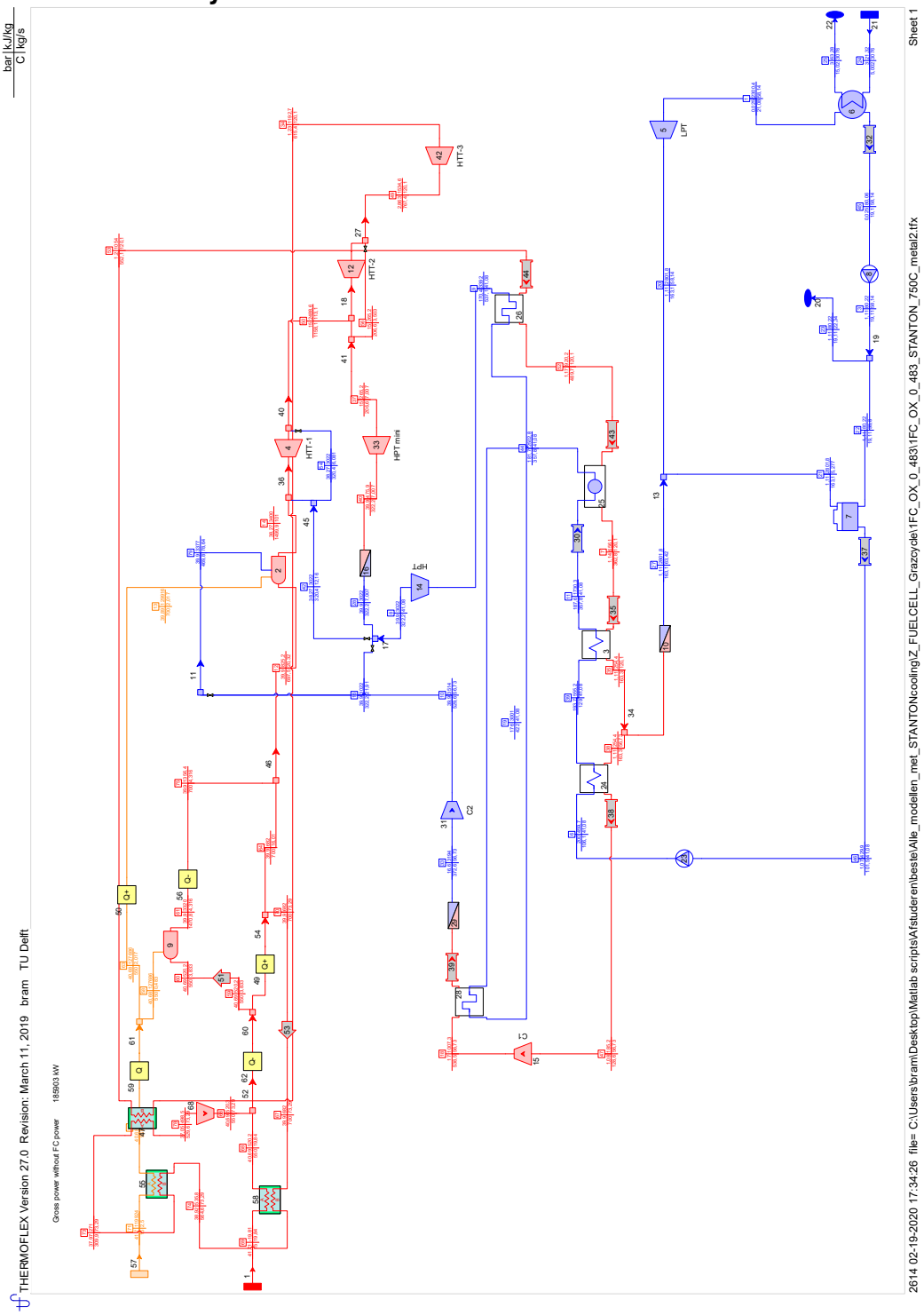

C.4 Graz-3FC-OX cycle Thermoflex model

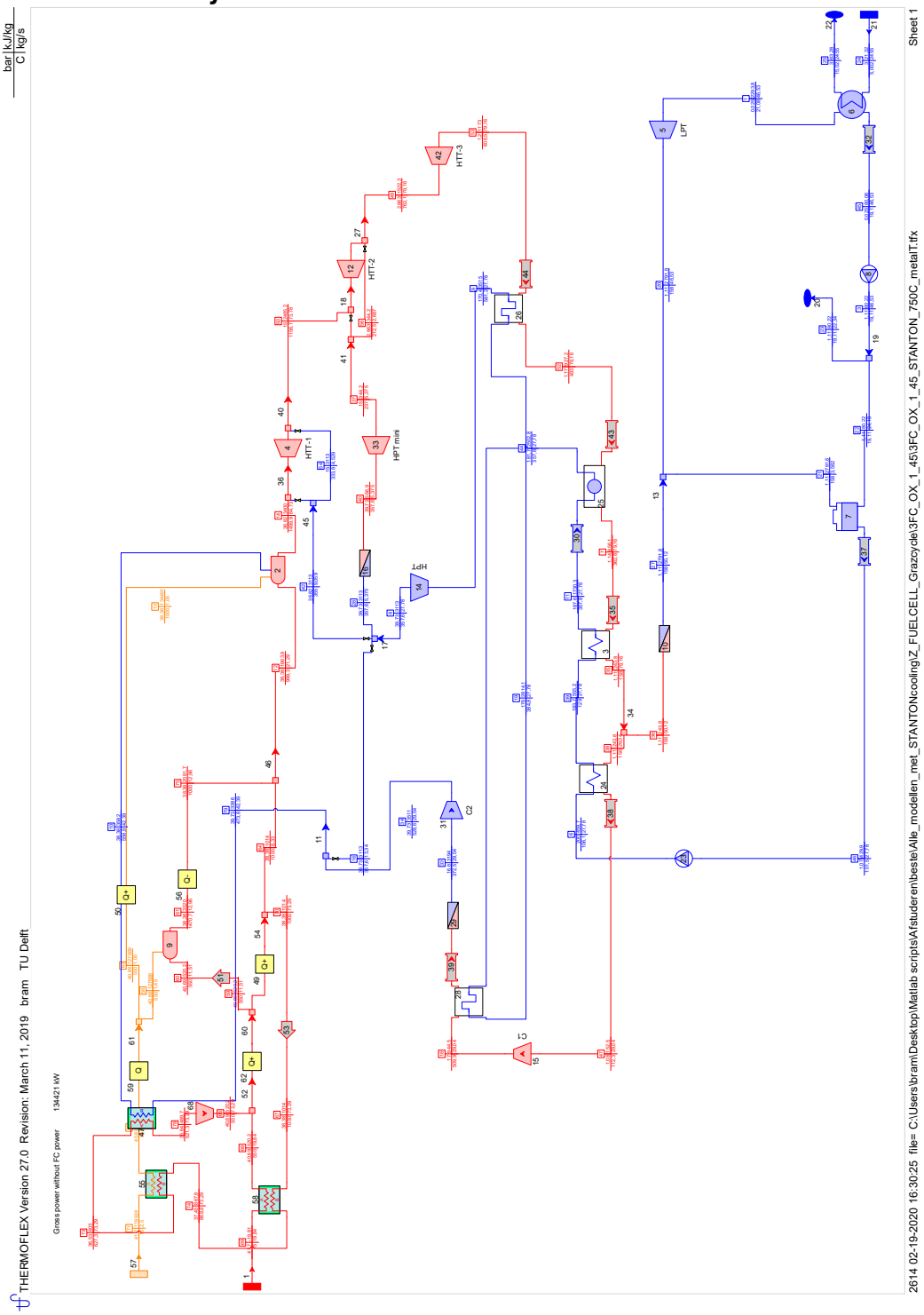

C.5 U-Graz-3FC-OX cycle Thermoflex model

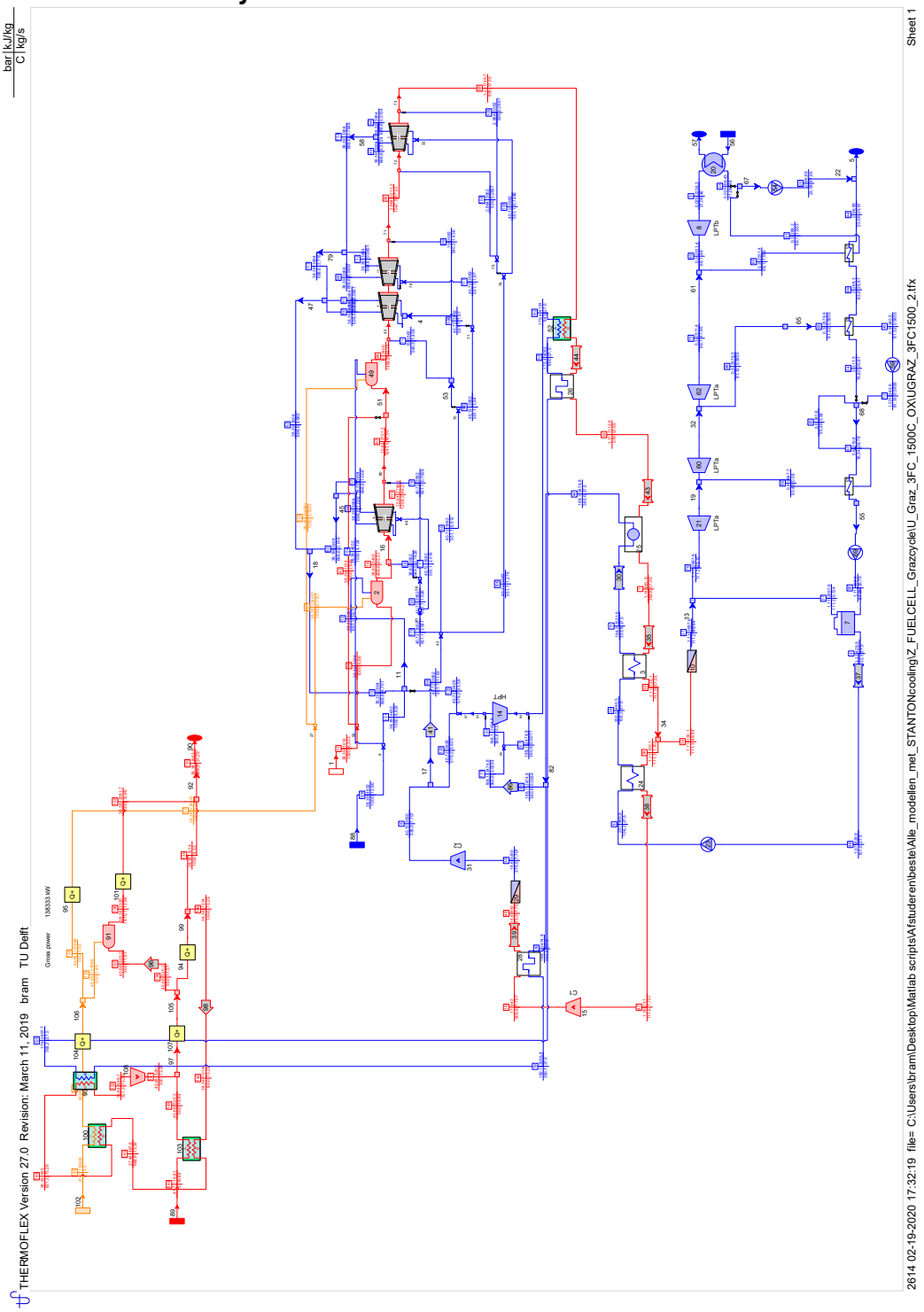

C.5.1 U-Graz-3FC-OX cycle Thermoflex stage by stage cooling model (hybrid cooling)

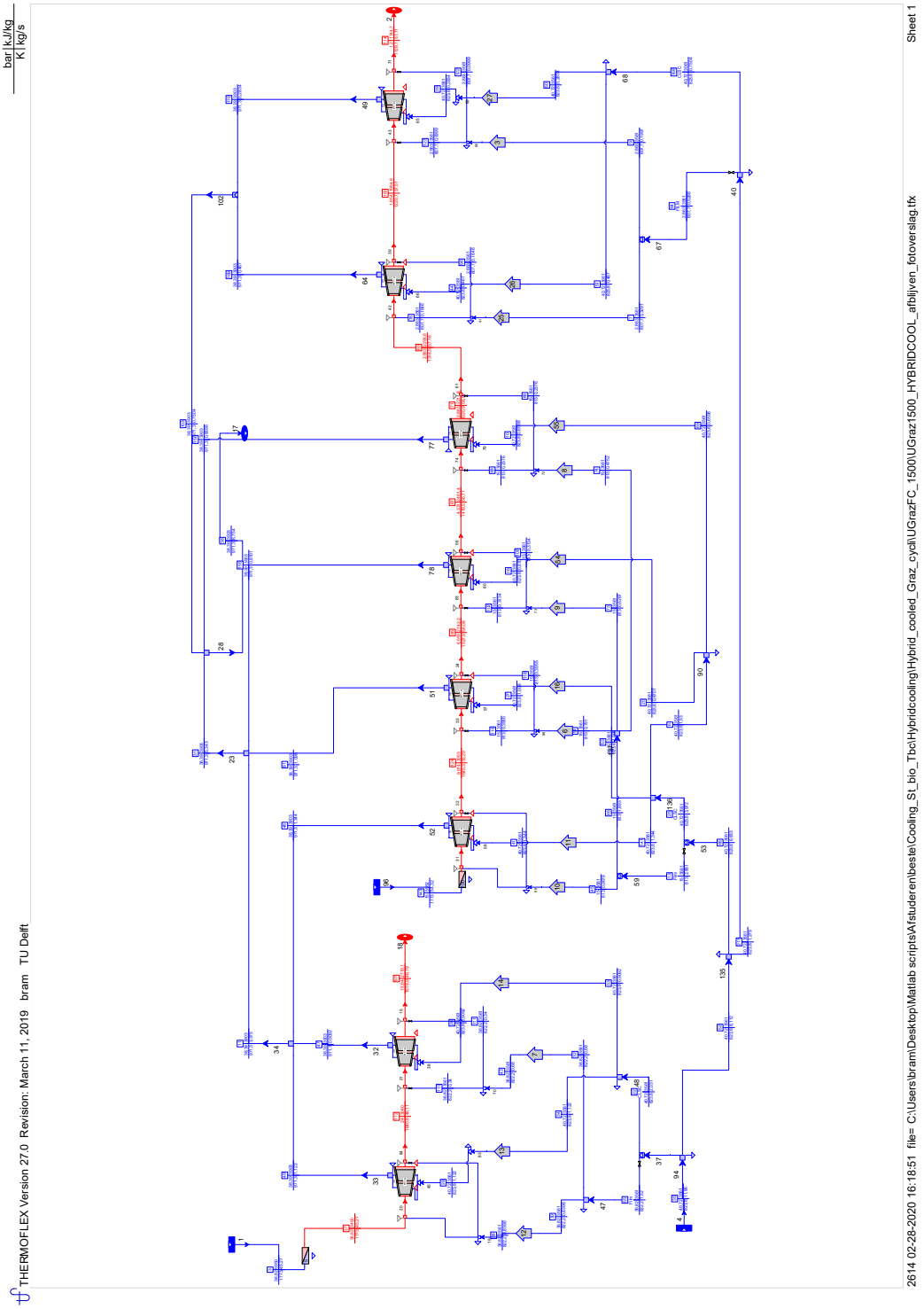

D MATLAB code

D.1 Scripts for calculating the cooling needs per turbine stage U-Graz-3FC-OX cycle(which uses hybrid cooling)

The cooling per turbine stage for the U-Graz-3FC-OX cycle is calculated using 2 scripts: The main script and a function file.

The main file calculates the cooling needs per turbine stage, using the temperatures from the detailed stage by stage cooling model, which is depicted in subsection C.5.1. The function file retrieves the heat capacity, from the Fluid-prop database.

D.1.1 Main script, HTT cooling of stages

```
clc
clear all

K=273.15;
St=0.00067;%stanton *FOB
St_film=0.00082;%stanton *FOB

Bi_tbc=0.9;
Ag_Aw=2*6;      %%%%*2 is truukje zodat je alleen stator berkent maar ook rotor meeneenmt

CoefficientFilm=Ag_Aw*St_film/2*1/(1+Bi_tbc);
CoefficientCLSC=Ag_Aw*St/2*1/(1+Bi_tbc); % is in literatuur standaard 0.012

Tw=1061;%1150
Twrot=1061; %1150
Tce=971.6;
Tci=824.1;
Pci=40.72;%bar
CPc=cpverkrijg(Pci,Tci-K);


Tcifilm=822.5;
CPcfilm=cpverkrijg(Pci,Tcifilm-K);
Tcifilm_HTT2=813.3;
Tcifilm_HTT3=808;
TciHPT=630.9;
P_HPT=181.7;
mdotHPT=26.61;
CPc_HPT=cpverkrijg(P_HPT,TciHPT-K);


CF=1/(1+Bi_tbc);
%% elke ronde aanpassen
%% HT1
mdotg1ja=45.27;
Tg1=1773;
Tg2=1640.8;
```

```
%%%%%%%%%%%%%%%%%%%%%%
%% HT2
mdotg3ja=54.32;
Tg3=1773;
Tg4=1645.3;
Tg5=1527.9;
Tg6=1419.8;
%% HT3
Tg7=1319.1;
Tg8=1220.8;%  bar en K


%% stator 1+rotor CLSC
mdotg1=mdotg1ja;
Tg=Tg1;
Pg=36.82;
Cpg=cpverkrijg(Pg,Tg-K);

mdotc1_clsc=CF*Cpg/CPc*St*Ag_Aw*(Tg-Tw)/(Tce-Tci)*mdotg1;
eps1=(Tg-Tw)/(Tg-Tcifilm);
mdotc1__film=CF*Cpg/CPcfilm*St_film*Ag_Aw*(eps1/(1-eps1))*mdotg1;


%% stator 2+rotor CLSC
mdotg2=mdotg1+mdotc1__film;
Tg=Tg2;
Pg=23.5;
Cpg=cpverkrijg(Pg,Tg-K);

mdotc2_clsc=CF*Cpg/CPc*St*Ag_Aw*(Tg-Tw)/(Tce-Tci)*mdotg2;
eps1=(Tg-Tw)/(Tg-Tcifilm);
mdotc2__film=CF*Cpg/CPcfilm*St_film*Ag_Aw*(eps1/(1-eps1))*mdotg2;

mdottotalcoolingCLSC_HTT1=mdotc1_clsc+mdotc2_clsc;
mdottotalcoolingfilm_HTT1=mdotc1__film+mdotc2__film;
%%%%%%%%%%%%%%%%%%%%%%%%%%%%

%% HTT-2
Tcifilm=Tcifilm_HTT2;
%% stator 3+rotor CLSC
mdotg3=mdotg3ja;
Tg=Tg3;%
Pg=15;
Cpg=cpverkrijg(Pg,Tg-K);

mdotc3_clsc=CF*Cpg/CPc*St*Ag_Aw*(Tg-Tw)/(Tce-Tci)*mdotg3;
eps1=(Tg-Tw)/(Tg-Tcifilm);
mdotc3__film=CF*Cpg/CPcfilm*St_film*Ag_Aw*(eps1/(1-eps1))*mdotg3;

%% stator 4+rotor CLSC
mdotg4=mdotg3+mdotc3__film;
Tg=Tg4;
Pg=9.914;
Cpg=cpverkrijg(Pg,Tg-K);

mdotc4_clsc=CF*Cpg/CPc*St*Ag_Aw*(Tg-Tw)/(Tce-Tci)*mdotg4;
eps1=(Tg-Tw)/(Tg-Tcifilm);
```

```
mdotc4__film=CF*Cpg/CPcfilm*St_film*Ag_Aw*(eps1/(1-eps1))*mdotg4;

%% stator 5+rotor CLSC
mdotg5=mdotg4+mdotc4__film;
Tg=Tg5;
Pg=6.553;
Cpg=cpverkrijg(Pg,Tg-K);

mdotc5_clsc=CF*Cpg/CPc*St*Ag_Aw*(Tg-Tw)/(Tce-Tci)*mdotg5;
eps1=(Tg-Tw)/(Tg-Tcifilm);
mdotc5__film=CF*Cpg/CPcfilm*St_film*Ag_Aw*(eps1/(1-eps1))*mdotg5;

%% stator 6+rotor CLSC
mdotg6=mdotg5+mdotc5__film;
Tg=Tg6;%  bar en K
Pg=4.331;
Cpg=cpverkrijg(Pg,Tg-K);

mdotc6_clsc=CF*Cpg/CPc*St*Ag_Aw*(Tg-Tw)/(Tce-Tci)*mdotg6;
eps1=(Tg-Tw)/(Tg-Tcifilm);
mdotc6__film=CF*Cpg/CPcfilm*St_film*Ag_Aw*(eps1/(1-eps1))*mdotg6;



mdottotalcoolingCLSC_HTT2=mdotc3_clsc+mdotc4_clsc+mdotc5_clsc+mdotc6_clsc;
mdottotalcoolingfilm_HTT2=mdotc3__film+mdotc4__film+mdotc5__film+mdotc6__film;

%%%%%%%%%%%%%%%%%%%%%%%%%%%%%%%%%%

% %% Film part Rankine HTT 2 is the same for this cycle as HTT-1 thus keep commented
% Tce=868;
% Tci=728;
% Tcifilm=648;
% Pc=70;
% CPc=cpverkrijg(Pc,Tci-K);
% Pcfilm=7.5;
% CPcfilm=cpverkrijg(Pcfilm,Tci-K);

%%%%%%%%%%%%%%%%%%%%%%%%%%%%

%% HTT-3
Tcifilm=Tcifilm_HTT3;
%% stator 7+rotor
mdotg7=mdotg6+mdotc6__film;
Tg=Tg7;%  bar en K
Pg=2.863;
Cpg=cpverkrijg(Pg,Tg-K);

mdotc7_clsc=CF*Cpg/CPc*St*Ag_Aw*(Tg-Tw)/(Tce-Tci)*mdotg7;
eps1=(Tg-Tw)/(Tg-Tcifilm);
mdotc7__film=CF*Cpg/CPcfilm*St_film*Ag_Aw*(eps1/(1-eps1))*mdotg7;

if mdotc7_clsc <= 0
mdotc7_clsc=0
end
if mdotc7__film <= 0
```

```
mdotc7_film=0
end
%% stator 8+rotor
mdotg8=mdotg7+mdotc7_film;
Tg=Tg8;
Pg=1.854;
Cpg=cpverkrijg(Pg,Tg-K);

mdotc8_clsc=CF*Cpg/CPc*St*Ag_Aw*(Tg-Tw)/(Tce-Tci)*mdotg8;
eps1=(Tg-Tw)/(Tg-Tcifilm);
mdotc8_film=CF*Cpg/CPcfilm*St_film*Ag_Aw*(eps1/(1-eps1))*mdotg8;
if mdotc8_clsc <= 0
mdotc8_clsc=0;
end
if mdotc8_film <= 0
mdotc8_film=0;
end

mdottotalcoolingCLSC_HTT3=mdotc7_clsc+mdotc8_clsc;
mdottotalcoolingfilm_HTT3=mdotc7_film+mdotc8_film;
%% HPT COOLING ENKEL OPENLOOP
St_filmHPT=0.00704;%0.8%fictive value for CLSC
StantonfHPT=St_filmHPT;%real stanton number to be able to calc Bi_tbc
mdotg=mdotHPT;
Tg1=1116;%40bar
P1=170.4;
P2=181.7;
Cpg_HPT=2.55;%REFPROP P170.4 T1116 %THis is supecritical dus dit kannie cpverkrijg(P2,Tg1-K);
eps1=(Tg1-Tw)/(Tg1-TciHPT);
mdotcHPT=CF*Cpg_HPT/CPc_HPT*St_film*Ag_Aw*(eps1/(1-eps1))*mdotg


%% Results knallen


mdotCLSCTOTAL=mdottotalcoolingCLSC_HTT1+mdottotalcoolingCLSC_HTT2+mdottotalcoolingCLSC_HTT3;
mdotfilmTOTAL=mdottotalcoolingfilm_HTT1+mdottotalcoolingfilm_HTT2+mdottotalcoolingfilm_HTT3;
coolingtotal=mdotfilmTOTAL+mdotCLSCTOTAL

name_cooling={'HTT1_CLSC';'HTT2_CLSC';'HTT3_CLSC';'HTT1_FILM';'HTT2_FILM';'HTT3_FILM';'
    CLSC_total';'Film_total'};
Cooling_tabel=[mdottotalcoolingCLSC_HTT1;mdottotalcoolingCLSC_HTT2;mdottotalcoolingCLSC_HTT3;
    mdottotalcoolingfilm_HTT1;mdottotalcoolingfilm_HTT2;mdottotalcoolingfilm_HTT3;
    mdotCLSCTOTAL;mdotfilmTOTAL];
Cooling_gewild=[0;0;0;0;0;0;0;0];
TabUITGFC=table(name_cooling,Cooling_tabel,Cooling_gewild)

%% fraction of valves
Fraction_Htt1=(mdottotalcoolingCLSC_HTT1+mdottotalcoolingfilm_HTT1)/coolingtotal;
Fraction_Htt2=(mdottotalcoolingCLSC_HTT2+mdottotalcoolingfilm_HTT2)/coolingtotal;

Fraction_Htt1_film=mdottotalcoolingfilm_HTT1/(mdottotalcoolingCLSC_HTT1+
    mdottotalcoolingfilm_HTT1);
Fraction_Htt2_film=mdottotalcoolingfilm_HTT2/(mdottotalcoolingCLSC_HTT2+
    mdottotalcoolingfilm_HTT2);
Fraction_Htt3_film=mdottotalcoolingfilm_HTT3/(mdottotalcoolingCLSC_HTT3+
    mdottotalcoolingfilm_HTT3);
```

```
name_fractions={'HTT1';'HTT2';'HTT1film';'HTT2film';'HTT3film'};
Fractions=[Fraction_Htt1;Fraction_Htt2;Fraction_Htt1_film;Fraction_Htt2_film;
    Fraction_Htt3_film];
tablefrac=table(name_fractions,Fractions)
```

D.1.2 Function file, HTT cooling of stages

```
function [cp] = mywaarde(P,T)
Cmp   = 'water';
FP = actxserver ('FluidProp.FluidProp');
Model = 'IF97';
ErrorMsg = invoke(FP,'SetFluid_M',Model,1,Cmp,[1,0]);

[Enthalpy,ErrorMsg] = invoke(FP,'Enthalpy','PT', P, T);
[cp,ErrorMsg] = invoke(FP,'HeatCapP','PT', P, T);
% SpecVolume
Enthalpy;
cp;
end
```

D.2 Scripts for calculating the FC parameters

The FC parameters are calculated using 3 scripts: The main script, the first function file and the second function file.

The FC script calculates the fuel utilisation and other electrochemical results per FC, using a certain amount of oxygen recirculation/steam cathode cooling as input for the calculation. Furthermore, it makes the fuel cell figures (figure 31 and 32) displayed in section 6.3 of this thesis.

D.2.1 Main script set to retrieve 3FC-OX data, needed to calculate the FC parameters

```
clear all
clc
close all
%% welke plot wil je zien
FCwanttoplot=1;%FC 1 2 of 3
%% TFLEX FUELCELL values afbijvenc
effi=0.65;
LHV_H2=120067.5;%KJ/kg
heatloss=0.02;%heatloss of LHV
P1=39.9;%bar exit FC1
P2=39.2;%bar exit FC 2
P3=38.4;%bar

%% cycle kiezen   5 is 3FC—OX   6is 3FC—steam
cycle=5;

%% 3FC—OX
if cycle==5 % 3 FC—OX
fuelin=2.5;%kg/s
oxin=93.13;%19.84;%kg/s
fuelusedtot=1.45;%kg/s eerste schatting
steamin=0;
%% 3FC Steam
elseif cycle==6 % 3 FC_steam
fuelin=2.5;%kg/s
oxin=19.84;
fuelusedtot=1.45;
steamin=33.8;
%% 1FC steam
elseif cycle==8 % 1FC steam in
fuelin=2.5;%kg/s
oxin=19.84;%19.84;%kg/s
fuelusedtot=1.45;%kg/s eerste schatting
steamin=34.19;
end
%%


MH2=2.0156*10^—3;%kg/mol molar mass
MO2=2*15.999*10^—3;%kg/mol molar mass
MH2O=18.01528*10^—3;%kg/mol molar mass
RatioO2_H2=0.5*MO2/MH2;
RatioH2O_H2=MH2O/MH2;
```

```
HHV=0;
fuel_h550=127686.4+HHV;%—LHV_H2;%enthalpy Kj/kg at 550c
fuel_h700=129916.4+HHV;%—LHV_H2;%enthalpy Kj/kg at 700c
fuel_h850=132183+HHV;%—LHV_H2;%enthalpy Kj/kg
fuel_h1000=134491+HHV;%—LHV_H2;%enthalpy Kj/kg
% fuel_h15=119923.5+HHV;%

ox_h550=520.26;%enthalpy Kj/kg at 550c
ox_h700=682.05;%enthalpy Kj/kg at 700c
ox_h850=846.98;%enthalpy Kj/kg
ox_h1000=1014.5;%enthalpy Kj/kg
ox_h15=—9.16;%

hvap=2547;%2547;
steam_h=3558.61—hvap;%enthalpy Kj/kg at 550c
steam_h700=3905.4—hvap;%enthalpy Kj/kg at 700c
steam_h850=4261.7—hvap;%enthalpy Kj/kg at 850c
steam_h1000=4630.62—hvap;%enthalpy Kj/kg at 850c

%% FC's samen
aaerror=2;
for k=1:100
fuelusedtot=fuelusedtot—aaerror/100000;
oxuit=oxin—(fuelusedtot)*RatioO2_H2;
oxuitmol=oxuit/MO2;
steamuit=steamin+fuelusedtot*RatioH2O_H2;
steamuitmol=steamuit/MH2O;
fueluit=fuelin—fuelusedtot;
huit=fueluit*fuel_h1000+oxuit*ox_h1000+steamuit*steam_h1000;
hin1=fuelin*fuel_h550+oxin*ox_h550+steamin*steam_h;
qinall=LHV_H2*fuelusedtot;
Wfc=effi*qinall;
qintot=LHV_H2*(1—effi)*fuelusedtot;
% aaerrorq=hin1+qintot—huit
qloss=heatloss*LHV_H2*fuelusedtot;
aaerror=hin1—Wfc—huit—qloss;
if abs(aaerror) <= 0.00001
    break
end
end
%% FC 1
fuelused1=0.1;%kg/s
aaerror1=2;
for k=1:100
fuelused1=fuelused1—aaerror1/100000;
oxused1=fuelused1*RatioO2_H2;
Wfc1=LHV_H2*effi*fuelused1;
fuelin2=fuelin—fuelused1;
oxin2=oxin—oxused1;
steamin2=steamin+fuelused1*RatioH2O_H2;
hin2=fuelin2*fuel_h700+oxin2*ox_h700+steamin2*steam_h700;
qloss1=heatloss*LHV_H2*fuelused1;
aaerror1=hin1—Wfc1—hin2—qloss1;
if abs(aaerror1) <= 0.00001
    break
end
```

```
end

%% Fc 2

fuelused2=0.3462;
aaerror2=2;
for k=1:100
fuelused2=fuelused2-aaerror2/100000;
oxused2=fuelused2*RatioO2_H2;
Wfc2=LHV_H2*effi*fuelused2;
fuelin3=fuelin2-fuelused2;
oxin3=oxin2-oxused2;
steamin3=steamin2+fuelused2*RatioH2O_H2;
hin3=fuelin3*fuel_h850+oxin3*ox_h850+steamin3*steam_h850;
qloss2=heatloss*LHV_H2*fuelused2;
aaerror2=hin2-Wfc2-hin3-qloss2;
if abs(aaerror2) <= 0.00001
    break
end
end

%% FC3
fuelused3=fuelusedtot-fuelused2-fuelused1;
oxused3=fuelused3*RatioO2_H2;
Wfc3=LHV_H2*effi*fuelused3;
oxuit=oxin-(fuelusedtot)*RatioO2_H2;
steamuit=steamin3+fuelused3*RatioH2O_H2;
fueluit=fuelin-fuelusedtot;%
huit=fueluit*fuel_h1000+oxuit*ox_h1000+steamuit*steam_h1000;
qloss3=heatloss*LHV_H2*fuelused3;
aaerror3=hin3-Wfc3-huit-qloss3;



aaerror123=aaerror1+aaerror2+aaerror3;
%% Results
Fu1=fuelused1/fuelin;
Fu2=fuelused2/fuelin2;
Fu3=fuelused3/fuelin3;

x_H2_1=1-Fu1;%mol percentage at end fc1
x_H2O_1=Fu1;%mol percentage at end fc1

x_H2_2=1-(fuelused1+fuelused2)/fuelin;%mol percentage at end fc2
x_H2O_2=(fuelused1+fuelused2)/fuelin;%mol percentage at end fc2

x_H2_3=1-(fuelused1+fuelused2+fuelused3)/fuelin;%mol percentage at end fc3
x_H2O_3=(fuelused1+fuelused2+fuelused3)/fuelin;%mol percentage at end fc3

Oxi1=(oxin2/MO2)/(oxin2/MO2+steamin/MH2O);
Oxi2=(oxin3/MO2)/(oxin3/MO2+steamin/MH2O);
Oxi3=(oxuit/MO2)/(oxuit/MO2+steamin/MH2O);

%% Functiefile inknallen
%operating voltage moet ook meegenomen worden
[efficiency_FC1,E0_FC1,Enernst_FC1,Ecell_FC1,Powdens_FC1,q_FC1,ASR_FC1]=
    FC_mainmodel_efficientie_input3(P1,Oxi1,x_H2_1,x_H2O_1,973);
```

```
[efficiency_FC2,E0_FC2,Enernst_FC2,Ecell_FC2,Powdens_FC2,q_FC2,ASR_FC2]=
    FC_mainmodel_efficientie_input3(P2,Oxi2,x_H2_2,x_H2O_2,1123);
[efficiency_FC3,E0_FC3,Enernst_FC3,Ecell_FC3,Powdens_FC3,q_FC3,ASR_FC3]=
    FC_mainmodel_efficientie_input3(P3,Oxi2,x_H2_3,x_H2O_3,1273);



%% Tables
Fuelnames={'Fuelused_FC1';'Fuelused_FC2';'Fuelused_FC3';'Fuelused total'};
Fuelvar=[fuelused1;fuelused2;fuelused3;fuelusedtot];
Fueltable=table(Fuelnames,Fuelvar);

FC1names={'Fuel utilisation (Fu1)';'Cathode Oxygen molpercent';'Anode H2 molpercent';'Anode
    H2O molpercent';'Power in kW FC1'};
FC1var=[Fu1;Oxi1;x_H2_1;x_H2O_1;Wfc1];
FC1table=table(FC1names,FC1var);

FC2names={'Fuel utilisation (Fu2)';'Cathode Oxygen molpercent';'Anode H2 molpercent';'Anode
    H2O molpercent';'Power in kW FC2'};
FC2var=[Fu2;Oxi2;x_H2_2;x_H2O_2;Wfc2];
FC2table=table(FC2names,FC2var);

FC3names={'Fuel utilisation (Fu3)';'Cathode Oxygen molpercent';'Anode H2 molpercent';'Anode
    H2O molpercent';'Power in kW FC3'};
FC3var=[Fu3;Oxi3;x_H2_3;x_H2O_3;Wfc3];
FC1table=table(FC3names,FC3var);
%% Fuelcells compared to each other
FC_parrameters={'Cathode Oxygen molpercent';'Anode H2 molpercent';'E0';'Nernst Voltage';'Cell
     voltage';'Area specific resistence ohm/cm^2';'Power density in w/cm^2';'current density
    A/cm^2';'Power in kW'};
FC1_result=[Oxi1;x_H2_1;E0_FC1;Enernst_FC1;Ecell_FC1;ASR_FC1;Powdens_FC1;q_FC1;Wfc1];
FC2_result=[Oxi2;x_H2_2;E0_FC2;Enernst_FC2;Ecell_FC2;ASR_FC2;Powdens_FC2;q_FC2;Wfc2];
FC3_result=[Oxi3;x_H2_3;E0_FC3;Enernst_FC3;Ecell_FC3;ASR_FC3;Powdens_FC3;q_FC3;Wfc3];
FCvergelijktable=table(FC_parrameters,FC1_result,FC2_result,FC3_result)
FC_totalAREA=Wfc1/Powdens_FC1+Wfc2/Powdens_FC2+Wfc3/Powdens_FC3;
FC_totalPower=(Wfc1+Wfc2+Wfc3);
FC_totalPowerdensity=FC_totalPower/FC_totalAREA
```

D.2.2 First function file, needed to calculate the FC parameters

```
function [efficiency,E0,Enernst,Ecell,Pload_percm2,q,ASR,qfig,Ecellfig] = mywaarde(P,Oxi,x_H2
    ,x_H2O,T)


%% Calculation
F=96485;% Faradays constant in coulombs/mole
R=8.314;% Gas constant
T_ref=298;
Acell=5;%in cm^2;
n=1;%amount of cells
x_O2=Oxi; %hier zit dus 70%h2o bij
LHV_H2mol=242.36;%Mj/mol is
LHV_H2=LHV_H2mol/2.02*10^6;%MJ/kg
%% Perfect stuk

dH_H2_298K=0;A=3.249;B=.422*10^-3;C=0;D=0.083*10^5;
```

```
dG_H2_298K=0;dS_H2_298K=-(dG_H2_298K-dH_H2_298K)/298;
dH_H2=dH_H2_298K+R*(A*T+B/2*T^2+C/3*T^3-D/T)-R*(A*T_ref+B/2*T_ref^2+C/3*T_ref^3-D/T_ref);
dS_H2=dS_H2_298K+R*(A*log(T)+B*T+C/2*T^2-0.5*D/T^2)-R*(A*log(T_ref)+B*T_ref+C/2*T_ref^2-0.5*D
    /T_ref^2);


dH_O2_298K=0;A=3.639;B=0.506*10^-3;C=0;D=-0.227*10^5;
dG_O2_298K=0;dS_O2_298K=-(dG_O2_298K-dH_O2_298K)/298;
dH_O2=dH_O2_298K+R*(A*T+B/2*T^2+C/3*T^3-D/T)-R*(A*T_ref+B/2*T_ref^2+C/3*T_ref^3-D/T_ref);
dS_O2=dS_O2_298K+R*(A*log(T)+B*T+C/2*T^2-0.5*D/T^2)-R*(A*log(T_ref)+B*T_ref+C/2*T_ref^2-0.5*D
    /T_ref^2);

% Water vapor
dH_H2O_298K=-241.83*10^3;A=3.470;B=1.45*10^-3;C=0;D=0.121*10^5;
dG_H2O_298K=-228.6*10^3;dS_H2O_298K=-(dG_H2O_298K-dH_H2O_298K)/298;
dH_H2O=dH_H2O_298K+R*(A*T+B/2*T^2+C/3*T^3-D/T)-R*(A*T_ref+B/2*T_ref^2+C/3*T_ref^3-D/T_ref);
dS_H2O=dS_H2O_298K+R*(A*log(T)+B*T+C/2*T^2-0.5*D/T^2)-R*(A*log(T_ref)+B*T_ref+C/2*T_ref^2-0.5
    *D/T_ref^2);

dH_reactie=dH_H2O-dH_H2-.5*dH_O2;
dS_reactie=dS_H2O-dS_H2-.5*dS_O2;
dG_reactie=dH_reactie-dS_reactie*T;

%% Calculation
dG=dG_reactie;
dGkg=dG_reactie*18.02;
dH=dH_reactie;
E0=-dG/(2*F);

%% Standard cell values  as Samuel
t_CAT=0.2;%0.2;%0.2;%cathode thickness in cm
t_elec=0.004;%40*10^-6*10^2;%electrolydte thickness in cm
t_ANO=0.015;%150*10^-6*10^2;%Anode thickness in cm
t_int=0.01;%100*10^-6*10^2;%interconnect thickness 9mm breed

C1_CAT=8.114*10^-3*10^2;C2_CAT=600;%coefficients ressesivity
C1_elec=2.94*10^-3;C2_elec=10350;%coefficients ressesivity
C1_ANO=2.98*10^-3;C2_ANO=-1392;%coefficients ressesivity
% C1_inter=1.256*10^-1;C2_inter=4690;%coefficients ressesivity


Res_CAT=C1_CAT*exp(C2_CAT/T);
Res_elec=C1_elec*exp(C2_elec/T);
Res_ANO=C1_ANO*exp(C2_ANO/T);
Res_inter=1/((9.3*10^5/T*exp(-1100/T)))*10^2;% komt uit artikel Effect of Electrolyte
    Thickness on Electrochemical Reactions and Thermo-Fluidic Characteristics inside a SOFC
    Unit Cell Jee Min Park 1 , Dae Yun Kim

R_CAT=t_CAT*Res_CAT/Acell;%Acat is cross sectional area cathode
R_elec=t_elec*Res_elec/Acell;
R_ANO=t_ANO*Res_ANO/Acell;
R_inter=t_int*Res_inter/Acell;
Rint=R_CAT+R_elec+R_ANO+R_inter;

ASR=Rint*Acell;%in ohm/cm^2
ASR_SI=ASR*10^-4;
%% partial p
```

```
PH2=x_H2*P;
PO2=x_O2*P;
PH2O=x_H2O*P;

Enernst=E0+R*T/(2*F)*log((PH2*PO2^.5)/PH2O);



%% NOICE plotjes knallen
aaerror1=0.1;
kend=100;
Ecell=0.7;%linspace(0,Enernst,kend);%operating voltage must be lower then E0
efficiencywanted=0.65
for k=1:kend
Ecell=Ecell-aaerror1/10;
Icellfig=(Enernst-Ecell)/Rint;
RH2fig=Icellfig/(2*F);%consumption rate in moles / second
q=Icellfig/Acell;%current density in amperage/cm^2
Rloadfig=Ecell/Icellfig;
Ploadfig=Ecell*Icellfig;
Pload_percm2=Ploadfig/Acell;%load/cm^2 powdens
efficiency=Ploadfig/(-dH*RH2fig);
aaerror1=efficiency-efficiencywanted;
if abs(aaerror1) <= 0.00001
    break
end
end
end
```

D.2.3 Second function file, needed to calculate the FC parameters

```
function [qfig,Ecellfig,Pload_percm2fig,efficiencyfig,Enernst] = mywaarde(P,Oxi,x_H2,x_H2O,T,
    Ecell)

%% Calculation
F=96485;% Faradays constant in coulombs/mole
R=8.314;% Gas constant
T_ref=298;

Acell=5;%in cm^2;
n=1;%amount of cells
x_O2=Oxi; %hier zit dus 70%h2o bij

LHV_H2mol=242.36;%Mj/mol is
LHV_H2=LHV_H2mol/2.02*10^6;%MJ/kg
%% Perfect stuk

dH_H2_298K=0;A=3.249;B=.422*10^-3;C=0;D=0.083*10^5;
dG_H2_298K=0;dS_H2_298K=-(dG_H2_298K-dH_H2_298K)/298;
dH_H2=dH_H2_298K+R*(A*T+B/2*T^2+C/3*T^3-D/T)-R*(A*T_ref+B/2*T_ref^2+C/3*T_ref^3-D/T_ref);
dS_H2=dS_H2_298K+R*(A*log(T)+B*T+C/2*T^2-0.5*D/T^2)-R*(A*log(T_ref)+B*T_ref+C/2*T_ref^2-0.5*D
    /T_ref^2);


dH_O2_298K=0;A=3.639;B=0.506*10^-3;C=0;D=-0.227*10^5;
dG_O2_298K=0;dS_O2_298K=-(dG_O2_298K-dH_O2_298K)/298;
```

```
dH_O2=dH_O2_298K+R*(A*T+B/2*T^2+C/3*T^3-D/T)-R*(A*T_ref+B/2*T_ref^2+C/3*T_ref^3-D/T_ref);
dS_O2=dS_O2_298K+R*(A*log(T)+B*T+C/2*T^2-0.5*D/T^2)-R*(A*log(T_ref)+B*T_ref+C/2*T_ref^2-0.5*D
    /T_ref^2);

% Water vapor
dH_H2O_298K=-241.83*10^3;A=3.470;B=1.45*10^-3;C=0;D=0.121*10^5;
dG_H2O_298K=-228.6*10^3;dS_H2O_298K=-(dG_H2O_298K-dH_H2O_298K)/298;
dH_H2O=dH_H2O_298K+R*(A*T+B/2*T^2+C/3*T^3-D/T)-R*(A*T_ref+B/2*T_ref^2+C/3*T_ref^3-D/T_ref);
dS_H2O=dS_H2O_298K+R*(A*log(T)+B*T+C/2*T^2-0.5*D/T^2)-R*(A*log(T_ref)+B*T_ref+C/2*T_ref^2-0.5
    *D/T_ref^2);

dH_reactie=dH_H2O-dH_H2-.5*dH_O2;
dS_reactie=dS_H2O-dS_H2-.5*dS_O2;
dG_reactie=dH_reactie-dS_reactie*T;

%% Calculation
dG=dG_reactie;
dGkg=dG_reactie*18.02;
dH=dH_reactie;
E0=-dG/(2*F);

%% Standard cell values  as Samuel
t_CAT=0.2;%0.2;%0.2;%cathode thickness in cm
t_elec=0.004;%40*10^-6*10^2;%electrolydte thickness in cm
t_ANO=0.015;%150*10^-6*10^2;%Anode thickness in cm
t_int=0.01;%100*10^-6*10^2;%interconnect thickness 9mm breed

C1_CAT=8.114*10^-3*10^2;C2_CAT=600;%coefficients ressesivity
C1_elec=2.94*10^-3;C2_elec=10350;%coefficients ressesivity
C1_ANO=2.98*10^-3;C2_ANO=-1392;%coefficients ressesivity
% C1_inter=1.256*10^-1;C2_inter=4690;%coefficients ressesivity


Res_CAT=C1_CAT*exp(C2_CAT/T);
Res_elec=C1_elec*exp(C2_elec/T);
Res_ANO=C1_ANO*exp(C2_ANO/T);
Res_inter=1/((9.3*10^5/T*exp(-1100/T)))*10^2;% komt uit artikel Effect of Electrolyte
    Thickness on Electrochemical Reactions and Thermo-Fluidic Characteristics inside a SOFC
    Unit Cell Jee Min Park 1 , Dae Yun Kim

R_CAT=t_CAT*Res_CAT/Acell;%Acat is cross sectional area cathode
R_elec=t_elec*Res_elec/Acell;
R_ANO=t_ANO*Res_ANO/Acell;
R_inter=t_int*Res_inter/Acell;
Rint=R_CAT+R_elec+R_ANO+R_inter;

ASR=Rint*Acell;%in ohm/cm^2
ASR_SI=ASR*10^-4;
%% partial p

PH2=x_H2*P;
PO2=x_O2*P;
PH2O=x_H2O*P;

Enernst=E0+R*T/(2*F)*log((PH2*PO2^.5)/PH2O);
Icell=(Enernst-Ecell)/Rint;
% q=...???%
```

```
% Icell=q*Acell;
% Ecell=-Icell*Rint+Enernst
%% Results
RH2=Icell/(2*F);%consumption rate in moles / second
RO2=Icell/(4*F);%consumption rate in moles / second
q=Icell/Acell*10^4%current density in amperage/m^2
Rload=Ecell/Icell;
Pload=Ecell*Icell;
efficiency=Pload/(-dH*RH2);
voltage_efficiency=Ecell/Enernst;
Powdens=Pload/Acell*10;%in kwatt/m^2
EFFmax=dG/dH;%max achievable efficiency
Total_Power=Pload*n;
q_mAcm2=q/10;


RELAname={'ASR';'Power density in kwatt/m^2';'Power';'Enernst';'Potential V';'Operating V';'
    efficiency';'efficiencyMAX';'current density amperage/m^2'};
RELA=[ASR;Powdens;Pload;Enernst;E0;Ecell;efficiency;EFFmax;q];
TabRELA=table(RELAname,RELA)

%% NOICE plotjes knallen

kend=100;
Ecellfig=linspace(0,Enernst,kend);%operating voltage must be lower then E0

for k=1:kend

Icellfig(k)=(Enernst-Ecellfig(k))/Rint;

%% Results
% RH2=Icell/(2*F);%consumption rate in moles / second
% RO2=Icell/(4*F);%consumption rate in moles / second
RH2fig(k)=Icellfig(k)/(2*F);%consumption rate in moles / second
qfig(k)=Icellfig(k)/Acell;%current density in amperage/cm^2
Rloadfig(k)=Ecellfig(k)/Icellfig(k);
Ploadfig(k)=Ecellfig(k)*Icellfig(k);
Pload_percm2fig(k)=Ploadfig(k)/Acell;%load/cm^2
efficiencyfig(k)=Ploadfig(k)/(-dH*RH2fig(k));
end
```